

Photovoltaics

International

THE TECHNOLOGY RESOURCE FOR PV PROFESSIONALS



Edition 43

Heterojunction

Hevel Group details all steps for successful SHJ production

Shingling

Fraunhofer ISE demonstrates latest advances in PERC-based shingled solar cells

Industry 4.0

ISC Konstanz reveals the role and impact of digitalization in PV manufacturing

R&D report

In-house analysis of R&D expenditure of 21 PV manufacturers

Cell measurements

ISFH explains the importance of accurate solar cell measurements

www.pv-tech.org



PERC PATENT HOLDER

Harvest the Sunshine

Here Comes Another Reason to Choose JA Solar:

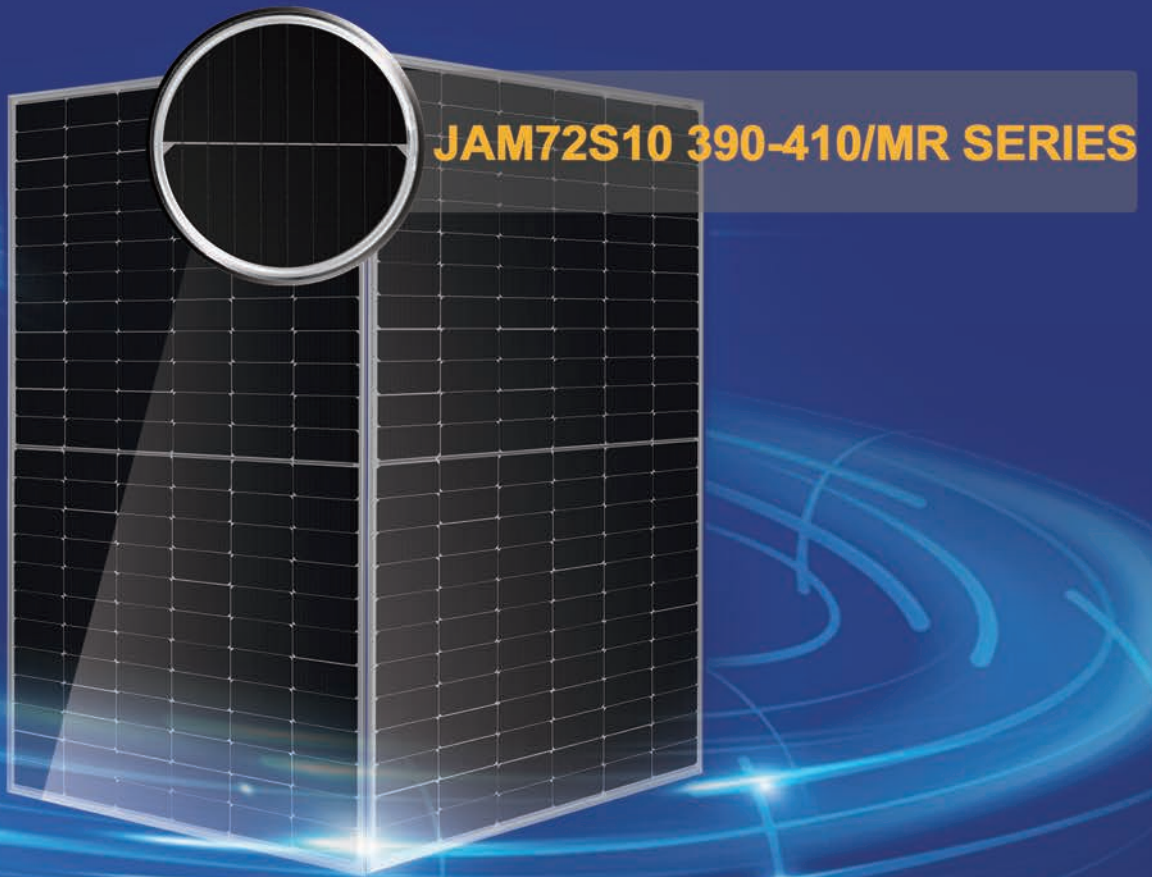
72-Cell Multi-Busbar Half-Cell Module

410W Higher Power Output

20.4% Higher Conversion Efficiency

3.70% Less Shading Loss

-0.35%/°C Better Temperature Coefficient



JA SOLAR

Tel: +86(10) 6361 1888
Email: sales@jasolar.com marketing@jasolar.com
www.jasolar.com

Published by:
Solar Media Ltd.,
123 Buckingham Palace Rd
Victoria, London SW1W 9SH
United Kingdom
T: +44 (0) 207 871 0122
T: +44 (0) 7827 885311
E info@pv-tech.org
www.pv-tech.org

Publisher: **David Owen**

Head of Content: **John Parnell**
Technical Publishing Director: **Mark Osborne**
Commissioning Editor: **Adam Morrison**
Sub-Editor: **Steve D. Brierley**
Design: **Tina Davidian**
Production: **Daniel H Brown, Sarah-Jane Lee**
Sales Director: **David Evans**
Account Managers: **Adam Morrison,**
Graham Davie, Lili Zhu

While every effort has been made to ensure the accuracy of the contents of this journal, the publisher will accept no responsibility for any errors, or opinion expressed, or omissions, or for any loss or damage, consequential or otherwise, suffered as a result of any material here published.

Cover image: Pilot process to apply an electrically conductive adhesive to shingled cells carried out on the industrial stringer in the Module-TEC of Fraunhofer ISE.

Printed by Buxton Press

Photovoltaics International
Forty Third Edition
September 2019
Photovoltaics International is a six monthly journal published in February and September each year.

Distributed in the USA by Mail Right International, 1637 Stelton Road B4, Piscataway, NJ 08854.

ISSN: 1757-1197

The entire contents of this publication are protected by copyright, full details of which are available from the publisher. All rights reserved. No part of this publication may be reproduced, stored in a retrieval system or transmitted in any form or by any means – electronic, mechanical, photocopying, recording or otherwise – without the prior permission of the copyright owner.

USPS Information
USPS Periodical Code: 025 313

Periodicals Postage Paid at
New Brunswick, NJ
Postmaster: Send changes to:
Photovoltaics International,
Solar Media Ltd., C/o 1637 Stelton Road,
B-4, Piscataway, NJ 08854, USA

Foreword

Welcome to Photovoltaics International 43. The PV industry continues its technological advance and downstream markets continue to grow, with the two elements remaining intrinsically linked. If this edition is an indication that technological advances are continuing to shape the industry and drive down the cost per-Watt to record lows, then we are set for many years of continued growth.

Our annual in-house analysis of the R&D spending trends of 21 PV manufacturers in this edition highlights the second consecutive year of combined expenditure topping the US\$1.0 billion mark, with the LONGi Group setting a industry record of US\$182.74 million of expenditure in 2018.

Linked with LONGi's R&D activities, Photovoltaics International has also reported on the rapid transition to larger wafer sizes, which will have a significant impact on the PV industry. Three companies driving this exceptional change - LONGi, GCL-Poly and Zhonghuan Semiconductor - are featured, including an exclusive picture of what Zhonghuan's "Kwafu" M12 series wafers (210mm x 210mm) look like in a 60-cell module format, boasting 610Wp performance.

Using 300mm semiconductor crystal pulling technology, significant R&D and over 100 patents in the making, Zhonghuan has also pioneered Industry 4.0 techniques to enter volume production of its king-size wafers. Edition 43 continues its own series of Industry 4.0 papers, with researchers from ISC Konstanz highlighting the role and impact of digitalization and self-learning concepts in PV manufacturing.

The topic of larger wafers is reprised in an extensive paper from Fraunhofer ISE that discusses the latest advances in PERC-based shingled solar cells and modules, with cell-to-module (CTM) losses needing to be reduced. Shingling is already being implemented at the gigawatt-scale by multiple companies and this trend is expected to accelerate considerably.

Also of note in this edition is a paper from ISFH that details the processes and the key importance of accurate solar cell measurement, especially, as noted in the last edition, in light of the swathe of solar cell conversion efficiency records already seen in 2019.

Another hot topic and one that is gaining in popularity as the post PERC technology of choice is silicon heterojunction (SHJ) technology. 2019 will be noted for the number of companies, many being new entrants, that are adopting turnkey solutions to produce, in volume, SHJ cells and modules.

One of the first to transition to SHJ technology was the Russia-based Hevel Group. A paper from Hevel in this edition is notable for detailing all the processing steps required for successful SHJ production.

Finally, we would like to thank all our contributors for their efforts and commitment in making this edition possible and, as ever, we look forward to our readers' response.

Mark Osborne

Senior News Editor and Technical Publishing Director
Solar Media Ltd

Editorial Advisory Board

Photovoltaics International's primary focus is on assessing existing and new technologies for "real-world" supply chain solutions. The aim is to help engineers, managers and investors to understand the potential of equipment, materials, processes and services that can help the PV industry achieve grid parity. The Photovoltaics International advisory board has been selected to help guide the editorial direction of the technical journal so that it remains relevant to manufacturers and utility-grade installers of photovoltaic technology. The advisory board is made up of leading personnel currently working first-hand in the PV industry.

Our editorial advisory board is made up of senior engineers from PV manufacturers worldwide. Meet some of our board members below:



Prof Armin Aberle, CEO, Solar Energy Research Institute of Singapore (SERIS), National University of Singapore (NUS)

Prof Aberle's research focus is on photovoltaic materials, devices and modules. In the 1990s he established the Silicon Photovoltaics Department at the Institute for Solar Energy Research (ISFH) in Hamelin, Germany. He then worked for 10 years in Sydney, Australia as a professor of photovoltaics at the University of New South Wales (UNSW). In 2008 he joined NUS to establish SERIS (as Deputy CEO), with particular responsibility for the creation of a Silicon PV Department.



Dr. Markus Fischer, Director R&D Processes, Hanwha Q Cells

Dr. Fischer has more than 15 years' experience in the semiconductor and crystalline silicon photovoltaic industry. He joined Q Cells in 2007 after working in different engineering and management positions with Siemens, Infineon, Philips, and NXP. As Director R&D Processes he is responsible for the process and production equipment development of current and future c-Si solar cell concepts. Dr. Fischer received his Ph.D. in Electrical Engineering in 1997 from the University of Stuttgart. Since 2010 he has been a co-chairman of the SEMI International Technology Roadmap for Photovoltaic.



Dr. Thorsten Dullweber, R&D Group Leader at the Institute for Solar Energy Research Hamelin (ISFH)

Dr. Dullweber's research focuses on high efficiency industrial-type PERC silicon solar cells and ultra-fine line screen-printed Ag front contacts. His group has contributed many journal and conference publications as well as industry-wide recognized research results. Before joining ISFH in 2009, Dr. Dullweber worked for nine years in the microelectronics industry at Siemens AG and later Infineon Technologies AG. He received his Ph. D. in 2002 for research on Cu(In,Ga)Se₂ thin-film solar cells.



Dr. Wei Shan, Chief Scientist, JA Solar

Dr. Wei Shan has been with JA Solar since 2008 and is currently the Chief Scientist and head of R&D. With more than 30 years' experience in R&D in a wider variety of semiconductor material systems and devices, he has published over 150 peer-reviewed journal articles and prestigious conference papers, as well as six book chapters.



Chen Rulong, Chief Technology Officer, Solar Cell R&D Department, Wuxi Suntech

Chen Rulong graduated from Changchun Institute of Optics and Fine Mechanics, majoring in applied optics. He began working in the field of R&D on solar cells from 2001. He is a visiting fellow at the University of New South Wales in Australia and an expert on the IEC Technical Committee 82, which prepares international standards on PV energy systems.



Florian Clement, Head of Group, MWT solar cells/printing technology, Fraunhofer ISE

Dr. Clement received his Ph.D in 2009 from the University of Freiburg. He studied physics at the Ludwigs-Maximilian-University of Munich and the University of Freiburg and obtained his diploma degree in 2005. His research is focused on the development, analysis and characterization of highly efficient, industrially feasible MWT solar cells with rear side passivation, so called HIP-MWT devices, and on new printing technologies for silicon solar cell processing.



Sam Hong, Chief Executive, Neo Solar Power

Dr. Hong has more than 30 years' experience in solar photovoltaic energy. He has served as the Research Division Director of Photovoltaic Solar Energy Division at the Industry Technology Research Institute (ITRI), and Vice President and Plant Director of Sinonar Amorphous Silicon Solar Cell Co., the first amorphous silicon manufacturer in Taiwan. Dr. Hong has published three books and 38 journal and international conference papers, and is a holder of seven patents. In 2011 he took office as Chairman of Taiwan Photovoltaic Industry Association.



Matt Campbell, Senior Director, Power Plant Products, SunPower

Matt Campbell has held a variety of business development and product management roles since joining the SunPower, including the development of the 1.5MW AC Oasis power plant platform, organized SunPower's power plant LCOE reduction programmes, and the acquisition of three power plant technology companies. Campbell helped form a joint venture in Inner Mongolia, China for power plant project development and manufacturing. He holds an MBA from the University of California at Berkeley and a BBA in Marketing, Finance, and Real Estate from the University of Wisconsin at Madison.



Ru Zhong Hou, Director of Product Center, ReneSola

Ru Zhong Hou joined ReneSola as R&D Senior Manager in 2010 before being appointed Director of R&D in 2012. Before joining ReneSola he was a researcher for Microvast Power Systems, a battery manufacturer. His work has been published in numerous scientific journals. He has a Ph.D. from the Institute of Materials Physics & Microstructures, Zhejiang University, China.



MEYER BURGER



Heterojunction: Superior cell efficiency

Discover Meyer Burger's outstanding Heterojunction manufacturing technology. HeliA bifacial heterojunction manufacturing platform delivers solar cell efficiencies of over 24% with best LCOE. Based on Meyer Burger's industry-leading modular cell coating platform, the HeliA system ensures excellent cell passivation and uniformity.

The powerful combination of Heterojunction and SmartWire Connection Technology ensures maximized energy yield and longest module lifetime.

Meyer Burger lifts you to new energy levels.
www.meyerburger.com





Contents

Section 1: Fab & Facilities

- 8** Competitiveness of a European PV manufacturing chain
Jochen Rentsch¹, Sebastian Nold¹, Lorenz Friedrich¹, Ralf Preu¹, Andreas Bett¹, Wolfgang Jooss², Jutta Trube³ & Peter Fath^{2,3}
¹Fraunhofer Institute for Solar Energy Systems (ISE), Freiburg, Germany; ²RCT Solutions GmbH, Konstanz, Germany; ³VDMA Photovoltaik Produktionsmittel, Frankfurt am Main, Germany
- 16** Future of PV production: Impact of digitalization and self-learning concepts on wafer, solar cell and module production
Swaytha Sasidharan¹, Florian Herzog¹, Johnson Wong² & Rudolf Harney¹
¹International Solar Energy Research Center Konstanz e.V. (ISC Konstanz), Germany; ²Aurora Solar Technologies, North Vancouver, Canada

Section 2: Materials

- 28** Why are monocrystalline wafers increasing in size?
Mark Osborne, Senior News Editor, Photovoltaics International

Section 3: Cell Processing

- 34** The monoPoly technology platform: Rapid implementation of passivating contacts in PERC/T production lines
Shubham Duttgupta, Naomi Nandakumar, John Rodriguez & Vinodh Shanmugam, Solar Energy Research Institute of Singapore (SERIS), National University of Singapore (NUS)

- 44** Precise and accurate solar cell measurements at ISFH CalTeC
Karsten Bothe & David Hinken, Institute for Solar Research Hamelin (ISFH), Emmerthal, Germany

Section 4: Thin Film

- 52** Heterojunction technology: The path to high efficiency in mass production
Igor Shakhray, Alexey Abramov, Sergey Abolmasov, Ekaterina Terukova & Dmitriy Andronikov, Hevel Group, Moscow, Russia

Section 5: PV Modules

- 63** PERC-based shingled solar cells and modules at Fraunhofer ISE
Puzant Baliozian, Nils Klasen, Nico Wöhrle, Christoph Kutter, Hannah Stolzenburg, Anna Münzer, Pierre Saint-Cast, Max Mittag, Elmar Lohmüller, Tobias Fellmeth, Mohammad Al-Akash, Achim Kraft, Martin Heinrich, Armin Richter, Andreas Fell, Alma Spribille, Holger Neuhaus & Ralf Preu, Fraunhofer Institute for Solar Energy Systems ISE, Freiburg, Germany

Section 6: Market Watch

- 80** R&D spending analysis of 21 key PV manufacturers in 2018
Mark Osborne, Senior News Editor, Photovoltaics International
- 85** Subscription / Advertisers Index
- 86** The new PV ModuleTech Bankability Ratings list
 The PV-Tech blog

Empowering Solar

with Qentys™ encapsulant film and PP based compounds for producing backsheets

ENCAPSULANT FILM

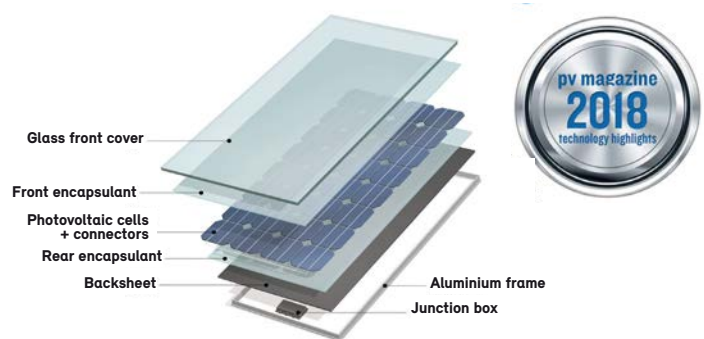
Qentys™ encapsulant film enabling module makers to significantly reduce module lamination cycle time while providing superior reliability.

Two versions are available:

- Qentys™ BPO 8828F – Transparent
- Qentys™ BPO 8828WH – White

Awarded by PV magazine:

Top 20 innovation highlights in 2018



BACKSHEET

Polypropylene (PP) based advanced compounds specially designed for production of backsheet layers, providing clear advantages over PET backsheets. Borealis makes these PP compounds available to the market by partnering with selected backsheet producers.

- Qentys™ SF700CL – core layer
- Qentys™ SF900WL – outer layer



Competitiveness of a European PV manufacturing chain

Jochen Rentsch¹, Sebastian Nold¹, Lorenz Friedrich¹, Ralf Preu¹, Andreas Bett¹, Wolfgang Jooss², Jutta Trube³ & Peter Fath^{2,3}
¹Fraunhofer Institute for Solar Energy Systems (ISE), Freiburg, Germany; ²RCT Solutions GmbH, Konstanz, Germany; ³VDMA Photovoltaik Produktionsmittel, Frankfurt am Main, Germany

Abstract

Today, solar power is one of the cheapest ways of providing energy internationally, partly because of the excellent R&D work in Europe. Prices of modules have fallen by half in the past three years, and at the same time the use of solar power has been steadily increasing. The reason why there has been an increase in the use of solar energy in Europe and Germany is the achievement of the climate targets of the Paris Agreement. While the machines for the production of solar modules are still manufactured in Germany, the production of cells has now almost completely migrated to Asia. Therefore, the VDMA commissioned a study from Fraunhofer ISE to evaluate whether the production of solar modules at competitive costs could again be realized in Europe. This paper presents the results of the VDMA study.

(see Fig. 1). Extracted values for Europe foresee a total installation base of around 1.5TWp in 2030 reaching up to 10TWp in 2050; this translates to annual installations of close to 200GWp by around 2030 and up to 500GWp in 2050.

More conservative short-term market growth expectations, such as those by Solar Power Europe [1] or Wood Mackenzie [6], usually estimate lower growth figures, as they typically only concentrate on the power sector. Nevertheless, SolarPower Europe experts also envisage a strong growth of the European PV Market already in the short term.

Introduction

Europe used to be the third-largest region for new installations, while maintaining its second-place ranking for total operating capacity [1] (see also Coleville [2], pp. 5, 12, 14). The region continues to represent a shrinking portion of cumulative global capacity as emerging economies with rapidly growing electricity demand deploy more and more solar PV [3] (see also Colville [2]). In 2018, however, demand increased significantly within the EU and beyond.

The EU added around 8,3GW of grid-connected solar PV in 2018, up 36% over the previous year's additions, bringing total capacity to 115GW. Compared with 2017, 22 of the 28 EU countries recorded more installations, driven by national binding targets for 2020, which many member states have yet to meet [1] (see also Colville [2], pp. 12, 79).

Almost all energy system scenarios show that PV technology will be the main pillar of the future energy supply. The full transition to 100% renewable energy across all sectors – power, heat, transport and desalination – can be seen as an upper boundary of possible future growth in Europe, as determined within a study from Energy Watch Group conducted at Lappeenranta University of Technology, Finland [4], and also published within the International Technology Roadmap for Photovoltaics (ITRPV) in 2019 [5]

Technology selections for the benchmark analysis of an EU PV manufacturing chain

The technology selections for this study have been primarily taken from the latest edition of the ITRPV roadmap 2018 in order to stay aligned as closely as possible with current technology and market trends [5]. Improvements in ingot, wafer and cell technologies, as well as in module design, will help raise the power rating bar of a crystalline solar module above the 400W level for a panel with 72 cells (or 144 half cells) within the next few years. Separated in respect of the different value chain steps, the technology routes below were chosen, resulting in the specific technology parameters in Table 1.

Ingot and wafer

Depending on the source, monocrystalline silicon was said to have reached parity with, or to have already taken over the leadership position from, multicrystalline silicon in 2018. In any case, the balance will swing further towards mono in the future, as all silicon ingot crystallization capacity expansions are focusing on the mono variant, which has fewer defects than multi, enabling the realization of higher cell efficiencies. The selected technology is based on CZ pulling including re-charging (total charge weight of approximately 300kg), where three ingots per crucible are grown. Wafering is performed by diamond wire sawing, since it is the current industry standard. A wafer thickness of 170µm is adopted, with a kerf loss of 80µm.

“The full transition to 100% renewable energy across all sectors can be seen as an upper boundary of possible future growth in Europe.”



EU PVSEC 2019

**36th European
Photovoltaic Solar Energy
Conference and Exhibition**

The Innovation Platform for the global PV Solar Sector



09 - 13 September 2019

**Marseille Chanot
Convention and Exhibition Centre**

Marseille, France



www.photovoltaic-conference.com • www.photovoltaic-exhibition.com

Cell

As passivated emitter rear contact (PERC) solar cell technology brings efficiency improvements of 1–1.5% points with little extra cost for additional production equipment, the bulk of crystalline silicon cell equipment investment these days is mostly for PERC tools. A cell design without a selective emitter is chosen for the specific technology selection, a layer stack of aluminium oxide and SiN_x is used for back-side passivation, and a five-busbar contact design based on screen printing (prepared for half-cut) is employed for metallization. There is a regeneration step at the end of the process chain, and the halving of the cells takes place after the cell measurement (this step can also occur at the beginning of module production).

Module

With today’s new high-efficiency cell generations all being ‘naturally’ bifacial, and issues with standardization or bankability mostly solved, the technology is rapidly gaining market share. Additionally, with the use of half cells the resistance losses can be reduced, providing a power boost of about 5 to 6W at the module level. The specific technology selection for the module technology in this study thus includes a bifacial module based on 144 half cells, with glass on the front and a transparent backsheets on the back. For interconnection, the half cells are classically soldered using cell connectors; a cell-to-module power loss of about 1.8% is assumed. For better stability, the modules are also equipped with an aluminium frame.

Methodology for the cost of ownership (COO) analysis

The following approaches are combined and applied in an integrated way for the economic analysis of the internal operating processes of a factory for the production of PV modules:

- A bottom-up approach for production modelling.
- A top-down approach for the modelling of other business areas (administration, sales, purchasing, personnel, etc.) as well as for the modelling of economies of scale.

The bottom-up approach for modelling production is based on the SCost calculation tool developed at the Fraunhofer Institute for Solar Energy Systems (ISE) [7]. With this tool it is possible to map the PV value chain of a vertically integrated PV factory, from polysilicon to the assembled PV system. SCost is based on the guidelines for the COO methodology of the Eo35 standard [8] of the international industry association of leading semiconductor manufacturers (Semiconductor Equipment and Materials International – SEMI).

In addition, technology-independent overhead

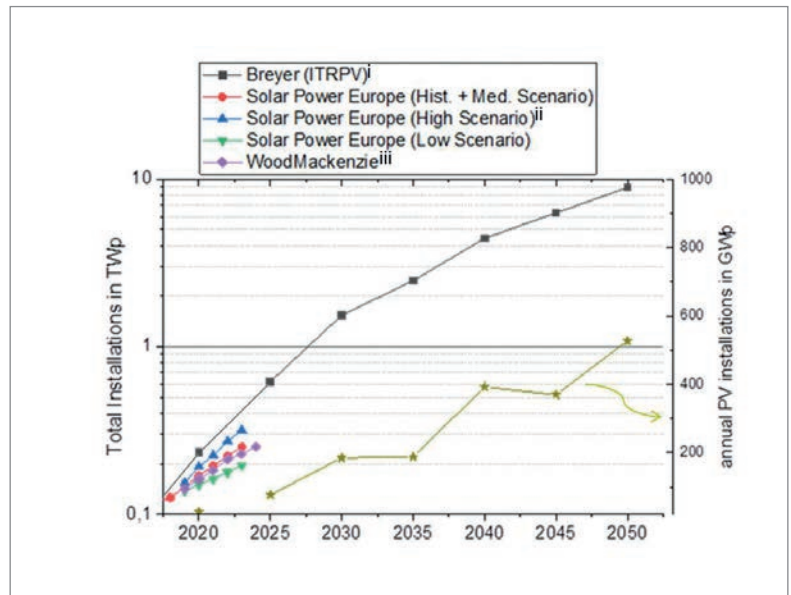


Figure 1. Expected market growth scenarios within the European Union for total as well as average annual installations in Europe. (Data taken from Ram et al. [4], SolarPower Europe [1] and Wood Mackenzie [6].)

	EU	CN
Ingot and wafer		
Type and base doping	Cz-Si, p-type	
Wafer thickness	170µm	
Kerf loss	80µm	
Wafer size	156.75mm × 156.75mm	
Silicon usage	16.2g/wafer	
Cell		
V _{oc}	685mV	680mV
j _{sc}	40.0mA/cm ²	39.8mA/cm ²
FF	81.4%	80.8%
Eta	22.3%	21.8%
Module		
No. of cells	144 half-cut	
Type	glass-backsheet (3.2mm glass)	
Module power	388W	
CTM power loss	1.8%	

Table 1. Performance parameters of selected technologies for this benchmark study.

costs as well as capital costs are incurred for the operation of a PV factory.

Technology-independent overheads

These costs comprise selling expenses, general and administrative expenses and research and development (R&D) expenses. In wafer, cell and module production, unit-related overhead costs of 3.5, 6.0 and 450€ct/piece respectively are assumed, which corresponds to an average PV module overhead cost share of 10.6% for the PV module technology. The latter figure is thus close to the average PV module overhead share of 10.5% for the world’s seven largest c-Si PV producers.

Capital cost

To calculate the cost of capital, an average cost of a capital rate of 5.0% is applied (pre-tax). This is calculated on the basis of the weighted average cost of capital (WACC) approach with the following assumptions. The equity ratio of the business units is assumed to be 20%, and hence the debt ratio is 80%. The return on equity is 10%, and the cost of debt 5%. The corporate tax rate used for Europe as well as for China is 25% [9]. The all-in costs determined in Fraunhofer ISE's study already include the (low) margins on equity capital gains of 10% and debt capital of 5%; the calculated all-in costs can therefore also be regarded as a calculated 'price' for the particular product.

Additional assumptions

- **Capacity:** for the calculation of the different scenarios within this study, a production capacity of ~1,000MWp/a is determined for PV module, solar cell and Si ingot/wafer production. It is assumed that the production sites for all three value-added units are located in the same place and that no additional transaction and transport costs are incurred between the value-added stages.
- **Utilization:** for the operational utilization of production, it is assumed that the bottleneck processes of the process chains, and thus also of the entire production, are fully utilized. PV products are usually manufactured around the clock, i.e. 24 hours a day, 7 days a week (24/7 production). Actual production facilities can achieve total capacity utilization rates of 95–100% [2]. In the scenarios examined here, 24/7 production is also assumed, with 5 days a year being set aside (e.g. for public holidays), so that 360 of 365 days or 8,640 hours per annum are devoted to production. With an operational utilization of production of 99–100%, this corresponds to a total utilization rate of around 96–97%.
- **Working time and shifts:** to cover the full operating time period of 8,640 h/a, it is assumed that, for all value-added stages, an average of 5.0 employees are required for each position in production in a shift-work operational schedule.

- **Depreciation period and additional capital expenditure (CAPEX):** a lifetime (or depreciation period) of 7 years is assumed for production equipment, 10 years for the facility area, and 20 years for buildings. In the context of the procurement of production equipment, additional expenses of 10% are assumed.

- **Area requirements:** the space required for each individual piece of equipment forms the basis for calculating the total space requirement for the production area. In addition to this, and all the other necessary equipment in the line (e.g. buffers), additional traffic areas are added according to length and width. As well as the production area, the amount of space taken up by additional building units for infrastructure equipment, logistics, support and offices is required in calculating the total area of the PV factory.

Definition of production scenarios

In order to compare the costs of a Chinese and a European PV production, different manufacturing scenarios are compared within the scope of the study (Table 2). A Chinese GW production with the detailed technology selection and process flows in Table 1 is the assumed benchmark. The Chinese reference scenario is based on a factory located in China with a complete local value chain (equipment, facilities, supply chain).

The Chinese scenario is contrasted with a counterpart factory fully localized in Europe with a complete value chain from Europe; analogously to the purely Chinese scenario, the economic advantages of individual regions (e.g. low electricity costs from hydropower in Scandinavia for particularly power-intensive value-added stages) are also taken into account here.

Unfortunately, a purely European scenario for a complete PV value chain from ingot to module is currently a somewhat hypothetical scenario. A third scenario is therefore considered, one in which the production site and buildings and equipment still originate in Europe, but large portions of the supply chain are imported from abroad. Possible transport costs for consumables are therefore taken into

Scenario	Manufacturing Location		Equipment		Supply Chain	
	EU	CN ¹	EU	CN	EU	CN / RoW
EU	✓		✓		✓	
EU / CN	✓		✓			✓
EU recover	✓		✓		✓ ²	
CN		✓		✓		✓

¹Within China, the PV value chain is also distributed across the country, with ingot/wafer manufacturing in the north (mainly Inner Mongolia because of cheap electricity) and cell and module production in the eastern parts of the country.

² Assuming a recovered EU supply chain which could result in similar prices for an EU supply chain.

Table 2. Assumed scenarios within this study.

account. This represents the most realistic scenario for many of today’s module manufacturers.

A fourth, currently also hypothetical, scenario is the ‘EU recover’ scenario. Here, production is assumed to take place in Europe, whereby the entire necessary supply chain (equipment, materials, etc.) is in turn sourced from Europe at the same cost as that achievable by a Chinese manufacturer in China. This scenario therefore assumes that the supply chain will increasingly resettle in Europe because of a future European market that is predicted to be steadily growing and the resettlement of GW scalable PV production capacity in Europe. Overseas transport costs could thus be avoided as far as possible.

For the cost comparison, additional different basic assumptions are made for a factory located in Europe or China. These assumptions are based on the assessments of the authors of this study and will be briefly explained below.

Equipment price

Within the scope of the study, it was possible to research a price difference of about 20% on average between Chinese and European plant manufacturers. This concerns in particular the price comparison for offers of equipment for the construction of a factory in China. If a factory is to be built in Europe, the relative differences between European and Chinese suppliers can be even smaller in some cases, since in this situation Chinese suppliers also have to include additional costs for export as well as for support in setting up the factory locally.

Building and facility

The cost difference for buildings and facilities between a Chinese and a European location can be very high. As the Fraunhofer ISE study initially assumes new greenfield sites, a difference of 50% in costs was assumed. This significant difference essentially has an impact on the initial CAPEX demand, but because of the typically long depreciation periods of 10 to 20 years, the difference is relatively small when considering the current production costs. In addition, it should be noted that, of course, existing locations that were only abandoned in recent years could be considered for the new construction of a production facility in Europe, and would therefore mean a significant reduction in the CAPEX initially required for buildings and infrastructure.

Equipment uptime, production yield and (cell) efficiency

The differences made in these aspects in the study are certainly the most debatable. The claim that derives from a better factory and technology performance in Europe is based on the existing close collaboration between industry (manufacturing companies as well as plant

“A purely European scenario for a complete PV value chain from ingot to module is currently a somewhat hypothetical scenario.”

construction) with highly innovative and high-performance R&D institutions in Europe. In such close collaborations, it must be possible to produce high-quality products in a highly automated production environment, including industry 4.0 concepts (machine learning, artificial intelligence, autonomous process control and logistics, etc.).

COO comparison of different scenarios

Fig. 2 shows the all-in module cost comparison for the scenarios of a PV value chain of size 1GWp that is entirely located in Europe or entirely located in China. The graph shows the split across the various stages of the value chain and the additional costs (SG&A, capital costs). In all scenarios, polysilicon is regarded as a (purchased) input material component and is therefore constant (as in all the following presentations). Fraunhofer ISE’s analysis is based on a module intended for the European market, i.e. for production in Asia, the necessary transport costs between Asia and Europe (usually sea freight) and the respective domestic transport routes to the seaports must be taken into account. A corresponding calculation of the costs to be considered shows an increasing share of transport costs in the total production costs: whereas in 2014 the share of transport costs was still about 4%, in 2019 it has already risen to about 9%.

In Fraunhofer ISE’s modelling, the consideration of the transport costs for a module from Chinese production leads to an increase of about 1.2€ct/Wp in the price of the same module on the European market. So far, the European scenario has been based on the material costs determined

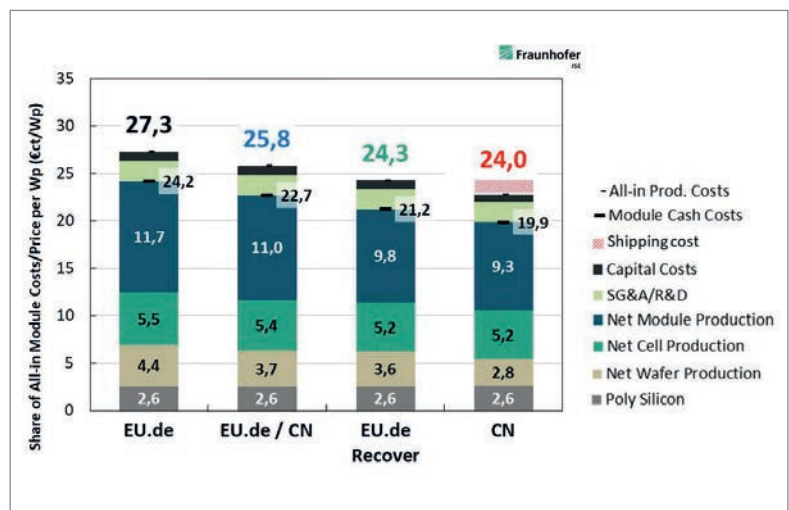


Figure 2. Overview of all-in module costs in all scenarios calculated within this study, including the ‘EU recover’ scenario for a manufacturing site in Germany. In the latter scenario, the sourcing of materials can be executed from a ‘recovered’ supply chain in Europe at a comparable cost to that in China.

“Scaling production capacity brings significant competitive advantages.”

from research, in particular of the smaller module manufacturers in Europe still in existence. A scenario that is also currently fairly realistic is therefore the inclusion of Asian, in particular Chinese, material manufacturers who can supply a potential European GW-scale manufacturer. In this scenario, transport costs will therefore continue to be incurred for the procurement of materials, especially for module glass, as one major component. As a result, however, a further reduction in manufacturing costs for European production of 1.5€/Wp can be determined (scenario EU.de / CN).

Within the currently still hypothetical ‘EU recover’ scenario (see Table 2), it is assumed that as a result of the several GW-scalable PV factories in Europe, material production, and thus essential parts of the supply chain, will also return to Europe. If there is sufficient demand and sales volume, European manufacturers (e.g. of PV module glass or Al frames) can also offer manufacturing costs and prices in the supply chain similar to those of their Chinese competitors, thus eliminating the need for additional transport surcharges. A further reduction of all-in costs for a manufacturer of PV modules in Europe by 1.5€/Wp (in particular by eliminating transport costs for the procurement of module materials) can thus lead to a real cost leverage for PV modules manufactured in Europe.

Scaling matters – economy of scale effects within the PV value chain

Economies of scale effects occur with increasing output (with a given production technology) and are reflected in a reduction in unit costs. The economies of scale to be considered within this study are examined in the following three steps:

1. Because of the principle of the smallest common multiple for successive process steps with different optimal capacities, a more balanced capacity adjustment of the process steps results. This leads to a reduction in standby times, and thus to an increase in equipment utilization and an overall decrease in the volume-specific number of machines.
2. The increased demand for consumables and the upscaling of production capacities make it easier for the purchasing department to call up more favourable prices from the respective manufacturers. Consumables account for by far the largest share of operational costs (Fig. 3).
3. Additional economies of scale include the increasing dilution of administrative, sales, marketing and R&D expenses as production capacity increases, and a tendency towards lower interest rates with higher corporate value.

All effects together result in the dependence of production costs on production capacity shown in Fig. 4. On the basis of Fraunhofer ISE’s benchmark scenario of a purely European 1GW production with full supply chain coverage from Europe (in this case the calculation has been made for a production location in Germany), it can be seen that, compared with Chinese competitors with production sizes in the range 7 to 10GW, similar costs/prices to those in China for comparable products should be achieved. Such a scenario, however, presupposes in particular that the essential consumables are available on the European market in large quantities at competitive prices.

Overall, the results show that scaling production capacity – as can be observed in many PV companies – brings significant competitive advantages. With a simultaneous overcapacity of global PV production, as has prevailed in recent years, and the associated price pressure on producers, it is clear that company size is a decisive competitive factor and that large PV producers can benefit from several economies of scale. Vertical integration along the PV value chain at one location is key to reducing the production costs associated with PV modules, as profit margins and logistics costs within the value chain are eliminated.

Conclusion and recommendations

After years of stagnation, the European PV market recorded significant growth again in 2018, which, according to various market research companies, will continue in the near future. The market potential for the further expansion of PV can still be estimated to be very high; the sector coupling (electricity, heat, transport) offers significant development potential for the European domestic market, with annual expansion rates of 200GWp from 2025 required in order to achieve the CO₂-reduction targets. Such a market perspective or market potential will also

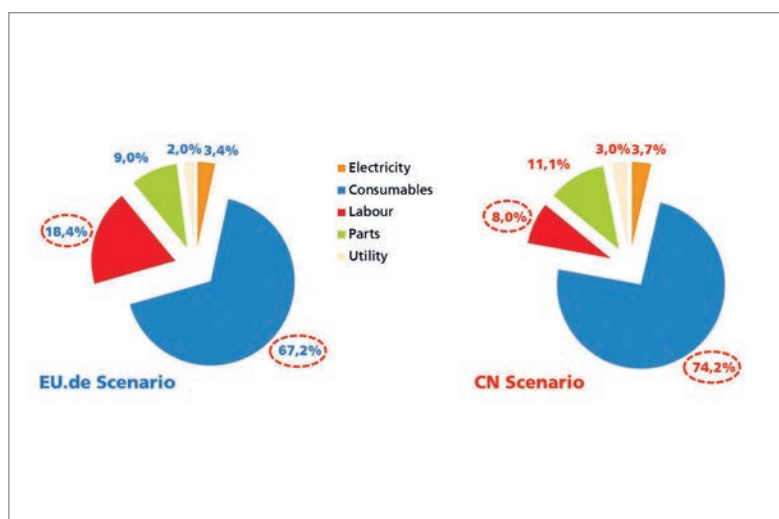


Figure 3. Operational expenditure (OPEX) cost split. Consumables by far represent the largest cost share, with the main contributors being from module production: glass, Al frames, backsheet, EVA, ribbons, junction box.

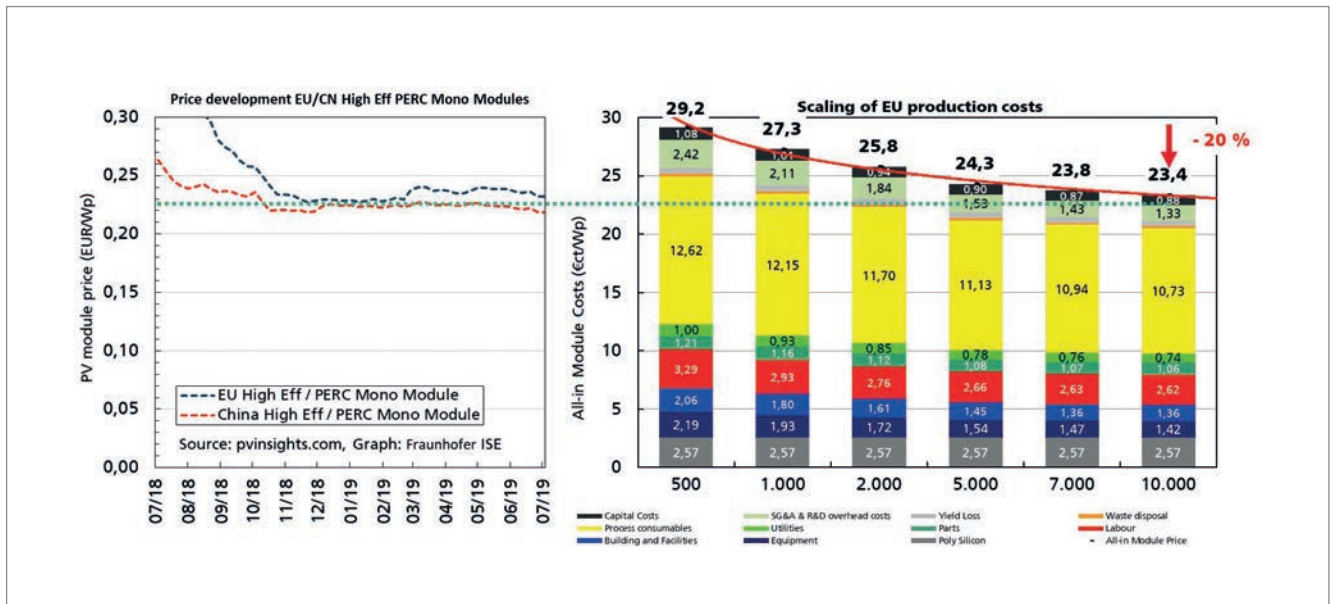


Figure 4. SCost model result for the all-module cost of the EU.de scenario (in relation to the price trend for high-efficiency PERC modules from pvinsights.com), taking into account all relevant economy of scale effects for targeted production sizes between 500 and 10,000MWp.

facilitate the necessary investments in Europe in order to regain lost ground in the PV production capacity sector across the entire value chain compared with Asian competitors.

Politicians can support the market recovery and market expansion within Europe by reducing additional market caps, by maintaining the feed-in priority of PV-generated electricity, by making greater efforts to expand the grid infrastructure and by developing decentralized distribution concepts for electricity integration.

For ‘Made in Europe’ products, additional voluntary environmental standards could also apply; for example, labels for products manufactured in a particularly sustainable manner can have a positive impact on purchasing behaviour.

In addition to these aspects influencing or promoting the market, this study compared the manufacturing costs of a PV value-added chain localized in Europe (ingot to module production) with production in China using a iGWp model factory. It was shown that a module manufactured in Europe for the European market can be produced at a competitive cost when certain conditions are met:

- The necessary transport costs for finished modules or materials from China to Europe are taken into account.
- European production achieves the necessary economy of scale, i.e. a factory size with a production capacity of the order of more than 5GWp per year.
- Ideally, as a result of the high market potential within the EU and the resettlement of several production sites on a GW scale, the supply chain for the manufacture of ingots, wafers, cells and modules returns to Europe, and essential

“A module manufactured in Europe for the European market can be produced at a competitive cost when certain conditions are met.”

materials can therefore be sourced locally at competitive prices.

A high degree of innovation undoubtedly exists within the European industry, in particular with equipment manufacturers in cooperation with worldwide leading R&D institutes in the field of PV located in Europe. In consequence, it must surely be the claim of European production to always maintain a certain advantage over Asian competitors, not only in terms of time but also in terms of performance (cell efficiency, module performance, uptime, yield, etc.), and to secure this sustainably through a clever intellectual property (IP) strategy.

References

[1] SolarPower Europe, “Global market outlook for solar power, 2019–2023”.

[2] Colville, F. 2015, “3GW annual cell production: The new benchmark for solar cell manufacturing”, PV-Tech [http://www.pv-tech.org/editors_blog/3gw_annual_cell_production_the_new_benchmark_for_solar_cell_manufacturing].

[3] IEA PVPS 2019, “Snapshot of global PV markets”.

[4] Ram, M. et al. 2017, “Global energy system based on 100% renewable energy – Power sector”, Technical Report, Lappeenranta University of Technology, Lappeenranta, Finland.

[5] ITRPV 2019, “International technology roadmap for photovoltaic (ITRPV): 2018 results”, 10th edn (Mar.) [https://itrpvdm.org/en/].

[6] Wood Mackenzie 2019, “Europe solar PV outlook 2019”.

[7] Nold, S. et al. 2012, "Cost modeling of silicon solar cell production innovation along the PV value chain", *Proc. 27th EU PVSEC*, Frankfurt, Germany, pp. 1084–1090

[8] Semiconductor Equipment and Materials International (SEMI) 2012, "E35-0312: Guide to calculate Cost of Ownership (COO) metrics for semiconductor manufacturing equipment" [www.semi.org].

[9] KPMG 2017 (Apr.), "Corporate tax rates table | KPMG | GLOBAL", [https://home.kpmg.com/xx/en/home/services/tax/tax-tools-and-resources/tax-rates-online/corporate-tax-rates-table.html].

About the Authors



Dr. Jochen Rentsch is head of the Production Technology – Surfaces and Interfaces department at Fraunhofer ISE. He studied physics at the Technical University of Braunschweig and obtained his diploma degree in 2002. In 2005 he received his Ph.D. in physics from the Albert Ludwigs University of Freiburg, Germany. His current work focuses on the acquisition and management of public- and industry-funded projects, and the transfer of processes and cell structures in the PV industry. He is also involved in consultancy and auditing work with PV manufacturing facilities worldwide.



Dr. Sebastian Nold studied industrial engineering at the University of Karlsruhe, Germany, and at the University of Dunedin, New Zealand, earning his diploma in industrial engineering at Karlsruhe in 2009. In 2018 he completed his doctoral thesis at Fraunhofer ISE on the economic assessment of silicon solar cell production technologies along the PV value chain. He has worked at Fraunhofer ISE since 2008 in the areas of cost calculation, technology assessment and economic evaluation of new concepts in the production of silicon solar wafers, cells and modules.



Dr. Ralf Preu received his diploma degree in physics in 1996 from the University of Freiburg, Germany, and his Ph.D. in electrical engineering in 2000. He also has a diploma degree in economics, awarded by the University of Hagen, Germany, in 2003. He joined Fraunhofer ISE in 1993 and is currently one of the directors of the PV division focusing on production technology and quality assurance.



Dr. Andreas W. Bett is director of Fraunhofer ISE. He received a diploma degree in physics and the state examination in physics and mathematics from the University of Freiburg, Germany, in 1988 and 1989

respectively, followed by his Ph.D. in physics from the University of Konstanz, Germany, in 1992. His main areas of research include solar silicon material, epitaxial growth of Si and III-V semiconductors, development of characterisation techniques for advanced solar cell devices, and the fabrication of solar cells.



Dr. Wolfgang Jooss received his Ph.D. from the University of Konstanz in 2002 for his work on multicrystalline and back-contact, buried-contact solar cells. Between 2002 and 2009 he worked for sunways AG as head of solar cells R&D, after which he joined centrotherm photovoltaics AG, where he held positions of director of integrated factories technology and director of PV technology. Since April 2016 he has been director of R&D at RCT Solutions GmbH in Konstanz, Germany.



Dr. Jutta Trube has been director of the VDMA Photovoltaic Equipment sector group since December 2015, where she focuses particularly on production equipment for solar cell and module production. She is also responsible for the publication of the ITRPV and its yearly updates. Prior to her current position at VDMA, she was R&D director and director of new technologies in vacuum equipment manufacturing. She studied physics at the University of Göttingen, Germany, and was awarded her doctorate in electrical engineering by the Technical University in Berlin.



Dr. Peter Fath is director of the Solar Equipment Machine Maker Department and a board member of the German VDMA. He received his Ph.D. in semiconductor physics from the University of Konstanz in 1998.

He is founder and director of the independent International Solar Energy Research Center ISC e.V., where he is responsible for relations with industry partners. His work experience includes responsibility for various due diligence and auditing reports in the PV sector, and M&A consultancy work (technology and market) for PV manufacturers, machine makers and material providers.

Enquiries

Dr. Jochen Rentsch
 Fraunhofer Institute for Solar Energy Systems (ISE)
 Heidenhofstrasse 2
 79110 Freiburg
 Germany

Email: jochen.rentsch@ise.fraunhofer.de
 Tel: +49 (0)761 4588-5199

Future of PV production: Impact of digitalization and self-learning concepts on wafer, solar cell and module production

Swaytha Sasidharan¹, Florian Herzog¹, Johnson Wong² & Rudolf Harney¹

¹International Solar Energy Research Center Konstanz e.V. (ISC Konstanz), Germany; ²Aurora Solar Technologies, North Vancouver, Canada

Abstract

Many of today's crystalline silicon (c-Si) PV production plants produce high-efficiency cells and modules on multi-GW scales. As the ratio of highly skilled development staff to production volumes decreases, there is greater demand for automation and production control, which will ultimately yield a higher return of investment in the form of better efficiency distributions, higher yield and improved equipment uptime. There are many feasible incremental improvements as a fab with a minimal degree of process control shifts towards sophisticated automation. An important Industry 4.0 concept is the *digital twin*, the detailed mapping of process and systems to physical and statistical models that will enable high-level optimizations for production and minimize maintenance downtime. Another concept developed at ISC Konstanz is *FlexFab*, which allows different cell types to be produced in one production line, with automatic scheduling according to demand. This paper explains how these modern production concepts are implemented in ISC's lab, and details the plans for their utilization in future production sites, with illustrations of the key benefits in practice. With these modern manufacturing concepts, it will even be possible to bring future c-Si PV production back to the EU with the choice of an appropriate cell concept (high efficiency but proven technology, e.g. interdigitated back-contact (IBC) cells, such as ZEBRA) and a sound business plan.

Introduction

Following the excellent article by Fraunhofer ISE on this topic in edition 42 of *Photovoltaics International* [1], this paper discusses in more technical detail a number of topics relating to modern manufacturing concepts.

Industry 4.0 in PV

The transition to a smart factory is present in the roadmap of all manufacturers, SMEs and machine builders in every domain, not least PV. Most of the PV manufacturing facilities, including those of the top manufacturers, have integrated advanced automation and remote operation functionalities. In the next two years, most fabs will introduce automated fab logistic systems with machine learning, according to the 2019 International Technology Roadmap for Photovoltaic (ITRPV) (Fig. 1).

Although there have been relatively significant technical advances in machine technology and integration of automation technologies,

manufacturers are still not leveraging the value of the data generated in order to provide tangible improvements in production. Revamping and upgrading all the production equipment to support Industry 4.0 features are critical. A brief overview of the adoption of these concepts in several production facilities is presented next.

The Tongwei Solar Unmanned Production Line [2], opened in the last quarter of 2017, is the world's first Industry 4.0 smart-manufacturing high-efficiency cell production line; it comprises a 200MW monocrystalline solar cell production line, expanded in 2018 with 400MW HJT technology [3]. All the process technologies are automated and remotely controlled.

Jinko Solar [4] demonstrated an increase in cell efficiency as a result of the introduction of advanced automation and the inclusion of data analytics in the production life cycle, which facilitates a consolidated data-collection mechanism, enabling yield traceability, improving workflow efficiency and optimizing material transportation.

Silicon Module Super League (SMSL) member GCL System Integrated Technology (GCL-SI) presented the fully automated unmanned module assembly workshop in China to test manufacturing tools and software, with a test phase lasting about two years. Their ambitious targets included a 50% increase in efficiency, a 21% improvement in product quality, a 60% reduction in online manpower and a 30% decrease in processing costs.

SunPower has initiated the move towards lower-cost manufacturing with the introduction of its fab consisting of manufacturing tools with a high degree of automation for both high-efficiency cells and high-efficiency modules.

While a few examples can be observed, the adoption will ultimately depend on the price-performance ratio, as the return on investment (ROI) will be a critical factor for manufacturers.

A survey of manufacturing companies from different domains conducted by Ernst & Young and Bitkom Research shows that around 80% of the companies responded that Industry 4.0 plays

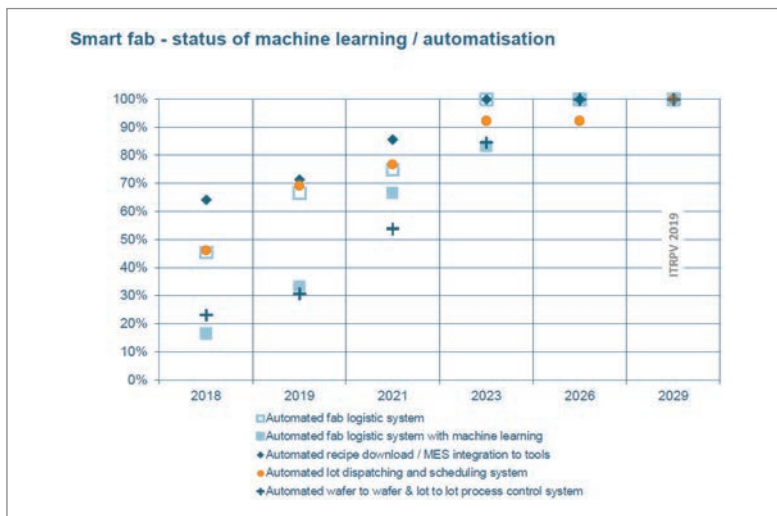


Figure 1. The high growth rate of automation predicted by the ITRPV 2019 [6].

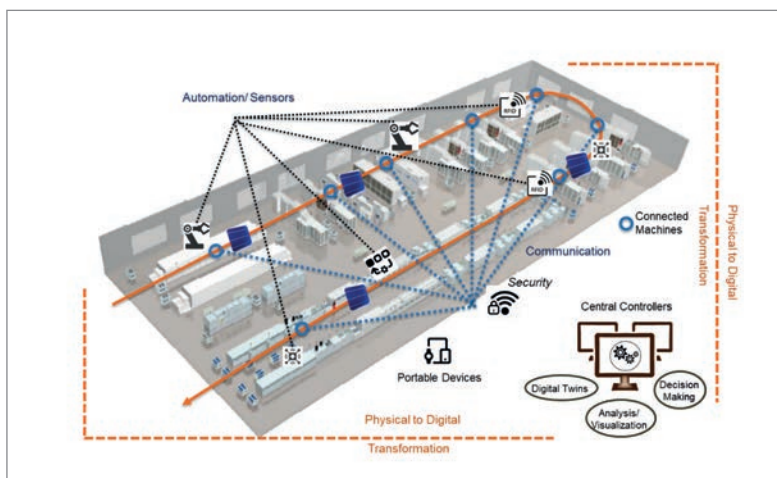


Figure 2. A smart factory visualization.

a part in their roadmaps. While the adoption rate was low, around 22%, most of the companies were in discussions to incorporate the concepts into their infrastructures. The biggest hurdles, according to the respondents, were the demand for investment, the lack of standards and the need for the transformation of the workforce in order to acquire the requisite skills to transition from having expertise in the field to having both software and subject expertise. The Sino-German Industry 4.0 Demonstration and Training programme on intelligent manufacturing and Industry 4.0 highlights the need for the training programmes to secure the transformation of both the manufacturing facility and the workforce. Platforms such as RAMI [5] define the framework of Industry 4.0 as a step towards its standardization.

“PV production is witnessing a shift in perception, moving from conventional manufacturing to smart manufacturing with the integration of functionalities from multiple domains.”

State of digitalization

PV production is witnessing a shift in perception, moving from conventional manufacturing to smart manufacturing with the integration of functionalities from multiple domains, such as the Internet of Things (IoT), data analytics with artificial intelligence, and robotics. This integration is now accepted as *Industry 4.0* [7], a term coined by the German strategic programme in 2011, and is achieved by the seamless incorporation of information technology (IT) and operational technology (OT) [8]. *Operational technology* includes the production-floor machines, automation units, sensors and actuators, and resources, which are now slowly transformed into a digital space. *Information technology* encompasses all software-related aspects, including (but not limited to) manufacturing execution systems (MES), enterprise resource planning (ERP), and supervisory control and data acquisition systems (SCADA).

The digital twin, a core component in a self-learning fab, is seen as one of the most promising technologies around the smart factory and the concept of Industry 4.0, because both in research and in industry it plays the role of bridging the physical and digital worlds. *Digital twins* are virtual representations of the physical assets/machines; they can store and display in real time the exact data, values and actions of their analogue twins, as well as simulating products, machines, etc. that are not yet available. These twins should be available for the entire production line, i.e. from each individual machine, as well as from the product itself. The concept is already being used in various industries – such as the automotive sector (Daimler, Audi, BMW) and the semiconductor sector (Applied Materials, Infineon, Texas Instrument, STMicroelectronics) – to make production more cost-effective and to accelerate the product development. Gartner predicts that by 2021, more than half of the big industries will have functional digital twins, resulting in a 10% improvement in overall effectiveness.

The large set of data coming from the heterogeneous data sources and digital twins, within the connected factory, will be the biggest game changer for the manufacturing sector. It opens up the field for analytical models, simulation and optimizations, with a move towards deriving value from the data, leading to significant improvements in cost and process efficiencies. Although data is generated from the current manufacturing facilities, most of it is not converted to intelligence that could transform the operations to minimize downtime, decrease ramp-up and optimization times, maximize production and reduce costs. A gradual evolution is required in order to incorporate the self-learning features by establishing intercommunication between the connected components to enable

diagnosis and prediction of equipment failures, self-configuration of parameters and adaptation to changing production environmental factors. This will facilitate improved flexibility in production, traceability, optimization and thereby manufacturing productivity.

The factory of the future

The set-up of fully digitalized PV factories requires a high degree of robotic workforce, and the entire production ecosystem is interconnected. The transformation from the physical space to the digital one is represented in Fig. 2; it shows a production floor with PV equipment and the movement of the wafers through the production steps. All parameters and measurements are easily accessible by those who need them, and alerts are sent to operators or to management on multiple devices. There should be a common standard for underlying communication, so that machines from different vendors can be installed hand in hand with automation. Single-wafer tracking is also necessary in such a factory.

Fig. 3 shows the flow of information, from an architectural perspective, with the various building blocks of a connected fab. The first layer represents a production floor with the processing equipment (such as diffusion furnaces and CVDs) and measurement devices (such as IV flashers and inline sheet resistance measurement for diffused emitters). In addition to the machines, the production floor is equipped with various sensor platforms, such as embedded PCs with connected sensors (temperature, humidity, vibration) and actuators, which provide contextual information. Other sources of data include details about maintenance, resources and personnel, all of which contribute to the semantic enrichment of the digital twin.

The second layer represents the digital twin layer. A *digital twin* can be defined as an evolving digital representation of the physical object, which captures both current and historical states and measurements. It is built with the help of real-time cumulative data sources and can provide an overview of the process/product, insights into the performance, etc. Digital twins have standard interfaces to communicate with the production floor to continually update and reflect the real-world states.

The architecture also includes the *self-learning loop*; this refers to the cycle of monitoring events and data from the production floor through the digital twins, analysing the data using models, algorithms and simulations, and providing feedback to the production floor operators and machines. With the digital twin layer, statistical patterns can also be detected and then further interpreted. For example, Fig. 4 shows an often-seen correlation between a midstream measurement tool which reads

the IR reflectance of a wafer after phosphorus diffusion, and end-of-line cell efficiency. Because the IR reflectance is sensitive to the peak dopant concentration, the digitalized PV factory, which maps this relationship and is capable of cell device simulation and diffusion process simulation, will have the ability to build a parameterized model that recommends steps towards optimizing the diffusion process or equipment. The initial phase includes a human expert in the loop who provides recommendations to the operators. Finally, the fab system will offer suggestions for improvements. Visualization and integration of tools such as CAD are also foreseen to be valuable in presenting a real-time view of the machines and the movement of the cell through the various process steps.

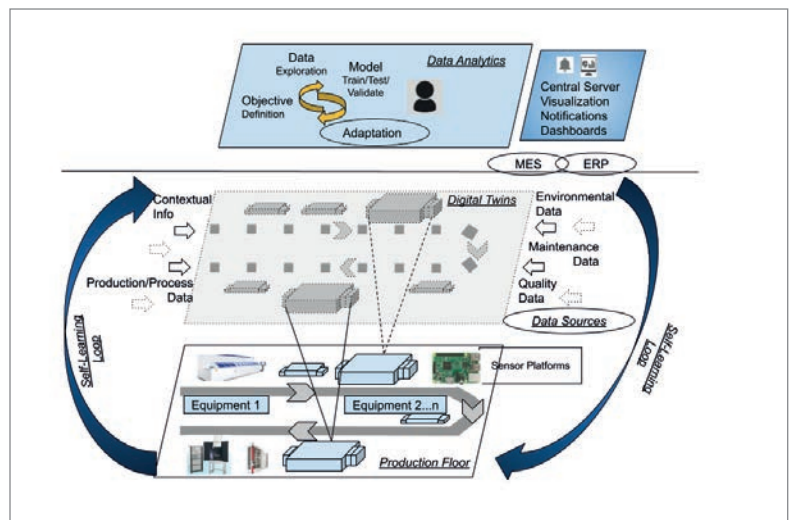


Figure 3. Architectural overview of Industry 4.0.

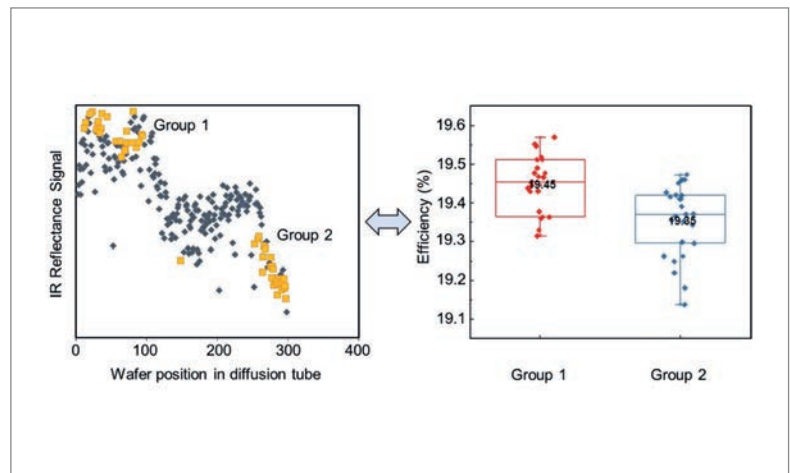


Figure 4. Correlations between the IR reflectance signals on phosphorus-diffused emitters, and the end-of-line cell efficiency.

“The introduction of standard communication technologies and the horizontal integration of information flow from several data sources enables the possibility to analyse and provide improved contextual real-time responses.”

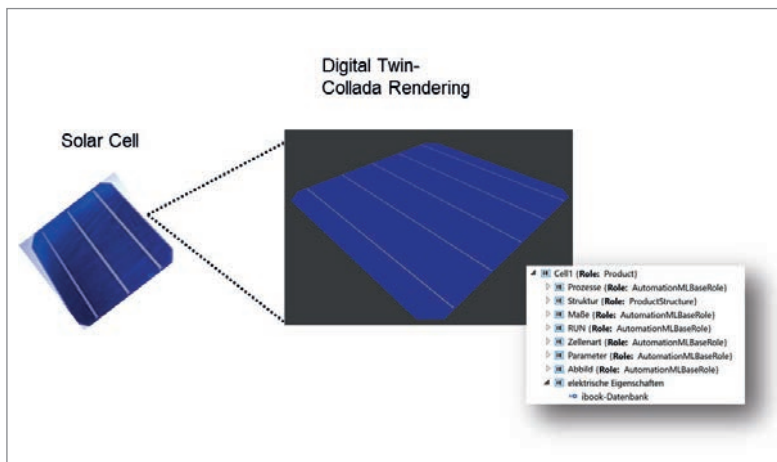


Figure 5. Visual representation of the digital twin of a solar cell.

What is Industry 4.0?

While Industry 4.0 is a culmination of several technologies, here an overview is presented of the contributing technologies from which functionalities will be integrated. In the current scenario, there are vertical information silos where the data flow is restricted to command and control. The introduction of standard communication technologies and the horizontal integration of information flow from several data sources enables the possibility to analyse and provide improved contextual real-time responses. The maturity of such cohesive interconnections along the entire value chain will then lead to the realization of the true value of Industry 4.0. The main drivers are:

- **Advanced manufacturing technologies:** this refers to the application of advanced technologies in product and process handling and also in management, e.g. scheduling, logistics and resource management. The use of robots and increased automation that will eventually be capable of intercommunicating help in achieving better production targets and in lowering manufacturing costs.
- **IoT and sensor technologies:** this refers to the networking and the management of interconnected sensors, tools and devices within the manufacturing facilities; it includes enablers such as cloud computing, edge computing and data analytics. From the smart factory perspective, parallels to the IoT architectural frameworks can be drawn in order to create distributed and horizontal information sharing possibilities.
- **Data analytics:** the analysis of the production requires a framework to monitor and collect relevant data from several sources. There should be interfaces to both statistical and machine-learning-based algorithms. It is foreseen to use open-source frameworks, such as Google's Tensorflow or Microsoft's Cognitive Toolkit. In PV, a lot of processing is done using statistical

tools, such as JMP, which are used for the design of experiments and statistical analysis. In order to remain compatible with the current tools, the digital twins need to interface with them. In addition, simulation tools, such as Quokka, which can simulate solar cells should also be interfaced to run a digital twin of a solar cell in order to provide improved simulations.

- **Security:** currently, the various components of security are managed individually. With the use of standard communication technologies, it is imperative to have security measures in place, as the system is more vulnerable to threats. It is also essential to have secure access management in place. Several companies collaborate with cybersecurity experts in the development and deployment of such interconnected systems.

Digital twins

As mentioned earlier, digital twins represent the digital counterparts of the physical assets. All physical things – machines, automation, materials and solar cells – can, and should in the future, have a digital twin. Digital twins are classified into several types [9]: product twin, process twin, entire production line twin or performance twin. The functionality is designed as per the requirements of the production plant. The different types of digital twin have different requirements: a machine requires sensors and actuators, while a product consists of different parameters.

One of the most important points in modelling is *granularity* (the level of detail). It is important to show some pragmatism and avoid academic completeness; incorporating every single detail can consume unnecessary computing power, slowing down the structure and possibly rendering real-time processing unfeasible. A digital twin requires a visualization tool that is clear and concise for both managers and operators. The facility should have the infrastructure to handle the real-time processing of large volumes of data. It should include interfaces to several algorithms that can model the data.

A clear advantage of using a digital twin is that the product can be 'produced' before it is actually physically created. This simulation of the product can then be used to carry out a wide variety of tests and put it through its paces. Fig. 5 shows a digital twin of a solar cell rendered using COLLADA, sourced from an AML file (described in the next section). For the production machines, a real-time view of the working components and the parameters can be easily made.

Digital twin: data model

With the various types of digital twin defined, two examples are considered here in the context of PV manufacturing: a 'product twin' corresponding to a solar cell, and a 'process twin' corresponding

to a piece of processing equipment, i.e. an inline wet-chemistry tool or a diffusion furnace. A digital twin of the solar cell enables us to analyse the cell through the various process steps. This further facilitates the possibility to optimize parameters in order to ensure that all the following cells fit the final quality evaluation criteria. The possibility to simulate virtual cells in real time speeds up the technology development cycle, as the number of development iterations can be reduced.

With regard to a product twin example, the design phase consists of identifying the relevant parameters to represent the asset; thus, the digital twin consists primarily of an underlying data model with all the relevant attributes of the solar cell. This structured representation allows information to be exchanged across components and systems. The data model includes metadata, process data, measurements and related contextual information. The life cycle of the product needs to be understood and captured in the digital twin.

A tight coupling of the physical object and the digital twin is established through communication interfaces and update mechanisms. Fig. 6 shows the modelling components in the realization of a digital twin. The physical assets here are the solar cell ('product') and an inline wet-chemistry process tool ('process'). All the parameters to be modelled are selected.

The modelling language adopted here is AutomationML, an emerging standard for the description of digital twins [10]: this is a standardized mark-up language for modelling and unifying all information used by engineering tools. AutomationML covers plant topology, geometry and kinematics, logic information, reference and relations, and referencing of other formats. It is an open standard and uses the XML format for programming. The language can be used to map and describe entire production lines in their hierarchy; it can also capture the inter-relationships between the several components. AutomationML comes with an in-built tool for conversion to the OPC UA data format. In addition, it can be interfaced to modelling tools for geometry and kinematics information, such as COLLADA and PLCopenXML.

The AutomationML editor provides a user-friendly interface in which it can be clearly programmed. A sample of the view of the digital twin data model for a solar cell designed using AutomationML using the editor is shown in Fig. 7, along with the corresponding XML schema. The figure indicates an instance hierarchy of a solar cell; metadata of the cell, the measurements made, the process steps performed and details relating to the process steps are included. The AML file can be used for sharing all the information relating to the solar cell twin; this file can then be converted to objects which can be accessed to update the parameters in real time or near real time.

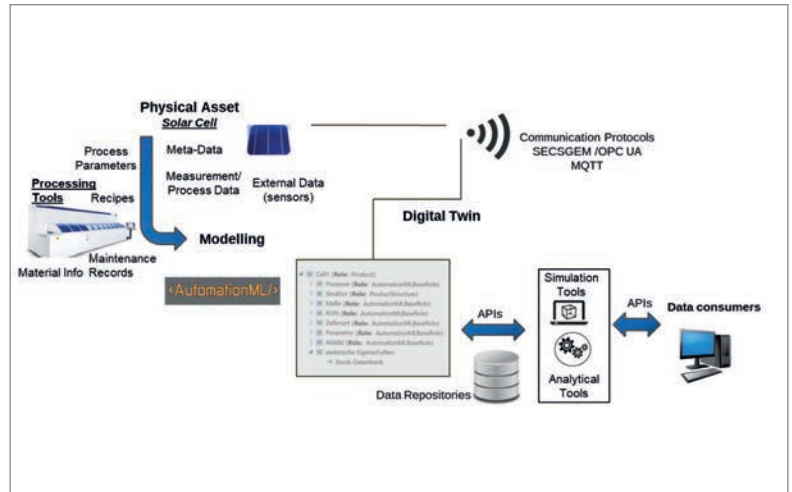


Figure 6. Communicating with the digital twin.

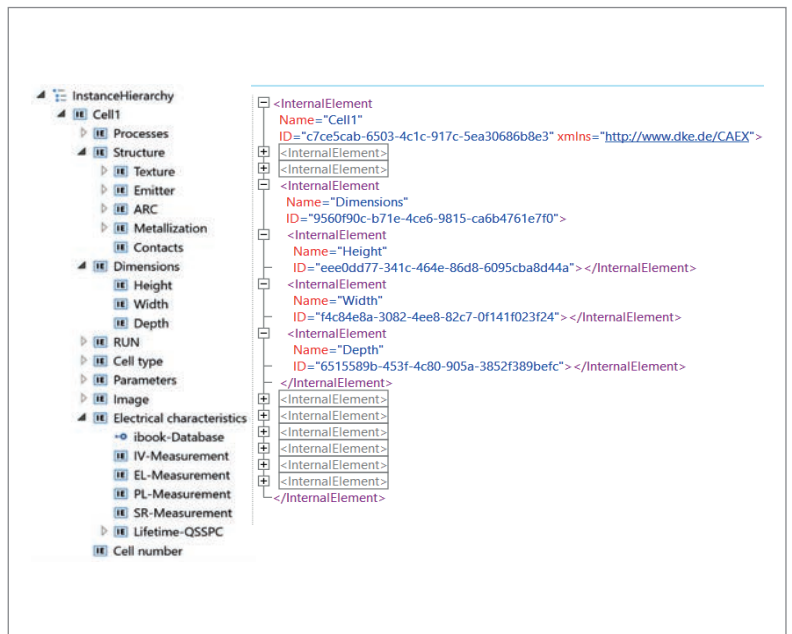


Figure 7. AutomationML and XML schema.

Digital twin: communication and interfaces – how to talk to machines

A critical component is the connectivity in order to ensure reliable and seamless connection of the digital twin to the heterogeneous data sources. While some factories have central information control software, such as MES, many facilities do not. Digital twins aim to use standard communication interfaces and to also facilitate a horizontal sharing of information in cases where MES is unavailable. Creating a single digital twin from a manufacturer might not be difficult, but having a standardized way to model and access several assets from different manufacturers is a challenge. For PV/semiconductor

“A critical component is the connectivity in order to ensure reliable and seamless connection of the digital twin to the heterogeneous data sources.”

production equipment, ISC has identified three communication categories adopted by the machine builders. The categories include:

- SEMI PV2 (SECS/GEM) [11]**
 The integration of the standards SEMI SECS-II (E5), GEM (E30) and HSMS (E37), which are already in use in semiconductor manufacturing, was recommended as the foundation for host communication throughout the PV industry. The SECS/GEM standard establishes the protocol for the communication link between a host computer and the machines. The host can issue remote commands to retrieve parameters, perform process program functionalities (such as run recipes), monitor material movement, etc. The information retrieved from the machines is classified into: 1) status variables – current parameters and measurements of the processing machine; 2) alarms – all the errors and warnings raised which indicate a non-optimum functioning of the machine; and 3) events – the possibility to monitor events and relevant machine parameters so that the host can continually get reports in a publish–subscribe mode. Additional functionalities include the possibility of using data spooling features to ensure no loss of information in the case of connectivity issues, defining and monitoring limits of parameters, and tracing functionalities.
- OPC UA [12]**
 This is the open-source communication protocol developed by the OPC foundation for machine to machine communication. It is a service-oriented architecture, supports multiple platforms and has an integrated information model and security features. The protocol includes the following specifications: data access (DA), historical data access (HDA), alarms and events (A&E), XML data access (XML-DA), data exchange (DX), complex

data (CD), security, batch, express interface (Xi) and unified architecture (UA). The main advantage of the OPC is its acceptance and use in several associated manufacturing sectors, such as automation, robotics, process control and manufacturing.

- Proprietary protocols**
 Several machines still follow proprietary communication protocols in the retrieval of data by a central server. This requires the development of drivers, wrappers and other translation tools to communicate with the machines and retrieve data in the required format. A standardized approach will reduce the amount of reworking that such proprietary protocols impose, but until the definition of the standards and widespread adoption occurs, workarounds will need to be in place.
- IoT and related protocols**
 For sensors and actuators, standard communication over TCP/IP is adopted. The highly adapted MQTT [13] transport protocol, which uses a publish/subscribe architecture, is suited to devices with smaller footprints. *REST interfaces* refer to the scalable architecture which facilitates communication over the hypertext transfer protocol (HTTP) to establish communication from an asset to a central web server.

An accepted standard for machine communication and a digital twin representation in the PV industry are needed in order to enable successful implementation of smart factories. Machine builders will have to offer this along with their machines and digital twin representation. SECSGEM or OPC UA are candidates for this standard, while AutomationML is a possibility for the digital twin representation.

Flexible factories

The digital transformation of the factory and the merging of all the data sources open up other interesting use cases of designing a flexible PV production line; for example, special cell types for certain niche products, or products with known variable demand, can be produced in this ‘FlexFab’ (Work on the concept of such a flexible factory is funded by the German Federal Ministry for Economic Affairs and Energy within the framework of the FlexFab project.) The changeover processes must be minimized and well known (e.g. necessary cleaning processes). The preparation of machines and the instruction of operators must be automated. The production schedule must be optimized automatically by a scheduler, as shown in the example in Fig. 8.

The requirements and design phase for this are twofold. The first is to identify commonalities and

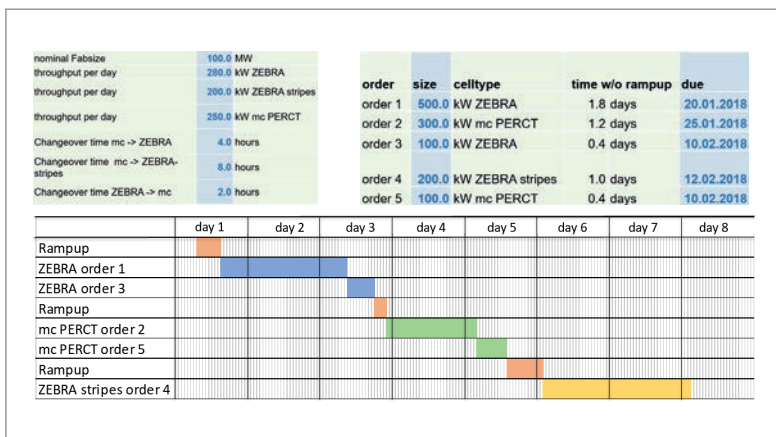


Figure 8. Example of a scheduler for a flexible production line: input fields for different cell types that can be produced at the site (top left) and orders for the fab with due dates (top right). The optimum schedule is then generated (bottom), and necessary information is sent to machines and operators.

differences in the technologies; this is established through several experimental batches to identify sources of contamination, possibilities of reuse of process steps, etc. A detailed design of experiments will allow the detection of conflicting and constructive factors.

The second is the possibility to remotely control and configure the parameters of the processing equipment. With the framework described above, ISC is working on the networking aspect for communicating with machines. A central control software is used to control and monitor equipment. In addition to control, the booking of machines is also handled by the software (presented later in this paper; see Fig. 14). On the arrival of a request to change the cell technology in a production line, all the required dependencies are checked and the machines are reconfigured to adapt to the new technology requirements. The basic requirement for doing this is to have all the machines connected and store all the necessary information in one place.

Self-learning factory

Imagine a factory that gets better all by itself... efficiencies steadily rise, small variations of production parameters are done automatically, and the fab achieves optimum production conditions unassisted. Take, for example, the introduction of a new silver paste for contact formation: the diffusion, printing and firing conditions are changed for some thousand wafers in a running production, and the optimum conditions and potential of the new paste are determined within hours. Fig. 9 shows a self-learning loop moving between the production floor and the digital data it generates to build models that will lead to the development of several applications.

The digital twins provide the interfaces to access the real-time and historical data from the machines; these data need to be converted to knowledge that can be leveraged. Traditional systems, such as ERPs, have rule-based routines in place. The production environment, however, is non-stationary and evolving; it is therefore necessary to build models that can learn and adapt in real time. The data analysis cycle starts with the identification of relevant data; the data are cleaned and filtered, and the appropriate statistical and learning models are then applied to the data. The inference obtained from the data is subsequently used in the decision making, for example in parameter optimization. Some of the applications include:

- **Predictive maintenance.** This is a disruptive approach [14] to performing maintenance, with the normal operations and parameters being continually monitored. Simulations and the ‘memory’ of the digital twin can be used to predict when a component or components

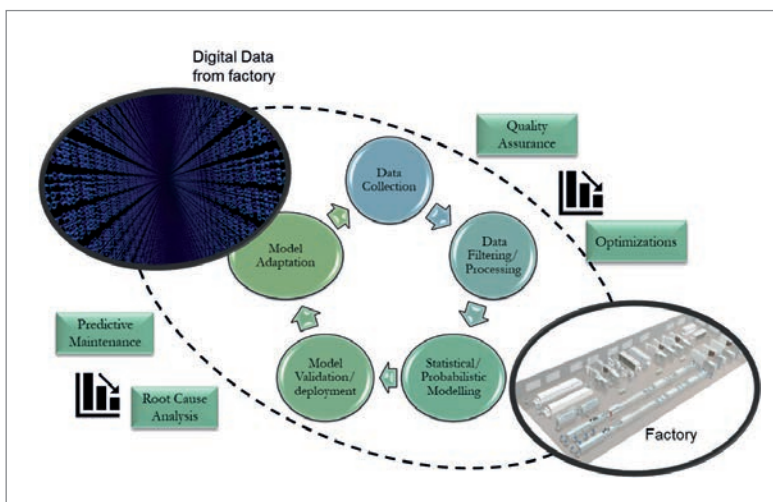


Figure 9. Applications based on learning from data.

within the production line will be faulty or even fail. It is also possible to avoid expensive on-site maintenance by experts from the manufacturer. If the company allows an online connection to the manufacturer, they can now use the digital twin to remotely service the machines. The likelihood of machine downtimes is estimated on the basis of load and usage patterns and environmental factors in order to reduce the mean time between failures (MTBF); estimates based on statistical and machine-learning models are provided. Errors in the equipment are anticipated by modelling (artificial neural networks), leading to early detection of failures, which means that warnings of abnormal patterns can be issued at an early stage. According to Deloitte [15], predictive maintenance will: 1) reduce the maintenance planning time by 20–50%; 2) diminish total maintenance costs by 5–10%; and 3) increase equipment uptime and availability by 10–20%.

- **Simulations and optimization.** A digital twin can be connected to simulation tools used by scientists in analysing production data and measurements. Simulation tools include Quokka3, PV Lighthouse and PC1D, which can be programmed to take in the data generated from the digital twin. While the implementation in the current state requires the development of wrappers and translation tools, a better integration is foreseen. By leveraging the digital twin data, improved simulations can be performed, thus mirroring the real-world status more accurately. Cost savings in the integration of simulation tools with the digital twin will be tremendous, and entire process chains can be simulated before production actually begins.

“It is necessary to build models that can learn and adapt in real time.”

- **Root cause analysis.** During the ramp-up phase, or during the introduction of newer technologies into the production line, several optimization cycles that are cost and time intensive are required. Identification of the source of errors or performance deviations can be performed with, for example, multivariate regression models.
- **Quality assurance.** The quality of the cell/module at the end of production can be ensured throughout the process line on the basis of the models.

ISC is also working on self-learning factories in the framework of the SelFab project, funded by the 'Ministerium für Wirtschaft, Arbeit und Wohnungsbau Baden-Württemberg' (Ministry of Economic Affairs of Baden Württemberg state).

Lab 4.0 at ISC Konstanz

In the development and integration of Industry 4.0 concepts for the factories, ISC's first step was the development and integration of a prototype using the same technologies, but on a smaller scale, i.e. in a solar cell research lab. The lab has all the production and process equipment for the complete fabrication of a solar cell; it also has the machines required for module development. Automation tools, such as loaders and unloaders, are not available, given the low throughput needed in a lab environment.

A pilot implementation provides an opportunity to explore specific aspects such as equipping the lab with sensors, exploring the standards for communication to the existing machines, identifying the gaps, collecting data and exploring analytical tools. The first phase was a survey of the equipment, resources and requirements for identifying the key areas of development and the possible challenges. The labs were fitted with environmental sensors, such as temperature, humidity and pressure sensors; Fig. 10 shows the historical trend of some of the values recorded in the labs.

Process equipment tools selected for communication include a diffusion furnace, a CVD, a firing furnace, an IV flasher and an inline wet-chemistry processing tool. Because some of the equipment was not PV2 compatible, upgrades were necessary in order to standardize the communication with all the equipment. This is an integral part, as it requires the development of one solution that can be extended to all the equipment. In the case of equipment that cannot be upgraded to support PV2, alternative communication strategies have to be in place.

The initial prototype uses the open-source Thingsboard platform [16] to visualize the data, device management and access management. A PostgreSQL database is the back-end database for storing all the data retrieved from the equipment and sensors. Fig. 11 presents a sample snapshot of connected devices in the lab.

The graph in Fig. 12 shows a sample overview of the trend in the machine parameters over a period of time. The data originate from the firing furnace and display the trend of temperature values of the furnace and the

**inter
solar**
connecting solar business | MEXICO

International Exhibition
and Conference for the
Solar Industry
WORLD TRADE CENTER,
MEXICO CITY

SEPT
03-05
2019
www.intersolar.mx



- Reach a market with extraordinary growth potential – Mexico ranks 5th for new solar capacity by 2021
- 13,000 attendees – join the largest gathering of professionals in the fields of solar, renewable energy and cleantech
- The perfect match: Intersolar and THE GREEN EXPO® are teaming up for a sustainable Mexico

Co-located Events



drive velocity. Fig. 13 shows some sample trends in the pressure values recorded from the inline wet-bench processing tool. This demonstrates the amount of information available for the analysis and study of cross-correlations, variance, etc. between parameters and final cell performance.

To integrate the concepts of a flexible factory, a web-based software management tool was developed. Referred to as the *iBook* (ISC booking tool), the front end offers a user interface for the managers and the operators to access all the information about the machines and booking information, as well as providing the ability to plan experiments (RUNs). In the case of the latter, the easy-to-use web interfaces have templates to choose cell technology, machine parameters, recipes, cell parameters, etc. here; for every RUN, all the associated data will be assimilated (see Fig. 14). The back end is again a PostgreSQL database. In addition, iBook will include information about personnel, maintenance statistics, details of the wafer (e.g. manufacturer, dimensions), etc. Communication between the iBook and the digital twin is planned through REST interfaces. The digital twin uses the iBook interface to retrieve metadata parameters and review information relating to booking times.

Impact of Industry 4.0

Industry 4.0 brings together a cohesion on all levels, linking investors, suppliers, consumers and other persons with a vested interest, creating a connected ecosystem. With the continuous stream of data, a degree of transparency is brought to the system, and everyone involved is able to take a proactive role in the functioning of the ecosystem. A shift from the vertical information silos to an interconnected open system will result in a transformation of not only the business models but also the way in which collaborative environments can be developed (Fig. 15).

Summary and outlook

A change in perspective is brought about by digitalization and Industry 4.0 in the manufacturing space. An adaptive system capable of learning from the environment and providing real-time recommendations and optimizations is the logical next step in the industrial evolution. Moving from rigid information silos to combining data sources to generate useful knowledge would result in improvements in several areas of manufacturing, focusing on the self-x functionalities of self-optimization, self-maintenance and self-configuration.

Incorporating Industry 4.0 into PV cell and module production will lead to significantly less downtime and improved efficiency through the higher level of process and inter-process control.



Figure 10. Environmental parameters – digital records.

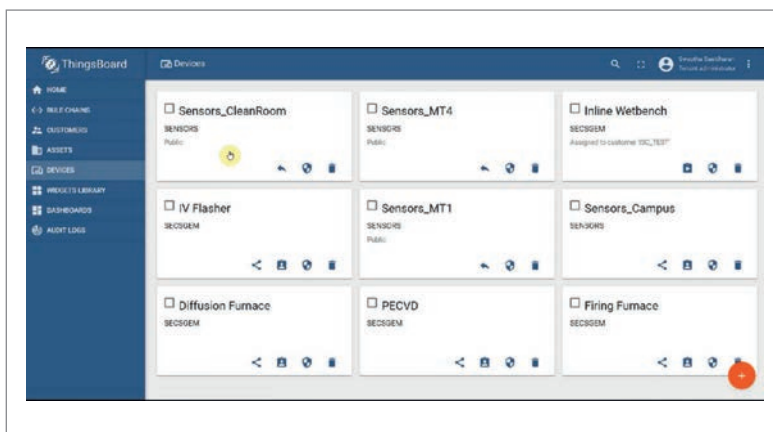


Figure 11. A view of several connected machines and sensors. MT1 and MT4 are characterization rooms in the ISC lab.

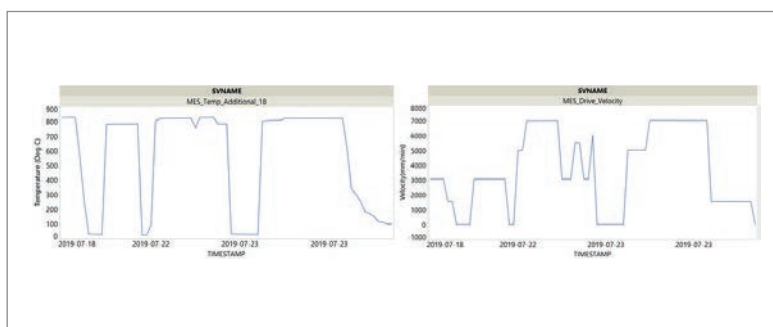


Figure 12. Machine parameter trends for the firing furnace.

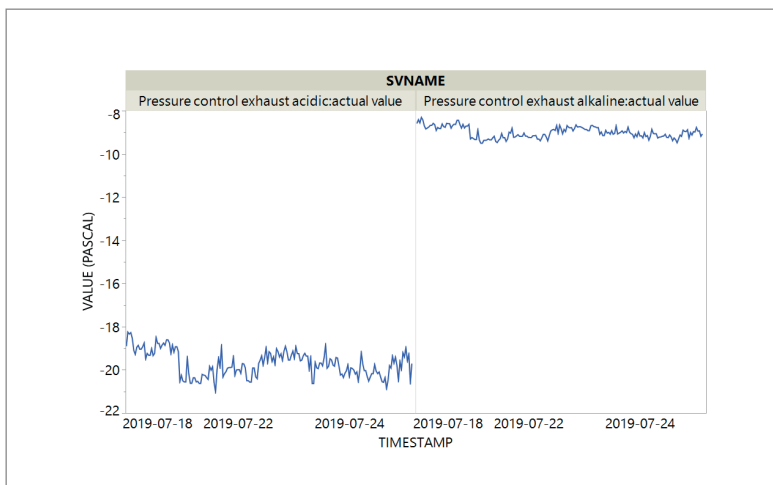


Figure 13. Machine parameters for the inline wet-bench processing tool.

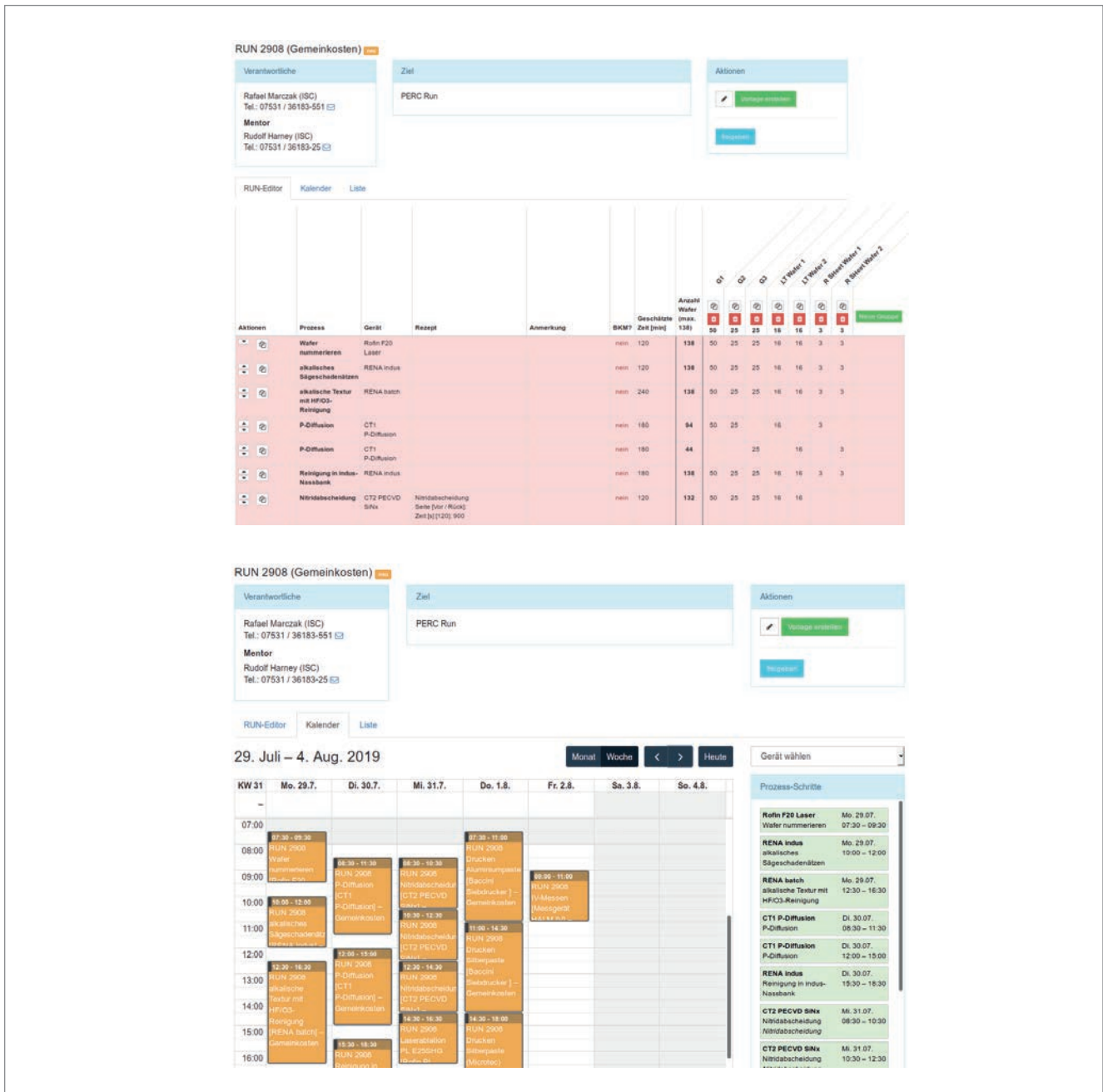


Figure 14. With the use of ibook ('ISC booking tool'), experiment planning, including group planning (a) and scheduling (b), is easily possible, as well as assignments to the operators. The earlier-described machine planning in a FlexFab is based on this system.

However, standards for communication interfaces (PV SECS/GEM or OPC UA) and digital twin representations (AutomationML) are essential (the authors' assumptions in brackets). Cell/module manufacturers will need to request appropriate interfaces and digital twin representations from their machine suppliers.

“Incorporating Industry 4.0 into PV cell and module production will lead to significantly less downtime and improved efficiency through the higher level of process and inter-process control.”

References

- [1] Zimmer, M. et al. 2019, “Digitalization meets PV production technology – Outline of a smart production of silicon solar cells and modules”, *Photovoltaics International*, 42nd edn.
- [2] [https://www.pv-tech.org/news/tongwei-initiating-20gw-solar-cell-capacity-expansion-plans].
- [3] [https://www.pv-tech.org/news/tongwei-to-start-heterojunction-pilot-production-with-migration-to-industry]
- [4] [https://www.jinkosolar.com/press_detail_1395.html?lan=en].
- [5] ZVEI – Industrie 4.0 News, Reference Architectural Model RAMI 4.0 [https://www.zvei.org/en/subjects/industry-4-0/the-reference-architectural-model-rami-4-0-and-the-industrie-4-0-component/].

[6] ITRPV 2019, "International technology roadmap for photovoltaic (ITRPV): 2018 results", 10th edn (Mar.) [<https://itrpvdma.org/en/>].

[7] Platform Industrie 4.0 [<http://www.plattform-i40.de/I40/Navigation/EN/Home/home.html>].

[8] Givehchi, O. et al. 2017, "Interoperability for industrial cyber-physical systems: An approach for legacy systems", *IEEE Trans. Ind. Inform.*, Vol. 13, pp. 3370–3378.

[9] [<https://www.plm.automation.siemens.com/global/en/our-story/glossary/digital-twin/24465>].

[10] Schroeder, et al. 2016, "Digital twin data modeling with AutomationML and a communication methodology for data exchange", *IFAC-PapersOnLine* 49.30, pp. 12–17.

[11] SEMI [<https://www.semi.org/en>].

[12] OPC Foundation [<https://opcfoundation.org/>].

[13] MQTT Foundation [<http://mqtt.org/>].

[14] Immerman, G. 2018, "The impact of predictive maintenance on manufacturing", *MachineMetrics* [<https://www.machinemetrics.com/blog/the-impact-of-predictive-maintenance-on-manufacturing>].

[15] "Making maintenance smarter" [<https://www2.deloitte.com/insights/us/en/focus/industry-4-0/using-predictive-technologies-for-asset-maintenance.html>].

[16] Thingsboard Platform [<https://thingsboard.io/>].

About the Authors



Dr. Swaytha Sasidharan received her Ph.D. in information and communication technology in 2019 and her master's in telecommunication engineering in 2009 from the University of Trento, Italy. She has several years' industrial experience working in the fields of Internet of Things, Industry 4.0, machine learning, embedded electronics, sensors and wireless sensor networks. She is currently working at ISC, focusing on Industry 4.0 aspects, particularly on the communication interfaces for PV equipment.



Florian Herzog graduated with his bachelor's in economical and electrical engineering from the University of Applied Science Konstanz in 2017. He studied the same subject for his master's in Konstanz and New York, and is currently employed at ISC Konstanz to work on his master's thesis, which deals with the creation of digital twins of solar cells.

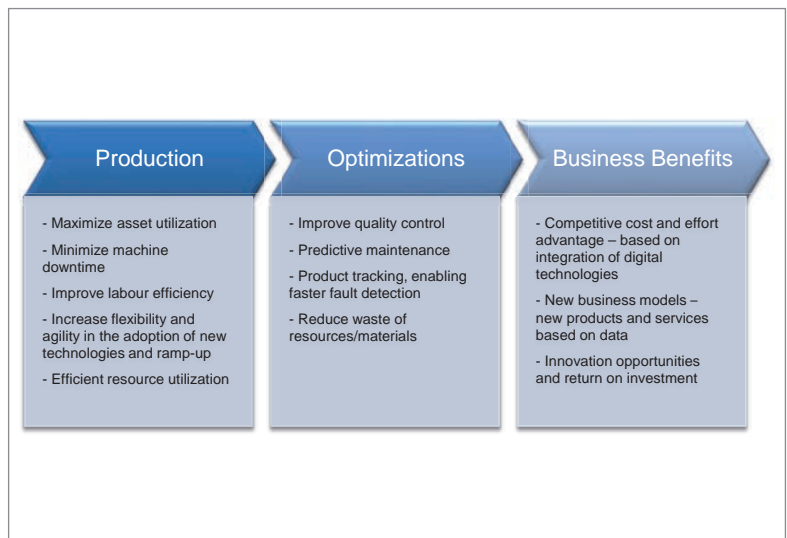


Figure 15. Impact of Industry 4.0.



Johnson Wong is a senior physicist at Aurora Solar Technologies, Canada, a company which develops inline tools for the measurement, visualization and control of critical processes during solar cell manufacturing. He previously headed the PV characterization group at the Solar Energy Research Institute of Singapore (SERIS), where he created various analytical tools to delineate the factors that contributed to solar cell power loss. He is the inventor of Griddler computer programs that apply full-area, two-dimensional finite-element analysis (FEA) to solar cells with arbitrary metallization geometries, as well as Module, a finite-element simulation program for solar panels.



Rudolf Harney studied physics in Tübingen, Canada, and in Oldenburg, Germany, obtaining his degree in 1998 on the characterization of CIGS thin-film solar cells. After graduation, he pursued several independent activities in the fields of wind energy, device development and programming. He joined ISC Konstanz in 2007, where he is currently a member of the Executive Board and Board of Directors, and the head of the Industrial Solar Cells Department.

Enquiries

Tel: +49-7531-36 18 3-25
 Email: rudolf.harney@isc-konstanz.de



www.snec.org.cn

14th (2020) International Photovoltaic Power Generation and Smart Energy Exhibition & Conference

See you in 2020

May 25-27, 2020

Shanghai New International Expo Center
(2345 Longyang Road, Pudong District, Shanghai, China)



关注SNEC微信



Follow us at WeChat

©Asian Photovoltaic Industry Association / Shanghai New Energy Industry Association

©Show Management: Follow Me Int'l Exhibition (Shanghai), Inc.

Add: RM905-907 No 425 Yishan Rd, Xuhui District, Shanghai 200235, PRC

Tel: +86-21-33685117 / 33683167

©For exhibition: info@snec.org.cn

For conference: office@snec.org.cn

Why are monocrystalline wafers increasing in size?

Mark Osborne, Senior News Editor, *Photovoltaics International*

Abstract

The PV industry is undergoing rapid technology changes that have been driven by the well-documented swift adoption of monocrystalline wafers. Less well understood, however, is that within this wafer technology transition comes a shift to larger wafer sizes, and this includes p-type and n-type mono-Si wafers.

The solar industry has been undergoing major technology changes, notably the shift to passivated emitter rear cell (PERC) and more recently the migration away from multicrystalline wafers to monocrystalline. These developments have led to the mass production of high-efficiency p-type mono-PERC bifacial cells, and half-cut and shingled technologies for modules, which are available in double-glass, multi-busbar and half-cell configurations. All of this is pushing high-efficiency products into the mainstream high-volume markets.

Various n-type cell options (for example, nPERT and selective emitter), as well as heterojunction (HJT) technologies, have secured a gradual but increasing foothold in the market, not least because of a shift in wafer size, which reduces overall production costs. The net result of the new capital investments has seen the number of (meaningful) n-type cell producers grow to approximately 20, with many others engaged at the R&D level too, or working with research institutes on collaborative projects. Consequently, global cell production of n-type has grown from the 2GW level in 2013 to just

over 5GW in 2018, and is projected to be more than 5GW in 2019 (Fig. 1).

Indeed, a big part of SunPower's latest next-generation technology (NGT) interdigitated back contact (IBC) cells, which will power its S-series modules, is the shift to larger n-type wafers (Fig. 2). This is also the path taken by LG Electronics.

Traditionally, monocrystalline silicon wafers before 2010 were classified as *small size* with dimensions 125mm × 125mm (164mm-diameter silicon ingot), and only a small number with dimensions 156mm × 156mm (200mm-diameter silicon ingot). These had been the dominant ingot size in the semiconductor industry until leading companies adopted 300mm-diameter ingots.

Monsoon Wang, Director of Product Marketing at LONGi Solar, told PV Tech that the wafer size change is occurring faster than many people realize.

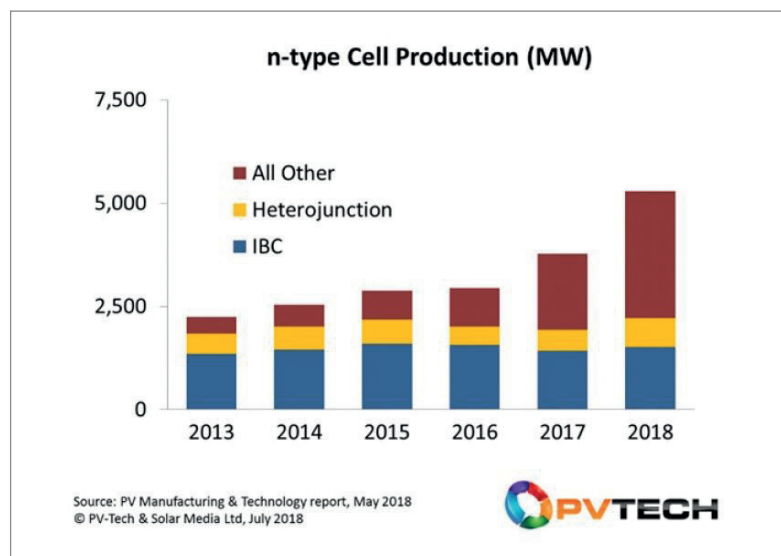
"Yes, this trend is happening," noted Wang. "Only ten years ago, almost all the mono wafers were 125mm. A few years later, some producers were starting to supply 156mm wafers, and we have seen that these almost complete transitions can take two to three years. So, by 2014, the transition to 156mm wafers had happened. The reason for this change is that the wafers were much smaller and production costs much higher, as the overall capacity was much lower than for multi. This was the driver for all cell producers to switch to the then larger wafer size."

After 2010, 156mm × 156mm wafers increasingly became the popular choice (lower cost per watt) for p-type mono and multi wafer sizes. As a result of the lower production costs, 125mm × 125mm p-type wafers were almost eliminated from the market by 2014, with only a few IBC and HJT cells using the 125mm × 125mm n-type wafers, as the larger-size technology lagged p-type investments because of the niche nature of the applications.

By the end of 2013, a number of China-based wafer producers (LONGi, Zhonghuan, Jinglong, Solargiga and Comtec) jointly issued the standards for (M2) 156.75 × 156.75 p-type mono wafers (205mm-diameter silicon ingot) and (M2) 156.75 × 156.75 p-type mono wafers (210mm-diameter silicon ingot).

Without increasing the overall dimensions of a 60-cell module, M2 wafers could increase module power by more than 5Wp, a significant boost for a competitive cost per watt, thus rapidly becoming the mainstream and maintaining that status for several years. During that period, there were also a few (M4) 161.7mm × 161.6mm (211mm-diameter silicon ingot) wafers on the market; the area of the M4 was 5.7%

Figure 1. New entrants to n-type manufacturing drive annual production levels to more than 5GW in 2018.



"Wafer size change is occurring faster than many people realize."

The Photovoltaics International technology journal is the only independent publication within the PV industry **focused entirely on PV manufacturing**. It is written by acknowledged experts in their chosen field – the Cell & Module manufacturers and their R&D partners.

It addresses their current and short to medium term technology requirements with special regard to increased conversion efficiencies, reduced manufacturing costs and other elements of their technology roadmaps via cutting edge technical articles and product reviews.

In each issue of the journal, we focus on the following areas:

- **Fab and Facilities**
Looks at the core functions and design considerations for PV facilities.
- **Materials**
Provides analysis of all materials used in manufacturing, including gases, liquids, silicon and other substrates.
- **Cell Processing**
Focuses on the technical aspects of solar cell production.
- **PV Modules**
Covers processes and technologies for packaging cells into modules.
- **Thin Film**
Presents papers on the production of all thin-film technologies.

SUBSCRIPTIONS

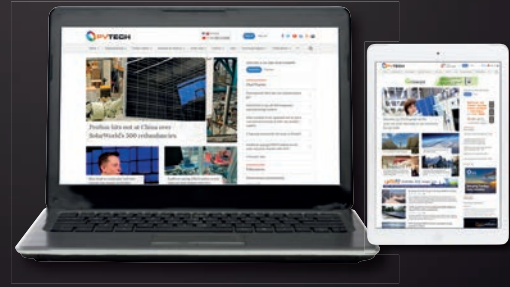
- Photovoltaics International Online Subscription **\$99**
- Photovoltaics International Print Subscription **\$199**
- Photovoltaics International Online & Print Subscription **\$249**
- Photovoltaics International Subscription **\$599**
- Photovoltaics International Institutional Licence - Great value for institutions that require multiple Photovoltaics Subscriptions for their members. **From \$1,999 to \$5,000**

VISIT OUR WEBSITE TO PURCHASE: www.pv-tech.org/photovoltaics-international/overview

OR CONTACT OUR TEAM FOR FURTHER INFORMATION: info@pv-tech.org

THE NO.1 SOURCE FOR IN-DEPTH & UP-TO-THE-MINUTE NEWS, BLOGS, TECHNICAL PAPERS, AND REVIEWS ON THE INTERNATIONAL SOLAR PV SUPPLY CHAIN COVERING:

MANUFACTURING | TECHNICAL INNOVATIONS |
MARKETS & FINANCE | LATEST PROJECTS



GET THE LATEST PV INDUSTRY INTELLIGENCE DIRECT TO YOUR INBOX.
SIGN UP FOR FREE NOW: WWW.PV-TECH.ORG/#NEWSLETTER



Join us again in 2020 for:



CONFERENCE PVCELLTECH 2020

10-11th March | Penang, Malaysia

Going into its 5th year, PV CellTech is a truly unique event attended by all of the world's top cell manufacturers, equipment and material suppliers to shape the PV cell technology roadmap. Join us to learn from and network with the PV industry's leaders.

"It is the brains of the drivers of industrial PV condensed in a conference room. I cannot think of a better event, where it is as easy as here to meet and talk to the leaders of key players."
Gerry Knoch, Exateq

"PV CellTech continues to draw technical leaders from all levels of the PV supply chain making it a premium venue for networking"
Bruce Lee, MacDermid Alpha

To get involved either as a speaker, partner or attendee please email: marketing@solarmedia.co.uk

larger than that of an M2, and these wafers were mainly used for n-type bifacial modules.

The move from 156mm × 156mm to the larger format of 156.75mm × 156.75mm in mass production started in 2016. The old 6" format (156mm × 156mm), recognized by all, is expected to disappear completely from the market by the end of 2019, according to the 2019 edition of the ITRPV survey (Fig. 3).

The transition to a new larger 'standard' wafer size, however, is going to prove difficult, as will comparing cell/module conversion efficiencies on a like-for-like basis going forward. Nevertheless, the industry is transitioning faster than expected and key PV module manufacturers, such as LONGi and JinkoSolar, are ramping up mono-Si wafer capacity, which is compatible with the production of larger silicon wafers.

Multicrystalline wafer sizes are also expected to follow suit. The dominant format is 156.75mm × 156.75mm in mass production but, according to the ITRPV 2019 edition, other sizes are also emerging in mass production, such as 157mm × 157mm; an even larger format, of dimensions 158.75mm × 158.75mm, could be the standard for the next few years. Driving the 158.75mm × 158.75mm format has been GCL-Poly as it transitions the largest installed base of multicrystalline DSS furnaces to its mono-cast technology.

Mono-cast move

On March 8, 2019, GCL-Poly gathered its major customers to highlight its new era of mono-cast production. Emphasis was placed on how comparable in performance to monocrystalline technology its mono-cast technology was. Highlights included presentations noting that PV modules using its cast mono wafers had no notable surface defects, and that the latest G3 wafer surface quality problem had been resolved completely. Low minority-carrier lifetime was said to have been greatly reduced, with a lower dislocation density.

The difference between the cell conversion efficiencies of cells produced on the same production line were therefore less than 0.3%. The power difference between a 72-cell GCL mono-PERC module and a 72-cell Cz module was said to be less than 5Wp. The power output of a 72-cell module was said to be able to reach 405Wp. By the end of 2018, several customers were reported to have started mass production of products using the GCL-Poly Mono G3 wafer.

GCL-Poly also noted, however, that in their opinion there were too many different wafer sizes, just ranging between 156.75mm and 158.75mm, on the market. Standardizing silicon wafer sizes is therefore conducive to the sustainable development of the entire industry.

GCL-Poly believed that its own market forecasts meant that the 158.75mm wafer size would become the dominant product on the market in 2019. The company said that by the end of 2019, the total production capacity of the Mono G3 wafer would range from 8GW to 10GW.



Image: SunPower Corp

Figure 2. SunPower is transitioning to larger n-type wafers.

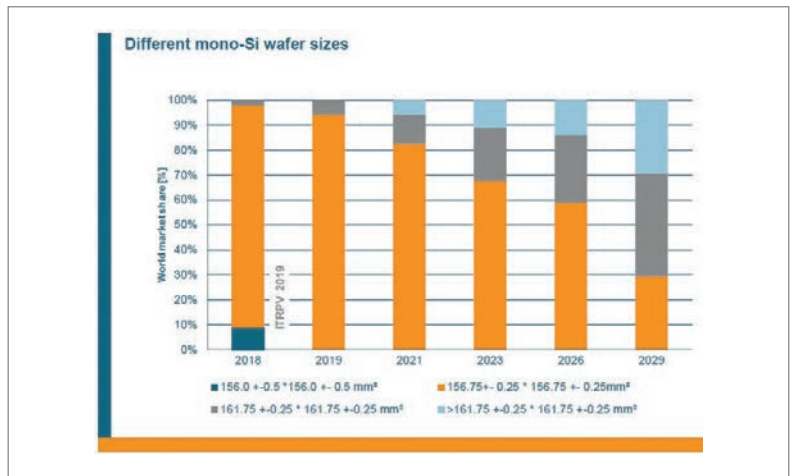


Figure 3. The ITRPV survey shows various wafer sizes gaining volume market penetration, but supersized wafers are already entering the market.

The roadmap for GCL cast mono cells in 2019 was said to focus on further quality improvements of the wafers and enhancing cell production techniques, notably for the introduction of selective emitter cells, which are not yet ready for mono-cast wafers. The company aims to achieve an average efficiency of 22.2–22.3% for mass-produced cells.

Established mono ingot/wafer producers, however, are already entering production with even larger wafer sizes, such as 166mm × 166mm. LONGi Solar rolled out its Hi-MO4 module in May 2019 (Fig. 4); this is a new generation of advanced monocrystalline PERC cell technology and encapsulation technology of half-cell and bifacial construction, using 166mm × 166mm p-type mono wafers. Reported module outputs are 420W, peaking at 430W.

The pace of launching larger sized wafers is more than likely due to intensified market competition seen in the second half of 2018, when China cut

“The old 6” format (156mm × 156mm) is expected to disappear completely from the market by the end of 2019.”



Figure 4. LONGi Solar's official launch of its Hi-MO4 module gained a large audience at Intersolar Europe.

support mechanisms for utility-scale and distributed generation markets under the '531 New Deal'.

"During the second half of last year [2018], due to market requirements customers were asking for higher module outputs in the 400Wp range," noted LONGi Solar's Monsoon Wang. "This is very difficult to achieve at the cell level in such a short time. Changing the wafer size and moving to half-cut cells was seen as the best option to get to 400Wp.

"However, several manufacturers had their own ideas on what the larger wafer size should be, such as 157.4mm, 158.75mm and 161.7mm, which Korean firms such as LG and Q CELLS selected for n-type wafer cells. So, in the second half of last year there was some uncertainty in the market, which led to discussions with a lot of customers. What we found was the key concern centred around the impact on the LCOE of PV projects.

"The [downstream] market will need time to be informed and educated about the next wafer transition, especially in module dimensions and weight comparisons with say glass/glass bifacial modules. A key point to consider when moving to slightly larger module dimensions is that the modules will still only need two people to install, so the LCOE will still be lower, as will the BOS (balance of system)."

"This also applies to cell manufacturing, with cost per watt also reduced, along with paste. Although it could be a little difficult for existing cell and module production capacity to adopt the larger wafer sizes, as capex would need to be spent on certain upgrades, new production lines would not have that difficulty," added Wang.

The thought process at play was the hope that a further increase in module power outputs by expanding the size of silicon wafers would be the cheapest route to securing product competitiveness.

"With larger wafers, the need for half-cut or multi-cut cells also increases."

According to LONGi, one route that PV manufacturers had evaluated was to adopt M2 wafers and continue to increase the width across the wafer, to 157mm, 157.25mm or 157.4mm, without increasing the overall dimensions of the module. However, modelling indicated that the increase in power output would be limited. Other factors, such as requirements on production accuracy, would also be increased. Furthermore, the certification compatibility could be affected (e.g. failing to meet the creepage distance requirement of UL certification).

LONGi also noted that another methodology was to follow the route of increasing the width across the wafer from 125mm to 156mm (increasing the size of the module), such as a 158.75mm pseudo-square wafer or square wafer (223mm-diameter silicon ingot).

LONGi stated that the latter increases the wafer area by about 3%, which in turn increases the power output of a 60-cell module by nearly 10Wp. What also seems to be happening is that n-type module manufacturers could be choosing 161.7mm M4 wafers, while some are planning to launch 166mm-size wafers in the future, according to LONGi.

Perhaps not surprising is that the largest mono wafer producer has chosen the 166mm wafer size, as this is apparently the maximum size compatible with all standard horizontal diffusion furnace production tools. On the one hand, the depreciation and manual labour per watt will be significantly reduced because of the increase in the production capacity for cells and modules. On the other hand, modules with larger wafers have higher power and can reduce BOS cost, which in turn will reduce the total cost of the system.

With larger wafers, the need for half-cut or multi-cut cells also increases, because of the increase in negative resistive losses for p-type mono-based cells. Less resistance between the cells clearly increases the power output of a module.

So, going forward, in the case of p-type mono-based cells, bigger is going to be better, as long as cut cells and other cell-to-module loss-reduction technologies, such as shingling, are adopted.

"There is a growing consensus amongst manufacturers that the next standard will be the 166mm size M6 wafer, after we publicly launched it at SNEC. There will be work undertaken to inform the market about this next standard wafer as, being the number one mono wafer producer, we have that responsibility," added Wang.

Maximum size wafer breakthrough

In mid-August 2019, Tianjin Zhonghuan Semiconductor (TZS) held a product launch for its mono silicon 'Kwafu' M12 series wafers in 205mm × 205mm and 210mm × 210mm sizes (Fig. 5), which were produced from a 300mm-diameter ingot.

Shen Haoping, chairman of Zhonghuan said, "The release of 'Kwafu' will significantly reduce the BOS (initial investment cost) and LCOE of photovoltaic power plants, helping manufacturers to obtain higher returns while also making parity in more regions. And

the successful implementation of the bidding project will effectively promote the further development of the global PV market.”

The 300mm-diameter wafer has been used in the semiconductor industry for just over 20 years and is the standard wafer size for CMOS IC fabrication. Efforts by industry consortiums to push the size to 450mm were abandoned on cost and lack of industry support.

Zhonghuan also announced that the new product involved more than 100 declared patents (partially accepted) and its own intellectual property technology, through new technological breakthroughs, to achieve new product iterations. According to Zhonghuan, using the same 144 half-piece (72 cut-and-halved) components, with cell efficiencies of 22.25%, the M12 p-type PERC 60-piece half-cut module produced 200W more than the equivalent M2 wafer-based module with a peak power in the 610W range (Fig. 6).

Lack of standards

In August 2019, LONGi Group reinforced to PV Tech that the solar industry must work together to agree on standardized larger wafer sizes, according to the monocrystalline solar manufacturer. The company revealed that it had now sold 2GW of its Hi-MO4 module. The firm is now increasing its backing of that wafer size with a series of upgrades across its own facilities.

“By end 2020, LONGi will upgrade its existing cell and module lines and transform them for production with the 166mm wafer,” said Wang Yingge, executive assistant to the chairman of LONGi Solar. “New lines such as the 5GW monocrystalline cell line in Yinchuan will be designed for the 166mm size from the start,” said Yingge, adding that large-scale production of Hi-MO4 will commence in the third quarter of 2019.

“The 166mm wafer has reached the allowable limit of production equipment which is difficult to overcome. This would be the upper limit of the standard for a considerable period,” said Professor Shen Wenzhong, Director of the Solar Energy Research Institute of Shanghai Jiaotong University.

“If manufacturers cannot reach an agreement on a size standard, it will restrict the development of the whole industry,” said Li Zhenguo, President of the LONGi Group.

Shen Wenzhong added, “Existing crystal drawing and slicing equipment are compatible with 166mm size silicon wafers. Production equipment for cells and modules needs to be modified, though the costs are lower and easier to achieve. Calculated by ‘flux’, cell and module production lines using 166mm wafers will increase capacity by 13% as compared with the 156mm size.”

“From LONGi’s perspective it will take around half a year to make its transition to the M6 wafer in a module, and perhaps a year for the industry to transition to the M6 wafer. There is a good incentive to transition as quickly as possible,” noted Wang.



Figure 5. Zhonghuan Semiconductor’s ‘Kwafu’ M12 series brick, launched in August 2019.



Figure 6. With larger and larger wafer sizes, the module dimensions increase significantly. On the far right of the picture is Zhonghuan Semiconductor’s M12 wafer-based 60-cell formatted PV module.


Conclusion

In just the last 18 months, a major shift to mono has been in full swing, including the shift by GCL-Poly to mono-cast production, sending multicrystalline to a place in the history books faster than expected.

Almost at the same time, the wafer size changes have been numerous and continue to expand in number, highlighting concerns of a lack of standard sizes in the future.

However, it would seem that the pace of the wafer size transition and increasingly larger formats being introduced to the market and ramped-up volume production is setting the industry on course to larger and larger module dimensions, with outputs exceeding 600W, perhaps as early as 2020. The ramifications of this in the upstream and downstream markets have yet to be fully understood.

“Wafer size changes have been numerous and continue to expand in number, highlighting concerns of a lack of standard sizes in the future.”



ENERGY TAIWAN

📍 Taipei Nangang Exhibition Center, Hall 1

Your all-in-one Green Energy Platform in Taiwan
Pre-Registration is now OPEN.



16-18 OCT
2019

-  *PV Taiwan*
-  *Wind Energy Taiwan*
-  *HFC Taiwan*
-  *Smart Storage Taiwan*

The monoPoly technology platform: Rapid implementation of passivating contacts in PERC/T production lines

Shubham Duttagupta, Naomi Nandakumar, John Rodriguez & Vinodh Shanmugam, Solar Energy Research Institute of Singapore (SERIS), National University of Singapore (NUS)

Abstract

Passivated emitter and rear cell (PERC) solar cell design is the industry standard for high-volume solar cell manufacturing today. The next challenge for the PV industry is to find a low-cost cell upgrade technology platform that can be easily retrofitted in existing production lines to modify the front side and enhance the rear. The monoPoly™ technology platform, developed at SERIS together with its strategic industry partners, offers an attractive solution and paves the way for the adoption of passivating contacts in large-scale manufacturing. This platform requires only one tool upgrade for most PERC/T production lines, has one less process step than a standard PERC production process, and yields a +1%_{abs.} efficiency boost over a standard PERC process. The authors believe that monoPoly will enable the PV industry to mass produce cells with efficiencies exceeding 24% in their existing lines in the near future.

Background

Global PV production continues to be dominated by p-type crystalline silicon (c-Si) solar cell technologies [1]. In particular, the passivated emitter and rear cell (PERC) solar cell design has been well established since the 1990s. Although PERC is currently the most popular, the GW-level adoption of this cell design in mass production has taken more than 20 years; this was mainly because of the unavailability of high-throughput equipment and process technology that could effectively passivate p-type surfaces in multi- and monocrystalline silicon wafer solar cells. By 2009, the development and commercial deployment of AlO_x for the passivation of p-type surfaces using high-throughput deposition schemes disrupted the (then mainstream) alloyed aluminium back-surface field (Al-BSF) technology, and PERC technology saw continuous growth in manufacturing in the 10 years that followed.

Today, PERC cells have demonstrated efficiencies exceeding 22% in mass production. However, as mainstream silicon PV progresses towards efficiencies greater than 24%, the challenge lies in boosting the solar cell's open-circuit voltage (V_{oc}) beyond 700mV – which is not easy to do for cells with screen-printed and fired contacts. Apart from the bulk material (which the authors believe can be

improved), the major voltage loss in most PERC/T solar cells arises from metal contact recombination at the front and rear surfaces, as well as partially from recombination loss at the phosphorus-diffused front surface. Passivating contacts using doped polycrystalline Si (poly-Si) materials provide an elegant solution to all these problems.

The first reports on passivating contacts for solar cells date back to the 1970s with structures such as SIPOS (semi-insulating polycrystalline Si), first used in transistor applications [4–7] and subsequently in PV applications [8–12]. The latter typically include full-area thin-film stacks that passivate the c-Si surface while selectively extracting only one type of charge carrier (i.e. either electrons or holes). There were only a few publications on the application of poly-Si for silicon solar cells during the period 1990–2010. It is likely that the first commercial application of poly-Si contacts was by SunPower in their interdigitated back contact solar cells [14].

There has been renewed interest in poly-Si passivating contact schemes since 2013, as evidenced by the excellent results obtained by Fraunhofer ISE with TOPCon technology and ISFH with POLO technology [16–20]. These were soon followed by reports from other institutes e.g. ECN with PERPoly and SERIS with monoPoly™ [22,23]. The concept of poly-Si-based passivating contacts in c-Si solar cells is 30–40 years old [8–12], and it could well be that a known method of deposition such as low-pressure chemical vapour deposition (LPCVD) was exercised by early adopters because of its legacy in microelectronics and the fact that tools were readily available. But, as was the case for PERC/T production lines, the passivating contact cell design now has the following requirements:

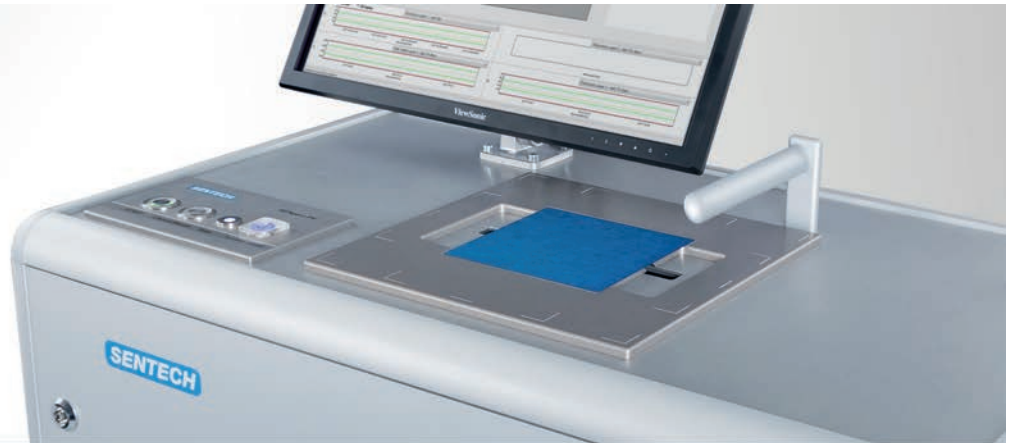
1. A production technology platform that has a smaller number of steps and enables ultrahigh deposition rates (>100nm/min).
2. A truly single-sided process that can be retrofitted to current solar cell lines.
3. Compatible with screen-printed (and fired) contacts and bifacial cell designs.

“The major voltage loss in most PERC/T solar cells arises from metal contact recombination at the front and rear surfaces.”

SENTECH

SENperc PV

QC for solar cell manufacturing



The innovative solution for quality control of coatings on PERC cells

- QC for multi- and c-Si based solar cell manufacturing
- Thickness measurement of AR coatings and passivation layers
- Long-term stability monitoring of deposition process
- Easy recipe based push button operation
- Software interface for data transfer
- Compact design

www.sentech.com

mail: marketing@sentech.de

phone: +49 30 63 92 55 20

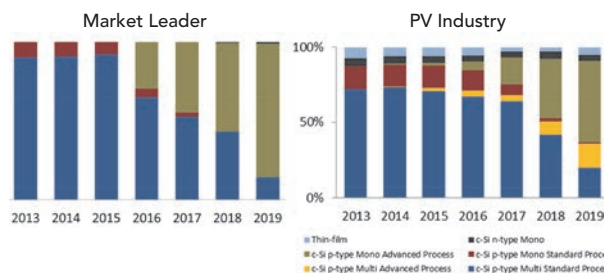


SOLAR MEDIA
MARKET RESEARCH

PV MANUFACTURING & TECHNOLOGY REPORT

Understand exactly what is really happening in PV manufacturing technology today – across the top-100 leading global module suppliers

This chart from the report, demonstrates how one company is driving the technology roadmap of the industry. The report includes insights as to how this has come about, what this means for global technology and supply offerings for the next 12-18 months, and what other companies are having to do in order to remain competitive going into 2021.



- Over 100 companies are analysed bottom-up, with quarterly effective capacities by region and technology type. Production levels for the different technologies are identified through mapping out utilization rates for lines throughout the year.
- Forecasts for new capacity, technology upgrades and expansions are given for all companies tracked.
- Capex and R&D spending is also provided for all manufacturers, with capex split into poly, ingot, wafer, cell and module segments and by region of capacity addition.
- The PV Manufacturing & Technology Quarterly report is a must-have quarterly addition for all PV manufacturers, and equipment and materials suppliers, and offers the most credible and detailed benchmarking tool available today within the industry.

REQUEST YOUR FREE DEMO

Call John Browne on +44 (0) 207 871 0150 or email marketresearch@solarmedia.co.uk to schedule your demo or for further information.

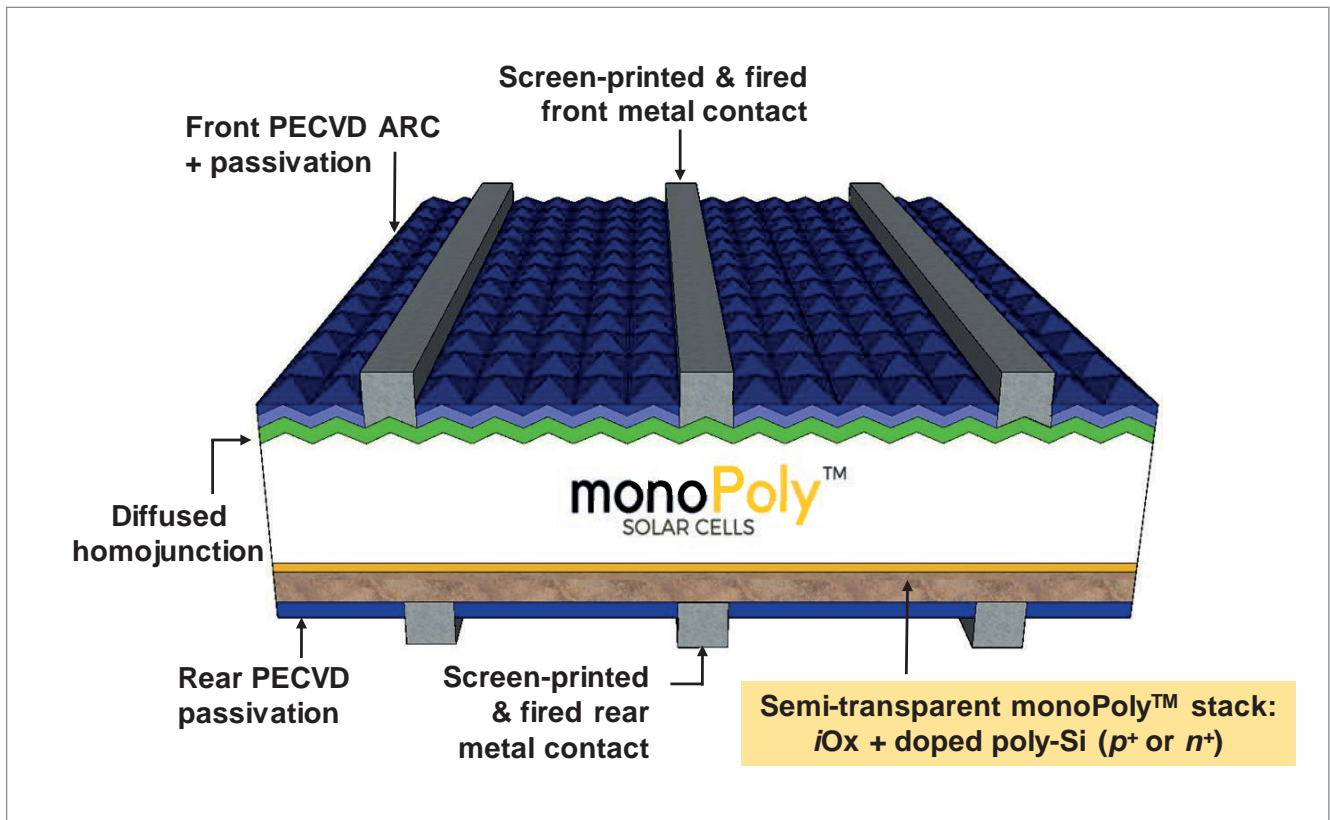


Figure 1. Schematic of a bifacial monoPoly c-Si wafer solar cell with a rear semi-transparent and thin electron-selective passivating contact, and screen-printed (and fired) front and rear metallization.

4. Cost-competitive when compared with standard PERC technology (the most important). This includes low (or no) maintenance and faster return on investment (ROI).
5. Sufficiently transparent layers, which can therefore be used for the front and rear, and which can be used for double-side contacts or all-back-contact designs.

This paper presents the monoPoly platform – an ideal combination, in the authors’ opinion, of all these requirements. The monoPoly technology platform is an upgraded PERC/T production methodology that incorporates the single-side (**mono**facial) application of a screen-printed and fired **poly**crystalline-based’ passivating contact which follows a very lean industrial process flow; moreover, the process can be retrofitted to existing production lines by adding one high-throughput polysilicon tool [26].

The monoPoly technology has achieved conversion efficiencies beyond 23.5% on M2-size wafers, with V_{oc} near 700mV and short-circuit current densities (J_{sc}) of more than 41mA/cm² because of the semi-

transparent nature of the layers. This technology platform is applicable for the rear side as well as for the front of today’s silicon wafer solar cells (Fig. 1).

monoPoly layer properties

The monoPoly stack consists of an interfacial oxide (SiO_x) capped by an n⁻- or p⁺-doped poly-Si layer. The SiO_x layer is grown in situ together with the in situ-doped poly-Si layer. Here the focus is on n⁻-doped poly-Si (n⁻:poly-Si) deposited by inline high-throughput, single-side plasma-enhanced chemical vapour deposition (PECVD). The properties of these layers are twofold: outstanding passivation and semi-transparency.

Outstanding passivation

The surface passivation quality of the interfacial SiO_x/n⁻:poly-Si stack on symmetrical n-type planar Cz-Si samples is summarized in Table 1. Excellent surface passivation properties (both at the c-Si-surface and the metal-doped poly-Si interface) are obtained, and this corresponds well to similar reports by other research groups for passivating contacts [27–29]. A TEM micrograph of 230nm-thick n⁻:poly-Si is also shown in Fig. 2(a).

Table 1. Summary of recombination properties for symmetrical test samples.

	τ_{eff} at $1 \times 10^{15} \text{cm}^{-3}$ [μs]	iV_{oc} at 1 Sun [mV]	J_0 per side at $1 \times 10^{16} \text{cm}^{-3}$ [fA/cm ²]	$J_{0,metal}$ per side [fA/cm ²]	$J_{0,metal}$ on solar cell [area-factored]
No deliberate oxidation step	1,680	711	8.9	-	-
In situ oxidation	3,080	730	3.0	20	~2

WET PROCESSING EQUIPMENT FOR HIGH EFFICIENCY CELLS

600 MW HJT FIELD EXPERIENCE DEMONSTRATES COMPETENCE

Is this also key to you?

- Innovative, young company – building on an engineering team designing and manufacturing for PV for 20 years
- On-site support by design and manufacturing engineers to stay ahead in development
- Engineering to manufacture the highest cell efficiencies in the market
- 20 years of supplying into the top technology cell manufacturers



Choose **exateq** and play safe with latest wet benches for n-type, IBC, and now HJT technology.

Take your process, your technology to the next step – **exateq** serves all needs of manual R&D to automatic pilot wet benches.

Go big - install GWs with exateq's q600 and Do 500 MW in one tool.

Gerry Knoch | gerry.knoch@exateq.de | www.exateq.de

exateq
experience aided techniques

Join us again in 2020 for:



CONFERENCE
PV CELLTECH
2020 10-11th March | Penang, Malaysia

Going into its 5th year, PV CellTech is a truly unique event attended by all of the world's top cell manufacturers, equipment and material suppliers to shape the PV cell technology roadmap. Join us to learn from and network with the PV industry's leaders.

"It is the brains of the drivers of industrial PV condensed in a conference room. I cannot think of a better event, where it is as easy as here to meet and talk to the leaders of key players."
Gerry Knoch, Exateq

"PV CellTech continues to draw technical leaders from all levels of the PV supply chain making it a premium venue for networking"
Bruce Lee, MacDermid Alpha

To get involved either as a speaker, partner or attendee please email: marketing@solarmedia.co.uk

celltech.solarenergyevents.com

Follow us during the year at PV-Tech.org



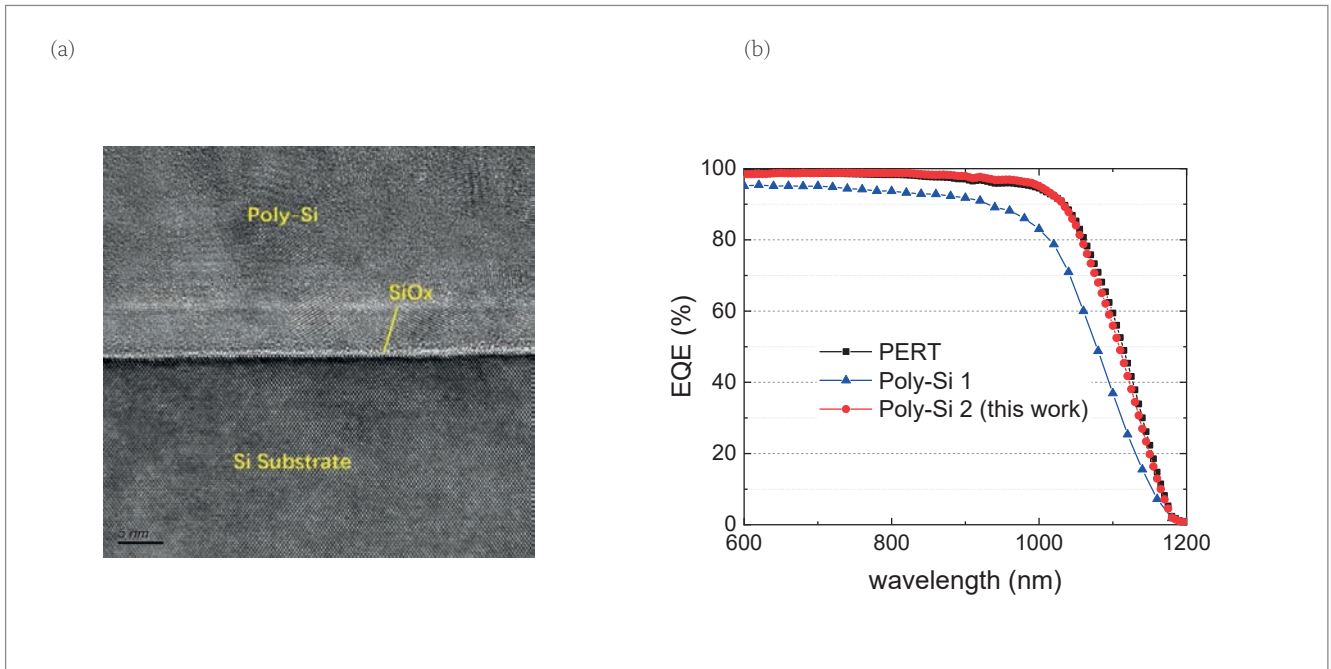


Figure 2. (a) TEM micrograph of the monoPoly stack. (b) External quantum efficiency (EQE) curves for a standard n-type passivated emitter rear totally diffused (PERT) cell with a homogeneous diffused BSF and two poly-Si layers with different optical properties, which affect the near-infrared (NIR) parasitic absorption in a cell. Poly-Si 2 is the optimized stack used in the monoPoly technology.

Semi-transparentcy

It is well known that poly-Si layers are highly absorbing as compared to c-Si. This is potentially detrimental to a solar cell, since it can lead to a loss in generated photocurrent when using doped poly-Si at the rear instead of a standard homogeneously diffused c-Si for the back-surface field (BSF). Fig. 2(b) presents comparisons of the quantum efficiency for 1) a standard n-type passivated emitter rear totally diffused (PERT) cell structure with a homogeneous diffused rear BSF ('PERT'); 2) a cell with a standard LPCVD-deposited poly-Si layer at the rear ('poly-Si 1'); and 3) a cell with a 'semi-transparent' monoPoly layer ('poly-Si 2'). The layer thickness and doping levels were kept similar for groups 2) and 3). The optimized and semi-transparent poly-Si 2 layer at the rear shows a much lower near-infrared (NIR) absorption that is on a par with that of the standard diffused PERT cell.

Application of monoPoly layers at the rear side of n-type bifacial solar cells

The monoPoly stack fabricated using inline PECVD (Meyer Burger, Germany) – when used as the rear passivating contact in an n-type bifacial monoPoly solar cell – yielded excellent cell voltages of greater than 695mV and a peak V_{oc} of 698mV. The rapid progress in the development of this technology (as a result of clever optimization of the inter-related fabrication processes) is highlighted in Fig. 3. Fig. 4 presents comparisons of the $I-V$ parameters of 1) standard n-type PERT (nPERT) cells with a diffused BSF; 2) monoPoly cells with and without the interfacial SiO_x; and 3) after further optimizations. The front and rear dielectric passivation for all

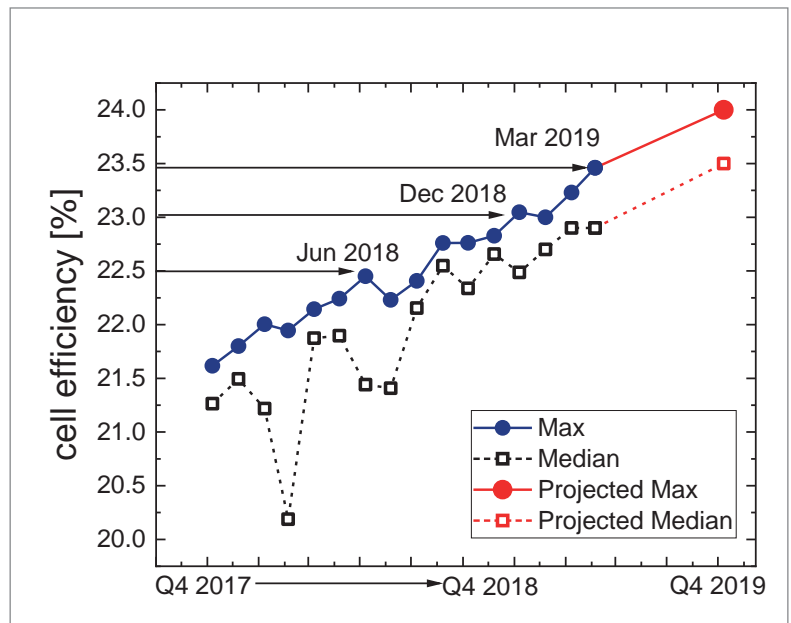


Figure 3. The rapid progress made in improving cell efficiencies for SERIS' n-type monoPoly solar cells.

groups was carried out using MAiA – a patent-protected process (stack) and equipment from Meyer Burger.

A reduction of the rear n⁺:poly-Si thickness to ~120nm gave a peak V_{oc} of 697mV together with a boost in fill factor (FF) due to improved conductivity and uniformity in the poly-Si layer, resulting in a peak cell efficiency of 23,5% and

“The monoPoly process is an eight-step simple and lean process flow that can be easily adapted to existing PERC/PERT production lines.”

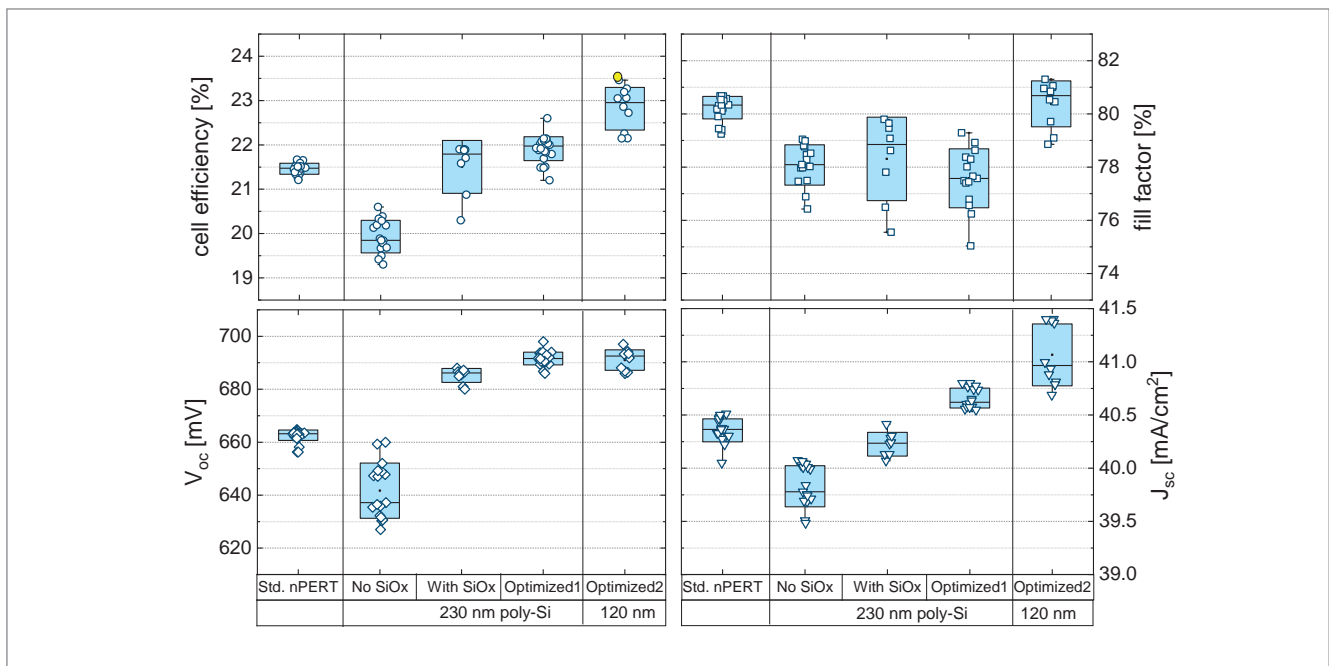


Figure 4. Batch I–V characteristics of n-type Cz-Si bifacial nPERT and monoPoly solar cells with a rear n⁺:poly-Si/SiO_x passivating contact stack fabricated by industrial PECVD with screen-printed front and rear contacts (in collaboration with Meyer Burger, Germany).

a batch median of 22.9%. The reduced poly-Si thickness will, in addition, lead to savings in operational cost and higher throughput in a high-volume production environment, both of which are important in reducing the cost of cell production. If a 100nm/min process is translated to high-volume manufacturing, then this would mean the deposition of the layer for an entire tray in around one minute; this in turn translates to a very high throughput, which has not yet been achieved in the industry. Further optimization of the n⁺:poly-Si layers is expected to further improve the *FF* values to more than 81.5% with a tighter distribution. The authors predict that these improvements, together with additional optimization of the front emitter and front metal pastes, will enable cell V_{oc} values greater than 720mV and efficiencies above 24% to be achieved in mass production.

Table 2 summarizes state-of-the-art *I–V* parameters for lab-type cells (mostly monofacial) and provides a striking comparison with commercially relevant screen-printed large-area (>6") solar cells (mostly bifacial) with high-temperature fired contacts. An attempt has been made to include selected module results available from various resources. This summary is the most comprehensive (to the authors' knowledge) at the time of publication. The module powers shown in Table 2 needs to be carefully recognized, as there is limited knowledge (known publicly) about the actual area of the module, cell gaps, module technology used and importantly the accountability of bifacial gains and method of measurement; therefore, these values are intended not for comparison purposes but rather for literature review.

monoPoly technology platform: retrofitting to existing PERC/T production lines

The introduction of passivating contacts to large-scale solar cell manufacturing is very appealing but at the same time challenging. It requires that the passivating contact be thermally stable when metallized with screen-printed industrial fire-through pastes. Moreover, high-throughput and low-cost deposition schemes for the passivating contacts are necessary.

The typical process flow (without a selective emitter) for standard pPERC and nPERT is presented in Fig. 5 for comparison purposes. The pPERC process has a laser step after passivation, whereas the nPERT process has an additional diffusion and wet-chemical clean to form the rear BSF. (It should be noted that the 'mandatory' stabilization tool widely used in PERC manufacturing lines today has not been included.) Furthermore, both processes use standard screen-printed metallization with high-temperature firing to form the metal contacts.

Over the past two years, SERIS and its key industry partners (including those involved in wet chemistry, boron diffusion, metal pastes and passivation layers) have been fine-tuning SERIS' proprietary monoPoly passivating-contact solar cell technology platform for mass production, which has produced a peak cell efficiency of 23.5%. The monoPoly process – presented in Fig. 5 – is an eight-step simple and lean process flow that can be easily adapted to existing PERC/PERT production lines, with one additional tool required while maintaining the same number of total process steps. This passivating contact process uses a unique 'patent-pending' PECVD process and equipment, enabling a streamlined method of manufacturing. The same lean process is used for the front-side monoPoly application (not shown here in this paper).

	Eff. [%]	V_{oc} [mV]	J_{sc} [mA/cm ²]	FF [%]	Cell details	Module power	Module details
Small-area cells ($\leq 100\text{cm}^2$)							
Fraunhofer ISE	25.7 [2]	724.9	42.5	83.3	n-type, rear poly-Si	–	–
ISFH	26.1 [3]	726.6	42.6	84.3	n-type, IBC	–	–
EPFL	22.6 [13]	719.6	38.8	80.9	p-type, both sides SiC _x	–	–
TU/e Delft	23.0 [15]	701	42.2	77.8	n-type, IBC	–	–
Georgia Tech	23.8 [21]	711.9	41.23	81.1	n-type, rear poly-Si	–	–
ANU	24.7 ^k	704.8	42.4	82.6	n-type, rear poly-Si	–	–
Large-area cells ($\geq 234\text{cm}^2$)							
ECN + Tempress	22.4 [24]	696	–	–	n-type, rear poly-Si	–	–
ISFH	22.3 [25]	714	38.5	81.1	n-type, both sides poly-Si	–	–
Georgia Tech	21.4 [27]	674	39.6	80.0	n-type, rear poly-Si	–	–
GCL	22.95 ^a	698	40.3	81.6	n-type, rear poly-Si	–	–
Jinko	24.2 ^b	724	40.7	82.4	n-type, rear poly-Si	469W (72) ^f	250.2cm ² , 5BB, half-cut
Jolywood	23.3 ^c	705	40.8	81.1	n-type, rear poly-Si	330W (60) ^g / 390W (72) ^g	246.21cm ² , 12BB, full-size
Trina	24.58 ^d	–	–	–	n-type, rear poly-Si	355W (60) [30] / 425W (72) ^h	M4-258.25cm ² , 9BB, half-cut
REC	–	–	–	–	–	330W (60) ⁱ	M2-244.32cm ² , 5BB, half-cut
LG	–	–	–	–	–	340W (60) ^j / 400W (72) ^j	M4-258.25cm ² , 12BB, full-size
SERIS + Meyer Burger	23.5 ^e	697	41.4	81.3	n-type, rear monoPoly	345W (60)	M4-258.25cm ² , SWCT, half-cut

^aPresented at PVCellTech 2019, ^bPress Release Jan. 2019, ^cPresented at nPV Workshop 2019, ^dPV Magazine May 2019, ^ePresented at 9th Silicon PV 2019, ^fPV Magazine Jun. 2019, ^gPresented at 9th Silicon PV 2019, ^hTrina website Jun. 2019, ⁱREC N-Peak White Paper (REC website), ^jPVCellTech 2018 and LG NeON 2 V5 Product Brochure, ^kPVQAT, China 2018.

Table 2. Summary of global state-of-the-art efficiencies of passivating contact cells and some selected module powers.

monoPoly module results

Having an independently verified module result is a testament of a promising commercially applicable technology. Since monoPoly is a new technology which, importantly, uses a new inline PECVD process, it is important to test the cells at the module level. The initial results obtained using the facilities at Meyer Burger for modules with 60 M4-size monoPoly passivating-contact solar cells, which yielded a power output of more than 345W (certified by TÜV Rheinland), are presented here. This power output corresponds to an open-circuit voltage of 41.2V, a short-circuit current of 10.5A and a fill factor of 79.5% for a 60-cell module (I - V parameters presented in Table 3) with a white backsheet and using Meyer Burger’s proprietary smart-wire interconnection technology (SWCT). The results are outstanding for an initial experiment and demonstrate a clear potential for the monoPoly platform to achieve a module power well above 350W with SERIS’ latest 23.5% cells, irrespective of the module interconnection technology. It should be noted that the results

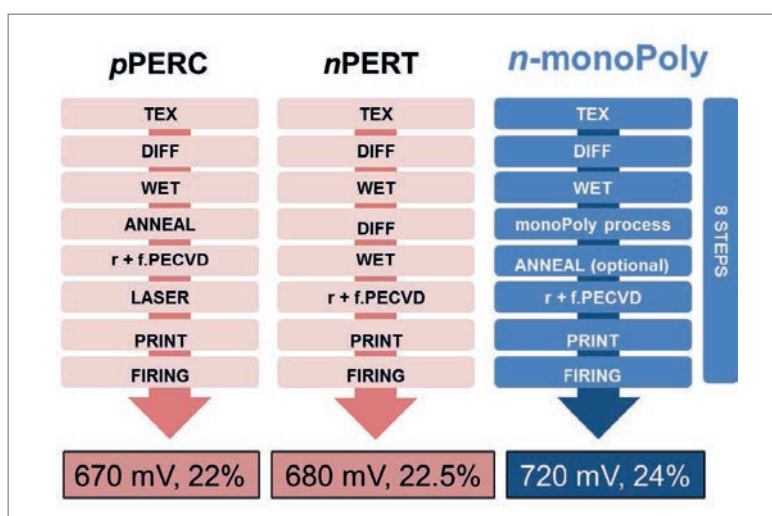


Figure 5. Comparison of the standard PERC and PERT process flows with the simple eight-step process flow for the fabrication of monoPoly solar cells, where the oxide and doped poly-Si can be deposited by PECVD, LPCVD or APCVD.

(for both cells and modules) are obtained in pilot conditions and are expected to further improve when trialled in a mass-production environment.

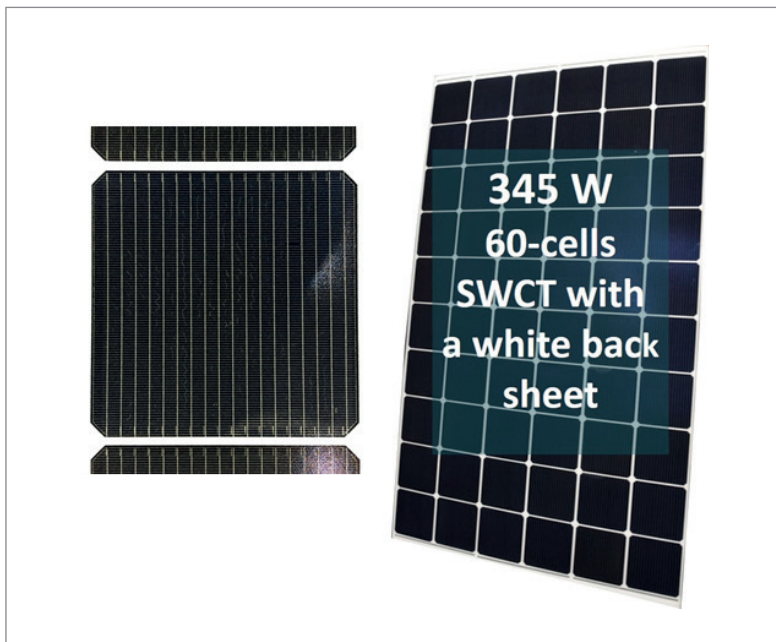


Figure 6. Preliminary module integration of monoPoly cells using smart-wire interconnection technology (SWCT) with 60 full-size cells (in collaboration with Meyer Burger, Germany).

P_{\max} [W]	V_{mpp} [V]	I_{mpp} [A]	V_{oc} [V]	I_{sc} [A]	FF [%]
345.1	34.72	9.94	41.24	10.53	79.5

Table 3. Summary of module I–V parameters for a 60-cell monoPoly module.

Summary

This paper has presented SERIS' monoPoly technology platform, a comprehensive solution for the adoption of passivating-contact solar cell technology in the c-Si PV industry. A simple eight-step process flow was outlined using well-established processes, a new industrial PECVD tool and high-temperature commercial screen-printed metallization. Cell efficiencies of up to 23.5% have been achieved on M2-size wafers, paving the way for the transfer of monoPoly technology to mass manufacturing. Furthermore, initial tests demonstrated a module power of 345W for a module comprising M4-size 60-cell monoPoly cells. The authors predict that next-generation front emitters and tailored screen-printed pastes will take the technology to 24% cell efficiencies.

Acknowledgements

The Solar Energy Research Institute of Singapore (SERIS) is sponsored by the National University of Singapore and Singapore's National Research Foundation (NRF) through the Singapore Economic Development Board. The authors thank Meyer Burger Technology AG for their kind cooperation in the development of the monoPoly cell and module.

“Cell efficiencies of up to 23.5% have been achieved on M2-size wafers, paving the way for the transfer of monoPoly technology to mass manufacturing.”

References

- [1] ITRPV 2017, “International technology roadmap for photovoltaic (ITRPV): 2016 results”, 8th edn (Mar.) [http://www.itrpv.net/Reports/Downloads/].
- [2] Richter, A. et al. 2017, “n-type Si solar cells with passivating electron contact: Identifying sources for efficiency limitations by wafer thickness and resistivity variation”, *Sol. Energy Mater. Sol. Cells*.
- [3] Haase, F. et al. 2018, “Laser contact openings for local poly-Si-metal contacts enabling 26.1%-efficient POLO-IBC solar cells”, *Sol. Energy Mater. Sol. Cells*, Vol. 186, pp. 184–193.
- [4] Mochizuki, H. et al. 1976, “Semi-insulating polycrystalline-silicon (SIPOS) films applied to MOS integrated circuits”, *Jpn. J. Appl. Phys.*, Vol. 15, No. S1, p. 41.
- [5] Matsushita, T. et al. 1976, “Highly reliable high-voltage transistors by use of the SIPOS process”, *IEEE Trans. Electron Dev.*, Vol. 23, No. 8, pp. 826–830.
- [6] Matsushita, T. et al. 1976, “Semi-insulating polycrystalline-silicon (SIPOS) passivation technology”, *Jpn. J. Appl. Phys.*, Vol. 15, No. S1, p. 35.
- [7] Matsushita, T. et al. 1979, “A silicon heterojunction transistor”, *Appl. Phys. Lett.*, Vol. 35, No. 7, pp. 549–550.
- [8] Fossum, J. & Shibib, M. 1980, “A minority-carrier transport model for polysilicon contacts to silicon bipolar devices, including solar cells”, *1980 Int. Electron Dev. Meet.*, pp. 280–283.
- [9] Lindholm, F. et al. 1985, “Heavily doped polysilicon-contact solar cells”, *IEEE Electron Dev. Lett.*, Vol. 6, No. 7, pp. 363–365.
- [10] Yablonovitch, E. et al. 1985, “A 720 mV open circuit voltage SiO_x :c Si: SiO_x double heterostructure solar cell”, *Appl. Phys. Lett.*, Vol. 47, No. 11, pp. 1211–1213.
- [11] Post, I.R., Ashburn, P. & Wolstenholme, G.R. 1992, “Polysilicon emitters for bipolar transistors: A review and re-evaluation of theory and experiment”, *IEEE Trans. Electron Dev.*, Vol. 39, No. 7, pp. 1717–1731.
- [12] Smith, D.D. et al. 2014, “Toward the practical limits of silicon solar cells”, *IEEE J. Photovolt.*, Vol. 4, No. 6, pp. 1465–1469.
- [13] Gizem Nogay, A.I. et al. 2018, “A simple process flow for silicon solar cells with co-annealing of electron and hole selective passivating contacts”, *Proc. 7th WCPEC*, Waikoloa, Hawaii, USA.
- [14] Smith, D.D. et al. 2014, “Toward the practical limits of silicon solar cells”, *IEEE J. Photovolt.*, Vol. 4, No. 6, pp. 1465–1469.
- [15] Yang, G. et al. 2018, “High-efficiency black IBC c-Si solar cells with poly-Si as carrier-selective passivating contacts”, *Sol. Energy Mater. Sol. Cells*, Vol. 186, pp. 9–13.
- [16] Feldmann, F. et al. 2013, “A passivated rear contact for high-efficiency n-type silicon solar cells enabling high V_{oc} s and $FF > 82\%$ ”, *Proc. 28th EU PVSEC*, Paris, France.
- [17] Brendel, R. et al. 2013, “Recent progress and

options for future crystalline silicon solar cells”, *Proc. 28th EU PVSEC*, Paris, France, pp. 676–691.

[18] Feldmann, F. et al. 2014, “Passivated rear contacts for high-efficiency n-type Si solar cells providing high interface passivation quality and excellent transport characteristics”, *Sol. Energy Mater. Sol. Cells*, Vol. 120, pp. 270–274.

[19] Feldmann, F. et al. 2014, “Carrier-selective contacts for Si solar cells”, *Appl. Phys. Lett.*, Vol. 104, No. 18, p. 181105.

[20] Haase, F. et al. 2017, “Interdigitated back contact solar cells with polycrystalline silicon on oxide passivating contacts for both polarities”, *Jpn. J. Appl. Phys.*, Vol. 56, No. 8S2, p. 08MB15.

[21] Rohatgi, A. et al., “Fabrication and modeling of high-efficiency front junction n-type silicon solar cells with tunnel oxide passivating back contact”, *IEEE J. Photovolt.*, Vol. 7, No. 5, pp. 1236–1243.

[22] Stodolny, M. et al. 2016, “n-type polysilicon passivating contact for industrial bifacial n-type solar cells”, *Sol. Energy Mater. Sol. Cells*, Vol. 158, pp. 24–28.

[23] Dutttagupta, S. et al. 2018, “monoPoly cells: Large-area crystalline silicon solar cells with fire-through screen-printed polysilicon contacts”, *Sol. Energy Mater. Sol. Cells*, Vol. 187, pp. 76–81.

[24] Stodolny, M. et al. 2019, “Review and outlook of doped and undoped LPCVD poly-Si based passivating contacts for industrial Si solar cells”, *Proc. 9th SiliconPV/nPV Workshop*, Leuven, Belgium.

[25] Peibst, R. et al. 2018, “Building blocks for industrial, screen-printed double-side contacted POLO cells with highly transparent ZnO:Al layers”, *IEEE J. Photovolt.*, Vol. 8, No. 3, pp. 719–725.

[26] Nandakumar, N. et al. 2019, “Approaching 23% with large-area monoPoly cells using screen-printed and fired rear passivating contacts fabricated by inline PECVD”, *Prog. Photovolt: Res. Appl.*, Vol. 27, No. 2, pp. 107–112.

[27] Tao, Y. et al. 2017, “Carrier selective tunnel oxide passivated contact enabling 21.4% efficient large-area n-type silicon solar cells”, *Proc. 44th IEEE PVSC*, Washington DC, USA, pp. 1–5.

[28] Stodolny, M.K. et al. 2017, “Material properties of LPCVD processed n-type polysilicon passivating contacts and its application in PERPoly industrial bifacial solar cells”, *Energy Procedia*, Vol. 124, pp. 635–642.

[29] Krügener, J. et al. 2017, “Improvement of the SRH bulk lifetime upon formation of n-type POLO junctions for 25% efficient Si solar cells”, *Sol. Energy Mater. Sol. Cells*, Vol. 173, pp. 85–91.

[30] Chen, Y. et al. 2019, “Mass production of industrial tunnel oxide passivated contacts (iTOPCon) silicon solar cells with average efficiency over 23% and modules over 345 W”, *Prog. Photovolt: Res. Appl.*, 10.1002/pip.3180.

About the Authors



Dr. Shubham Dutttagupta is deputy director of the Silicon Materials and Cells (SiMC) Cluster at SERIS and is also head of the Monocrystalline Silicon Wafer Solar Cell Group within the SiMC Cluster. His

research group focuses on the development and commercialization of large-area >25%-efficient crystalline silicon solar cells and high-efficiency processes. His Ph.D. research involved the development of advanced multifunctional materials required for high-efficiency crystalline silicon wafer solar cells.



Dr. Naomi Nandakumar is currently the team leader for advanced manufacturing concepts in the Monocrystalline Silicon Wafer Solar Cell Group within the SiMC Cluster at SERIS, where her research focuses

on the development of advanced high-efficiency silicon solar cells fabricated using industrial processes. She holds a Ph.D. in electrical engineering and an M.Sc. in applied physics from the National University of Singapore (NUS). For her Ph.D. she investigated functional thin films deposited by spatial atomic layer deposition for PV applications.



Dr. John Rodriguez graduated with a Ph.D. in photovoltaics and a bachelor’s in engineering (photovoltaics) from the School of Photovoltaics and Renewable Energy Engineering (SPREE),

University of New South Wales (UNSW), and was a UNSW Co-Op Program scholar. He has worked with leading PV research groups in Asia and Europe since 2006, and currently holds the position of team leader for passivated contact solar cells at SERIS.



Dr. Vinodh Shanmugam received his M.Sc. and Ph.D. in the metallization of silicon wafer solar cells from the National University of Singapore in 2016. He is currently the head of the PV Production Technologies Group

within the SiMC Cluster at SERIS. His research interests include advanced fabrication and characterization of high-efficiency industrial silicon wafer solar cells.

.....

Enquiries

Shubham Dutttagupta
shubham.dutttagupta@nus.edu.sg

inter solar

connecting solar business

The World's Leading Exhibition Series
for the Solar Industry

**INTERSOLAR
EVENTS
2019–2020**

www.intersolar-events.com



SEPTEMBER 3–5, 2019, MEXICO CITY, MEXICO

www.intersolar.mx

NOVEMBER 27–29, 2019, BANGALORE, INDIA

www.intersolar.in

FEBRUARY 4–6, 2020, SAN DIEGO, USA

www.intersolar.us

MARCH 3–5, 2020, DUBAI, UAE

www.intersolar.ae

JUNE 17–19, 2020, MUNICH, GERMANY

www.intersolar.de

AUGUST 25–27, 2020, SÃO PAULO, BRAZIL

www.intersolar.net.br

INTERSOLAR SUMMITS WORLDWIDE

www.intersolar-summits.com

FOLLOW US



Precise and accurate solar cell measurements at ISFH CalTeC

Karsten Bothe & David Hinken, Institute for Solar Research Hamelin (ISFH), Emmerthal, Germany

Abstract

This paper presents the calibration of solar cells, in accordance with the IEC 60904 standards, carried out at the solar cell calibration laboratory of the Calibration and Test Center (CalTeC) at the Institute of Solar Energy Research Hamelin (ISFH). For the calibration of a solar cell, the cell area, the spectral responsivity (SR) and the current–voltage (I – V) curve have to be determined. The I – V curve then yields the characteristic parameters, including the power conversion efficiency, fill factor, short-circuit current and open-circuit voltage. The required measurement facilities and contacting stages are explained in detail; in addition, the measurement procedures are introduced. The precision and accuracy of the resulting characteristic parameters and curves are demonstrated by recent intercomparisons between different international calibration laboratories.

open-circuit voltage V_{oc} , fill factor FF and power conversion efficiency η).

- The temperature coefficients α (for I_{sc}), β (for V_{oc}) and δ (for P_{max}).

Recently, the scope of accreditation was extended to include irradiance sensors as test objects too. For these sensors, ISFH CalTeC certifies the output signal (a voltage or a current) at a defined irradiance (e.g. $1,000\text{W}/\text{m}^2$) and a defined temperature (e.g. 25°C).

All parameters are reported with the accompanied uncertainty following an approved measurement uncertainty analysis. In order to ensure traceability to SI units, all reference devices are calibrated at Physikalisch-Technische Bundesanstalt (PTB) – the National Metrology Institute of Germany. The accreditation is carried out by Deutsche Akkreditierungsstelle (DAkkS) – the national accreditation body of the Federal Republic of Germany – under the registration number D-K-18657-01-00. It has been confirmed that ISFH CalTeC fulfils the ‘General requirements for the competence of testing and calibration laboratories’ of the International Organization for Standardization in ISO/IEC 17025.

Besides providing reference solar cells, calibration laboratories also act as independent bodies in confirming record efficiencies. Record efficiencies are listed most prominently in the regularly published ‘Solar cell efficiency tables’ (see, e.g., Green et al. [2]) in the international journal *Progress in Photovoltaics* (Wiley) as well as in the continuously updated ‘Research cell record efficiency chart’ [3] provided by the National Renewable Energy Laboratory (NREL). ISFH CalTeC is listed as one of seven ‘designated test centres’ participating in international round robins to demonstrate their required measuring accuracy and international comparability in measuring record efficiencies [4]. In three recent international intercomparisons [5–7], ISFH CalTeC showed excellent agreement with the other participants, indicating a high measurement accuracy and precision.

Here, insights into the calibration equipment used at ISFH CalTeC are given, and details of the calibration procedures are presented.

Introduction

As stated in the PV Status Report 2018 published by the European Commission [1], the global investment in 2017 to install about 100GW of solar PV power was €140bn. PV products are currently priced according to their power output measured under standard testing conditions (STC); thus, every per cent uncertainty in output power measurements LEADS to a financial uncertainty of around €1.4bn. Consequently, a precise measurement of PV devices in accordance with worldwide standards and traceable to SI units is of utmost importance. Calibration laboratories play a major role in this value chain, providing reference solar cells as standards for the calibration of solar simulators in laboratory and production environments.

For this purpose, the solar cell calibration laboratory of the Calibration and Test Center (CalTeC) at the Institute of Solar Energy Research Hamelin (ISFH) is accredited for the calibration of solar cells as defined in the IEC 60904 standards. The scope of accreditation includes:

- The area A of the cell or the aperture mask used for measurement.
- The spectral responsivity (SR) of the cell.
- The characteristic parameters of the current–voltage (I – V) curve (short-circuit current I_{sc} ,

“A precise measurement of PV devices in accordance with worldwide standards and traceable to SI units is of utmost importance.”

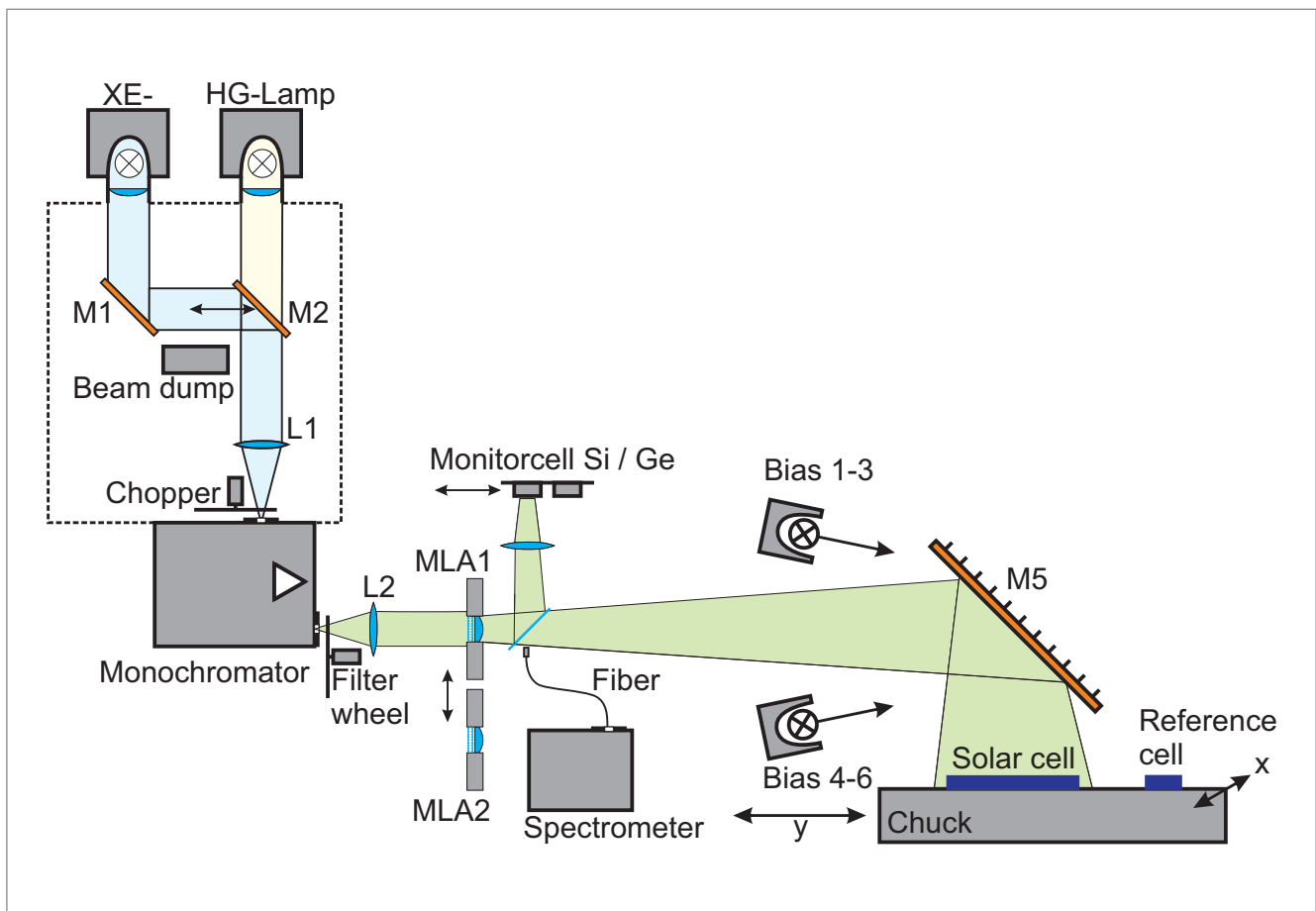


Figure 1. Schematic of the spectral responsivity measurement facility. Mirrors are labelled M while lenses are labelled L. By means of two micro-lens arrays (MLAs), monochromatically irradiated areas of 40×40 and $180 \times 180 \text{mm}^2$ are realized. The chuck is mounted on an x - y stage that allows either the reference cell or the solar cell under test to be irradiated.

Equipment

Three main measuring systems are required for the calibration of solar cells: one to determine the active area, another to determine the spectral responsivity, and a third one to measure the I - V characteristics.

Area measuring facility

The area of the solar cell under test (DUT) is of utmost relevance, since this value is required for calculating the energy conversion efficiency. CalTeC's area measurement system consists of a document and photo scanner which has a resolution of up to 9,600 dpi and is calibrated by means of a photolithographic-defined glass-chrome mask. Depending on the size of the object, expanded measurement ($k = 2$) uncertainties as low as 0.4% are obtained; for typical industrial solar cells with an area around 240.0cm^2 , this uncertainty corresponds to an area of 0.96cm^2 . The calibration of the glass-chrome mask is carried out by the National Metrology Institute of Germany (PTB).

Spectral responsivity measuring facility

The spectral responsivity of the solar cell under test is required for the calculation of the spectral mismatch factor MM, which compensates for differences in the current generation between the

target spectrum (usually AM_{1.5G}) and the spectrum of the sun simulator used for the measurement of the I - V characteristics.

Fig. 1 shows a schematic diagram of the differential spectral responsivity (DSR) facility developed in-house. The set-up consists of a two-beam assembly irradiating the entire solar cell under test simultaneously with white bias light and monochromatic probe light. The monochromatic light is generated using a grating monochromator into which the light of either a xenon or a halogen lamp is coupled. A homogeneous monochromatic illumination in the test plane with an inhomogeneity below 2% for most wavelengths is realized with the help of micro-lens arrays (MLAs), allowing areas of either 40×40 or $180 \times 180 \text{mm}^2$ to be illuminated. The remaining inhomogeneity is measured at 64 homogeneously distributed positions by shifting a world photovoltaic scale (WPVS) [8] reference cell in 20mm steps in the x and y directions. A precise knowledge of the light field homogeneity is essential, since it is necessary to correct for differences in monochromatic light field intensities between the position of the reference cell and the mean value of the large light field. An array of 48 halogen lamps allows bias light intensities of up to $1,600 \text{W/m}^2$ (1.6 suns) to be obtained. The current generation due to

the monochromatic light at the different bias irradiances is measured by means of a lock-in approach. The monochromatic light intensity is modulated using a mechanical chopper at the entrance slit of the monochromator. A transimpedance amplifier developed in-house keeps the solar cell under short-circuit conditions and outputs a voltage signal proportional to the current generated by the monochromatic light. The output signal is then measured with a lock-in amplifier. WPVS reference solar cells calibrated at the PTB are used for calibrating the DSR facility.

I-V curve measuring facility

I-V measurements are carried out using the light from a class AAA solar simulator (WACOM WXS-156 S-L2), shown in Fig. 2. The system comprises a two-lamp system (halogen and xenon) with a light field area of 175×175mm² and is thus compatible with wafer formats up to M6. The inhomogeneity is less than 2%, the long-term instability is under 1%/hour and the divergence (collimating angle) is below 3%.

For the compensation of short-term intensity fluctuations, the solar simulator is equipped with a monitor device and a fast feedback loop. The solar simulator is also equipped with a fast shutter unit, which is used to determine the 25°C-equivalent open-circuit voltage ($V_{oc,eq}$) from the open-circuit voltage measured as a function of time after opening the shutter [9]. A spectroradiometer, a contacting unit for the device under test (DUT) and a WPVS reference solar cell are mounted on a motorized *x* axis; this set-up allows a precise and fast control of the intensity and the spectrum of the solar simulator.

The solar cell measurement unit is equipped with a *z* stage to allow the compensation of contacting chucks of different thicknesses. The measurement unit consists of different components stacked on top of each other. At the bottom, there is a water flow cooling plate, which acts as a re-cooling unit for the array of 16 Peltier elements placed above. Positioned on top of this is a base plate to which different contacting plates can be screwed, depending on the cell type to be investigated. The device temperature can be adjusted to values between 20 and 80°C, allowing reliable measurements of the solar cell temperature coefficients. The contacting to the solar cell is implemented as a four-wire configuration.

A four-quadrant power supply is used for the measurement of the solar cell I-V curve. The current is measured by means of a voltage measurement across calibrated high-power precision shunt resistors. The measured values for voltage, current and temperature are recorded by separate and externally triggered calibrated multimeters. Both n- and p-type solar cells with edge lengths between 20 and 175mm and short-circuit currents of up to 15A are measured.



Figure 2. CalTeC's I-V curve measurement facility. A sun simulator provides a class AAA solar spectrum, while an x-z stage allows irradiation of the reference cell, the spectral radiometer or the solar cell under test.

Contacting units (front and rear)

No explicit standard exists for the design of the solar cell contacting scheme. The IEC 60904-1 recommends a four-wire connection at the cell busbars, and a note in this standard states that it is advisable to choose the contacting method appropriate to the intended use of the cell or of the measurement.

The design of contacting units that yield precise and accurate measurements of the solar cell I-V characteristics, however, represents one of the major challenges in solar cell calibration. Contacting units must be continuously developed to adapt to new metallization designs. For contacting the solar cell front busbars, some authors [10,11] demand a contacting method which reflects the module integration, while others [12,13] recommend a contacting scheme with an infinite number of contact points, thus neglecting the resistivity of the busbar.

Various contacting schemes are available. In order to contact the customer's cells as accurately as possible, the most suitable options are determined together with the customer. The contacting method used for the certified measurements is described in detail on the calibration certificate. In general, it is assumed that there is an infinite number of contact points on the area provided for the purpose of contacting, yielding the fill factor FF_{infc} . This definition

“The design of contacting units that yield precise and accurate measurements of the solar cell I-V characteristics represents one of the major challenges in solar cell calibration.”

enables reproducible measurements between different laboratories and measuring facilities, without explicitly defining the specific contacting scheme; it can also be extended to busbarless solar cells, where the area provided for the purpose of contacting are the fingers. Every real contacting scheme can only be an approximate solution to this. A potential distribution forms between two adjacent contact points and depends on the amount of current flowing and the conductivity of the metallization. It has been shown [14,15] that placing the sense contact at a certain distance from the current contacts yields the reference fill factor FF_{infcp} , even for very low-conductive busbars or fingers. Series resistance effects of the busbars or fingers are effectively cancelled out. A recent study on the impact of the contacting layout on the measured solar cell fill factor [14,15] shows that the best position for sensing corresponds very well to probing the average potential between two current contacts.

For solar cells with an edge length of approximately 156mm, a triplet structure with the voltage pin positioned between two current-carrying pins is used. In order to keep the mechanical load to a minimum, five triplets are homogeneously distributed over the busbar. Each single contact is realized by a spring-loaded contact pin, which is mounted in a 2.5mm-thick vertically positioned printed circuit board (PCB). When the aim is to contact thin busbars of widths smaller than those of the contact probes, the most reliable results are obtained when using probes with a multi-crown head. In all cases, the additional shading of the cell needs to be kept to a minimum in order to minimize the impact on fill factor [16]. Thus, for contacting the front of multi-busbar cells comprising up to 12 busbars, thin

contacting bars with an overall thickness of just 0.8mm have been developed (Fig. 3). The contact is made by means of copper sheets, into which a structure is cut that has a certain spring action.

A full-area brass chuck, shown in Fig. 4(a), is available for contacting the rear side of a solar cell; this particular chuck has integrated vacuum grooves to hold down the cell. In contrast to typical full-rear-area contacting plates, a sensing pin is intentionally not used here; instead, a sensing segment that is glued into the measuring plate is employed. This form of sensing was consciously chosen in order to be able to measure solar cells that are mechanically sensitive, which is often the case for cells comprising stacks of dielectric layers on the rear. Moreover, this contacting plate allows the contacting of the rear of bifacial solar cells, including busbarless bifacial solar cells.

A non-conductive chuck, shown in Fig. 4(b), is also available to allow the local contacting of the rear of bifacial solar cells. Electrical contact to the busbar is established by spring-loaded contact probes; these probes are located in the same positions as the front probes in order to minimize mechanical stress to the cell. The current design of this chuck is optimized for the measurement of solar cells with five busbars. To change the reflectivity of the chuck, optional plates are available.

Solar cell calibration procedure

There are three tasks involved in the standard method for taking a calibrated solar cell measurement: 1) measure the solar cell area or the area of the mask used to define the active area; 2) measure the DSR; and 3) measure the $I-V$ characteristics.

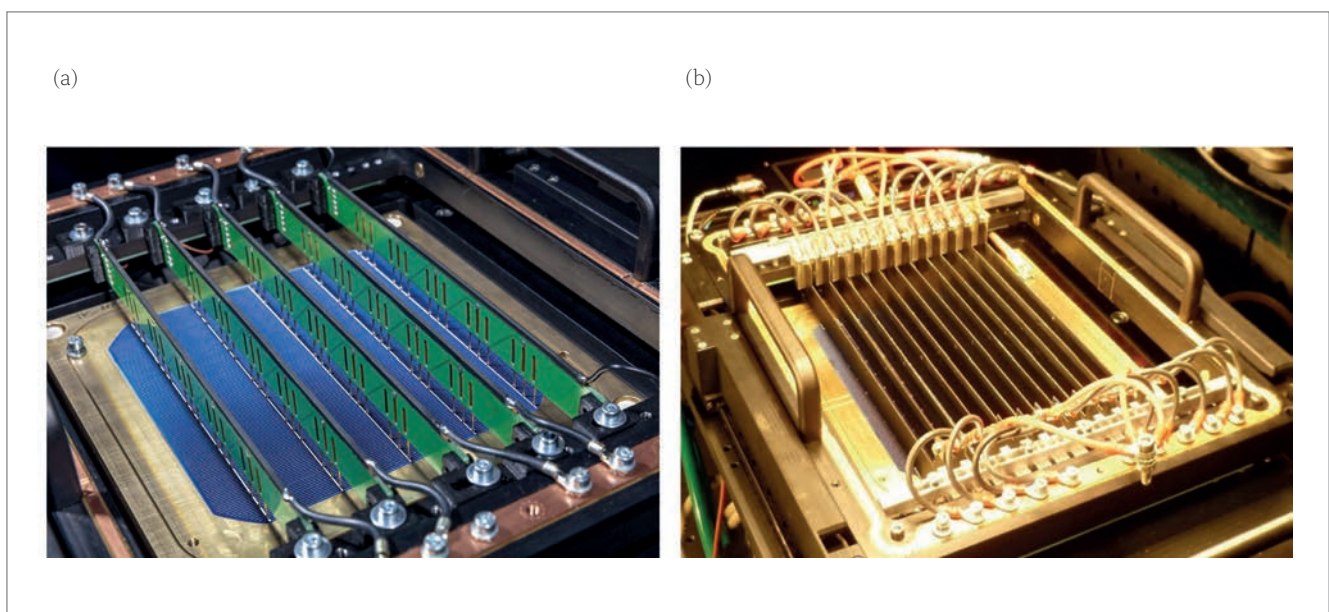


Figure 3. (a) Standard 2mm-wide contacting bars with spring-loaded contact pins for contacting solar cells with up to six busbars. (b) Thin 0.8mm-wide contacting bars for contacting solar cell with up to 12 thin busbars.

Area measuring procedure

The area measurement is a comparative measurement. In a first step, a photolithographic-defined segment of a chrome-glass mask reference sample is scanned. The sharp edge of the photolithographic-defined segment yields a scanned image with a well-defined edge. By means of a predefined threshold value, it is possible to specify which pixels will be counted to define the reference area. With the knowledge of the area of the reference segment from a primary calibration, the area of one pixel can then be calculated.

In a second step, the solar cell under test is measured and all pixels belonging to the cell area are counted by defining an appropriate threshold

“Since the measurement of the entire $I-V$ curve takes considerably longer than the measurement of I_{sc} alone, the correct thermal conditions must be ensured.”

value. Since the pixel area is known from the previous calibration, the area of the sample under test, or the area of the mask used to define the active solar cell area, can be calculated.

Spectral responsivity measuring procedure

To determine the spectral responsivity of the DUT, the relative DSR is measured between 280 and 1,200nm in 10nm steps at 25°C. To address

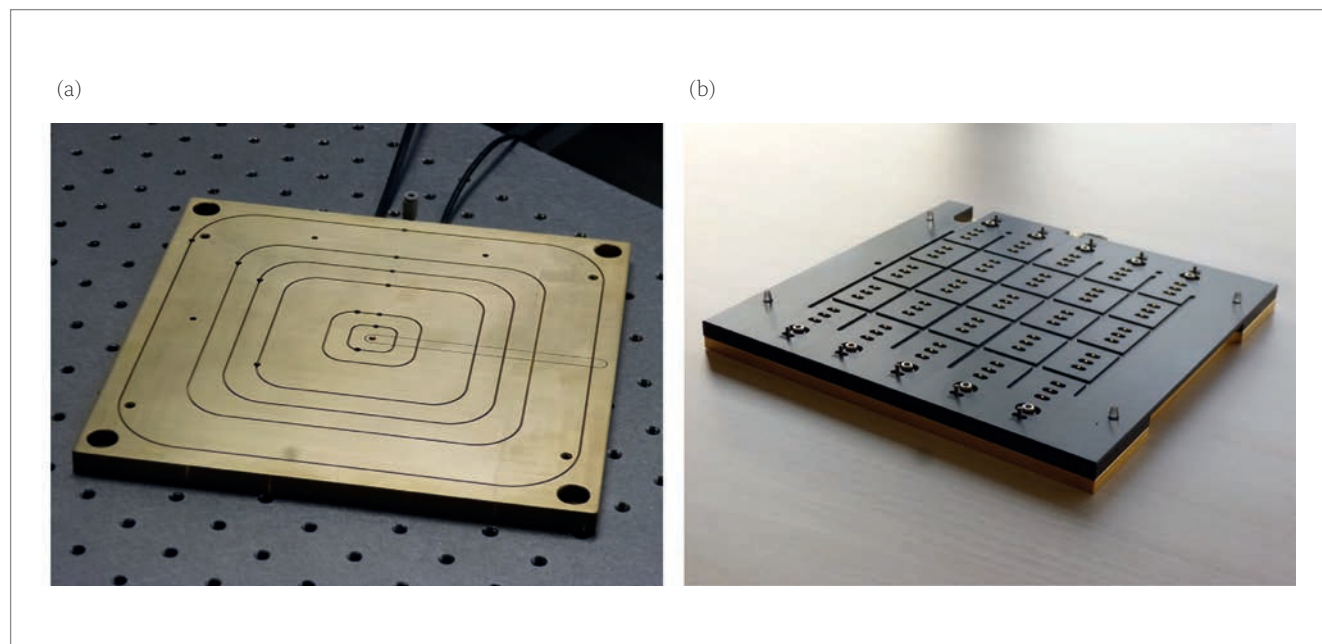


Figure 4. (a) A standard rear-contacting unit with an electrically isolated sensing segment embedded into the contacting plate. (b) A bifacial contacting unit for local rear contacting of solar cells with five busbars.

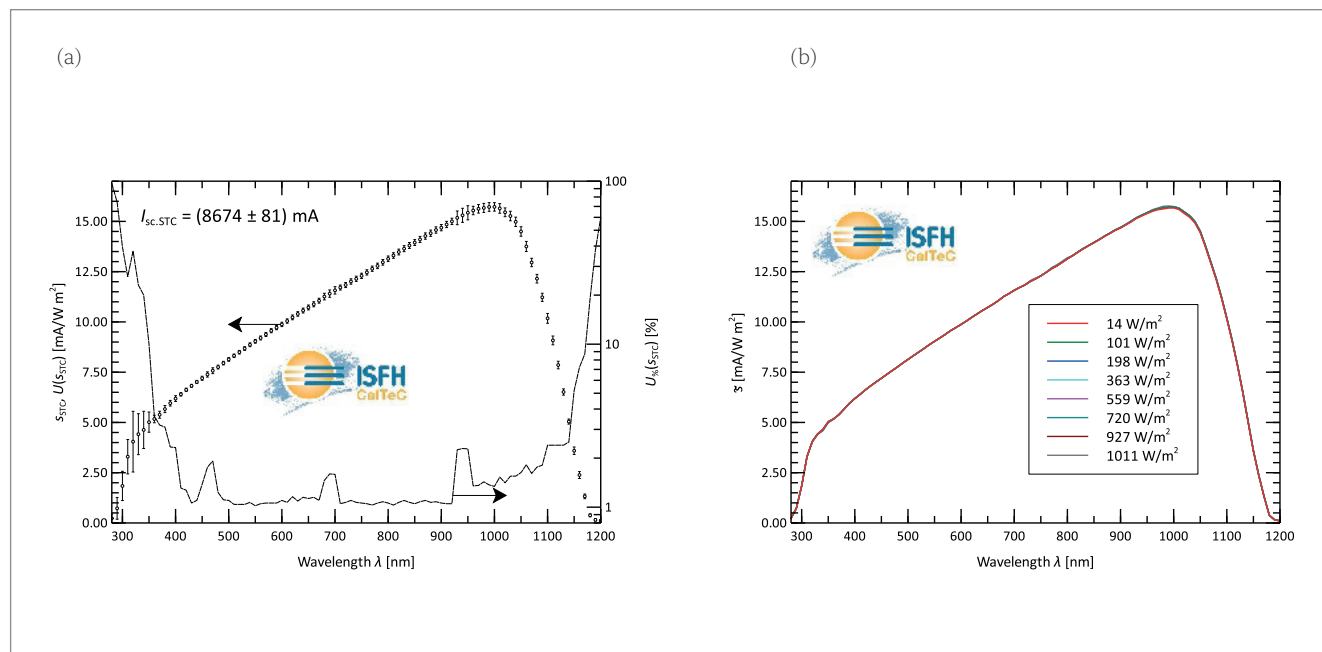


Figure 5. (a) Spectral responsivity curve of a 156x156mm² large-area industrial silicon solar cell; (b) the set of eight DSR curves used for the calculation.

non-linearities, this data acquisition is repeated at more than six bias irradiance levels E ranging from 10 to 1,100 W/m². If measurements of the solar cell temperature coefficients are requested, an additional set of measurements is performed at 50°C to account for temperature-dependent changes in the spectral mismatch factor MM.

The relative (non-differential) SR is derived mathematically from this DSR data set [17]. The SR curve is used in the subsequent I - V curve measuring procedure to calculate the spectral mismatch correction factor MM [18]. Thus, the correct short-circuit current I_{STC} of the DUT is determined; this I_{STC} value is then used to scale the measured relative DSR and the calculated relative non-differential SR curves to absolute units. A typical final spectral responsivity data set as provided in the calibration document is shown in Fig. 5.

I - V curve measuring procedure

The measurement of the I - V curve is carried out in three steps. The first step consists of determining the shadowing-free short-circuit current of the solar cell without any shading due to a contacting scheme. In the second step, the contacting scheme is implemented for the full I - V curve, and the irradiance of the sun simulator is increased to obtain the same shadowing-free short-circuit current measured in step 1. Finally, in the third step, the entire I - V curve is measured.

The DUT is kept at 25.0°C in darkness, and the I_{sc} measurement is performed directly after opening the high-speed shutter as a function of time. The minor heating of the solar cell during this short period of time can be neglected because of the small temperature coefficient of I_{sc} .

The measurement of I_{sc} requires that there is negligible shading from the contacting unit;

this is realized by electrically contacting the cell with Kelvin probes on the outer end of the cell busbars. Since a low busbar conductivity might cause considerable deviation from short-circuit conditions, the voltage on the busbar at the middle of the cell is measured. If this value is above 200 mV, a negative voltage is applied to the Kelvin probes until the centre voltage falls below 200 mV; the maximum allowed negative bias voltage is 1 V. If these requirements cannot be met at the same time, or if the solar cell has an interrupted busbar, a contact bar variation is performed. In this case, I_{sc} is measured as a function of the number of contacting bars, and the shading-free true I_{sc} value is determined by extrapolation to zero busbars.

After I_{sc} has been determined, all contact bars are mounted and the solar simulator irradiance is increased to compensate for the resulting shading. At this stage, the spectral mismatch correction MM is also determined; this factor is always calculated with respect to the actual sun simulator spectrum measured with the integrated spectral radiometer in advance of each calibration.

Since the measurement of the entire I - V curve takes considerably longer than the measurement of I_{sc} alone, the correct thermal conditions must be ensured. The approach taken here is to determine the 25°C-equivalent open-circuit voltage by applying the $V_{\text{oc}}-t$ method [9]. For this, the temperature of the solar cell under test is adjusted in darkness to 25°C, measured on the solar cell rear using a PT-1000 temperature sensor. Afterwards, the solar simulator high-speed shutter is opened and the open-circuit voltage is measured as a function of time. The maximum of the resulting curve is the best approximated value for $V_{\text{oc,eq}}$ at 25°C under illumination.

For the final measurement of the I - V curve, the shutter of the solar simulator remains open. The temperature of the measurement chuck is adjusted until the continuously measured V_{oc} equals $V_{\text{oc,eq}}$. The I - V curve is then measured using a four-quadrant current-voltage source. A defined voltage is applied and the current supplied by the cell is measured as a voltage drop across a calibrated high-power resistor. The current measurement for each data point takes about one second, and the entire I - V curve is measured within one to two minutes, depending on the number of voltage steps used. To check for possible hysteresis effects, two sweeps are performed: the first from V_{oc} to I_{sc} and the second from I_{sc} to V_{oc} . Finally, the characteristic solar cell parameters are extracted using the procedure published by Luque [19] and Paviet-Salomon [20]. A typical I - V curve together with the characteristic parameters is shown in Fig. 6.

Temperature coefficients

The temperature coefficients α , β and δ , corresponding to I_{sc} , V_{oc} and P_{max} respectively, are

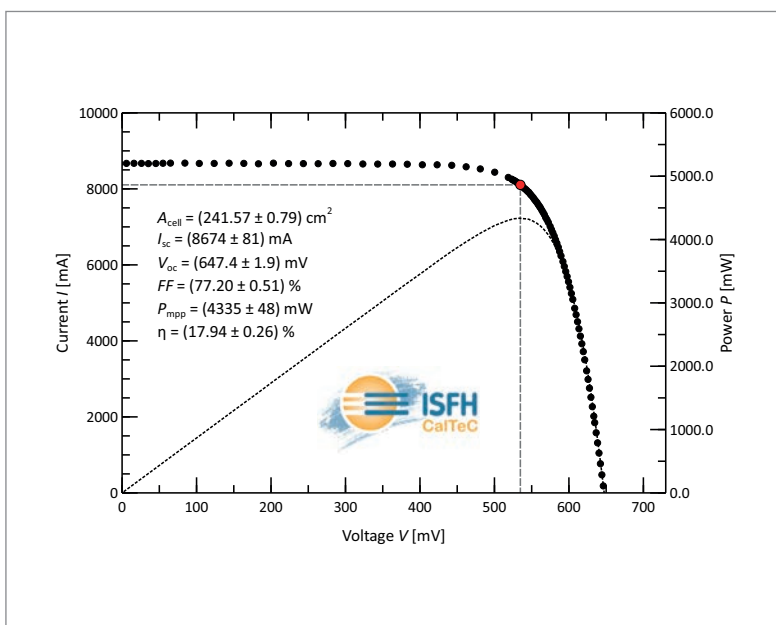


Figure 6. Measured I - V curve and calculated characteristic parameters for a 156×156mm² large-area industrial silicon solar cell.

determined from the $I-V$ curves measured at 20, 25, 30, 40 and 50°C. For each temperature, the desired characteristic parameters are determined and plotted as a function of temperature. Since the solar simulator spectrum is a good approximation of the AM1.5G reference spectrum [21], the change in the spectral mismatch factor is usually so small that an adjustment of the irradiance is subject to greater uncertainty than a mathematical correction. Instead, each $I_{sc}(T)$ value is multiplied by $C = f_{mm}(T_{STC}) / f_{mm}(T)$, with $f_{mm}(T)$ being the spectral mismatch factor at the temperature T , assuming that a spectral mismatch correction was performed for the 25°C measurement. The V_{oc} and P_{max} values need no further correction. The respective data sets are fitted linearly, and the slopes of the fits divided by the reference temperature T_{STC} of 25°C yield the temperature coefficients; as an example, this is shown for V_{oc} in Fig. 7.

International comparability

Within the framework of the EURAMET ENG55 ‘PhotoClass’ project, financed by the European Metrology Research Programme (EMRP), three intercomparisons were recently carried out between eight international solar cell calibration laboratories. One round robin was organized to document the current uncertainty in the measurement of the short-circuit current temperature coefficient [5], while a second one was performed to document variations in the calibration of reference solar cells [6]. A third intercomparison was carried out to provide information about the status of linearity measurements of short-circuit current versus irradiance [7]. In all three intercomparisons, ISFH CalTeC showed excellent agreement with the other participants, confirming the high measurement accuracy and precision of the ISFH solar cell calibration laboratory. To illustrate this, the results relating to α , the short-circuit current temperature coefficient, are shown in Fig. 8.

Summary

ISFH CalTeC provides solar cell calibration measurements in accordance with the requirements of the IEC 60904 standards for laboratory and industrial solar cells as well as for reference cells in WPVS design. The German accreditation body DAkkS confirms that ISFH CalTeC fulfils the general requirements for the competence of testing and calibration laboratories as defined in the IEC/ISO 17025 standard. ISFH CalTeC offers solar cell calibration as a worldwide service.

References

- [1] Jäger-Waldau, A. 2018, “PV status report 2018”, EUR 29463 EN, Publications Office of the European Union, Luxembourg. DOI: 10.2760/826496.
- [2] Green, M.A. et al. 2019, “Solar cell efficiency

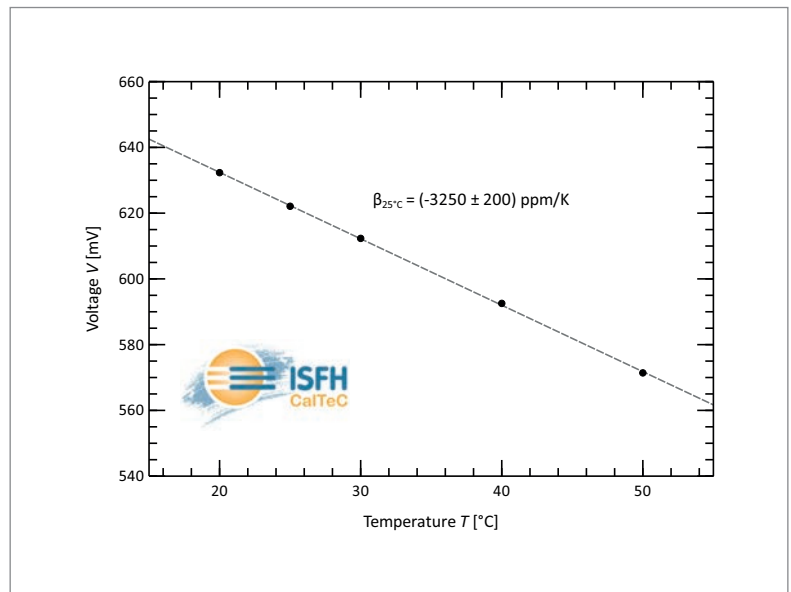


Figure 7. Temperature coefficient β of the open-circuit voltage determined from the slope of a linear fit to a $V_{oc}-T$ data set.

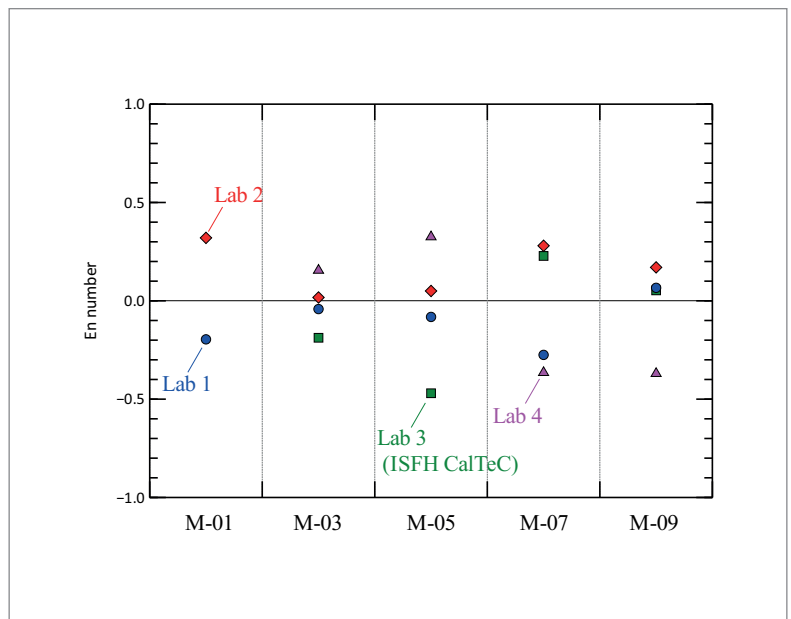


Figure 8. E_n numbers of the temperature coefficient α of the short-circuit current for five different reference cells measured by four different calibration laboratories; ISFH CalTeC is Laboratory 3. The E_n value [22,23] is a measure of how good the agreement is of two measured values when taking into account their measurement uncertainties: $E_n = 0$ corresponds to complete agreement, and $|E_n| < 1$ ensures an overlap of the uncertainty ranges and is often taken as the reference condition. The E_n values are calculated with respect to the weighted mean.

tables (Version 53)”, *Prog. Photovolt: Res. Appl.*, Vol. 27, pp. 3–12. DOI: 10.1002/pip.3102.

[3] National Renewable Energy Laboratory (NREL) 2019, “Best research-cell efficiencies” [https://www.nrel.gov/pv/assets/images/efficiency-chart.png].

[4] Green, M.A. et al. 2018, “Solar cell efficiency tables (version 51)”, *Prog. Photovolt: Res. Appl.*, Vol. 26, pp. 3–12. DOI: 10.1002/pip.2978.

[5] Salis, E. et al. 2019, “Results of four European

“In all three intercomparisons, ISFH CalTeC showed excellent agreement with the other participants.”

Figure adapted from Salis et al. [5].

- round-robins on short-circuit current temperature coefficient measurements of photovoltaic devices of different size", *Sol. Energy*, Vol. 179, pp. 424–436. DOI: 10.1016/j.solener.2018.10.051.
- [6] Kröger, I. et al. 2018, "Results of the round robin calibration of reference solar cells within the PhotoClass project", *Int. J. Metrol. Qual. Eng.*, Vol. 9, p. 8. DOI: 10.1051/ijmqe/2018006.
- [7] Bliss, M. et al. 2019, "Interlaboratory comparison of short-circuit current versus irradiance linearity measurements of photovoltaic devices", *Sol. Energy*, Vol. 182, pp. 256–263. DOI: 10.1016/j.solener.2019.02.031.
- [8] Osterwald, C.R. et al. 1999, "The world photovoltaic scale: An international reference cell calibration program", *Prog. Photovolt. Res. Appl.*, Vol. 7, No. 4, pp. 287–297.
- [9] Emery, K. et al. 1996, "Temperature dependence of photovoltaic cells, modules, and systems", *Proc. 25th IEEE PVSC*, Washington DC, USA, pp. 1275–1278. DOI: 10.1109/PVSC.1996.564365.
- [10] Sinton, R.A. 2012, "Characterization issues for bifacial solar cells", 1st Bifi PV Workshop, Konstanz, Germany.
- [11] Emery, K.A. 2016, "How [NOT] to measure a solar cell to get the highest efficiency", *Proc. 43rd IEEE PVSC*, Portland, Oregon, USA.
- [12] Geisemeyer, I. et al. 2014, "Contacting bare silicon solar cells with advanced cell metallisation", *Proc. 29th EU PVSEC*, Amsterdam, The Netherlands. DOI: 10.4229/EUPVSEC20142014-2BV.8.29.
- [13] Hohl-Ebinger, J. et al. 2008, "Contacting bare solar cells for STC measurements", *Proc. 23rd EU PVSEC*, Valencia, Spain, p. 2012.
- [14] Kruse, C.N. et al. 2017, "Impact of contacting geometries when measuring fill factors of solar cell current–voltage characteristics", *IEEE J. Photovolt.*, Vol. 7, pp. 747–754. DOI: 10.1109/JPHOTOV.2017.2677084.
- [15] Kruse, C.N. et al. 2017, "Impact of contacting geometries on measured fill factors", *Energy Procedia*, Vol. 124, pp. 84–90. DOI: 10.1016/j.egypro.2017.09.329.
- [16] Raj, S. et al. 2017, "Impact of nonuniform illumination and probe bar shading on solar cell I-V measurement", *IEEE J. Photovolt.*, Vol. 7, pp. 1203–1208. DOI: 10.1109/JPHOTOV.2017.2726558.
- [17] Bothe, K. et al. 2018, "Accuracy of simplifications for spectral responsivity measurements of solar cells", *IEEE J. Photovolt.*, Vol. 8, pp. 611–620. DOI: 10.1109/JPHOTOV.2018.2793758.
- [18] IEC 60904-7, edition 3.0, 2008-11, "Photovoltaic devices – Part 7: Computation of the spectral mismatch correction for measurements of photovoltaic devices".
- [19] Luque, A. & Hegedus, S., Eds, 2010, *Handbook of Photovoltaic Science and Engineering*. Chichester, UK: John Wiley & Sons, Ltd. DOI: 10.1002/9780470974704.
- [20] Paviet-Salomon, B. et al. 2017, "New guidelines for a more accurate extraction of solar cells and

modules key data from their current-voltage curves", *Prog. Photovolt. Res. Appl.*, Vol. 25, pp. 623–635. DOI: 10.1002/pip.2872.

- [21] IEC 60904-3, edition 4.0, 2019-02, "Photovoltaic devices – Part 3: Measurement principles for terrestrial photovoltaic (PV) solar devices with reference spectral irradiance data".
- [22] ISO/IEC Guide 43-1, edition 2.0, 1997, "Proficiency testing by interlaboratory comparisons – Part 1: Development and operation of proficiency testing schemes".
- [23] Wöger, W. 1999, "Remarks on the En-criterion used in measurement comparisons" (in German), *PTB Mitteilungen*, Vol. 109, No. 1, pp. 24–27.
-

About the Authors



Karsten Bothe studied physics at the Technical University Braunschweig, Germany, the University of Sussex, Brighton, U.K., and the University of Oldenburg, Germany. In 2006 he received his Ph.D. in physics from the University of Hannover, Germany, for his work on oxygen-related trapping and recombination centres in boron-doped crystalline silicon. After an appointment as a research fellow at the Nara Institute of Science and Technology (NAIST), Japan, in 2007, he became head of the solar cell characterization group at ISFH. Since 2016 he has been in charge of the solar cell calibration laboratory at ISFH CalTeC.



David Hinken studied physics at the University of Hannover, Germany, and the University of La Laguna, San Cristóbal de La Laguna, Spain. He received a Diploma degree in physics from the University of Hanover in 2007, followed by a Ph.D. in physics from the same university in 2012, with a thesis topic of luminescence-based characterization of crystalline silicon solar cells. In 2015 he joined the solar cell calibration laboratory of ISFH CalTeC as deputy head, where he is responsible for solar cell calibration equipment, scientific supervision and customer service.

.....

Enquiries

Dr. Karsten Bothe
Institute of Solar Energy Research Hamelin (ISFH)
Calibration and Test Center
Solar Cells and Sensors
Am Ohrberg 1
31860 Emmerthal
Germany

Email: solarcells@caltec.isfh.de
Website: www.caltec.isfh.de

Heterojunction technology: The path to high efficiency in mass production

Igor Shakhray, Alexey Abramov, Sergey Abolmasov, Ekaterina Terukova & Dmitriy Andronikov, Hevel Group, Moscow, Russia

Abstract

Heterojunction technology is currently a hot topic actively discussed in the silicon PV community. Hevel recently became one of the first companies to adopt its old micromorph module line for manufacturing high-efficiency silicon heterojunction (SHJ) solar cells and modules. On the basis of Hevel's own experience, this paper looks at all the production steps involved, from wafer texturing through to final module assembly.

Introduction

In recent years, many solar cell and module producers in the silicon PV industry have been forced to adapt their existing production lines to new technologies in order to be able to deliver highly efficient and low-cost modules to the market. The most popular transfer has been from Al back-surface field (Al-BSF) to passivated emitter and rear cell (PERC) technology, since the latter is compatible with existing production lines used for standard technology. Nevertheless, excellent crystalline silicon (c-Si) surface passivation by hydrogenated amorphous silicon (a-Si:H) offers the possibility to employ the most expensive part of silicon thin-film production lines, namely plasma-enhanced chemical vapour deposition (PECVD) systems, for silicon heterojunction (SHJ) technology, as recently realized by Hevel LLC.

The simple structure of SHJ solar cells, in combination with their high efficiency and low-temperature processing, makes them very attractive to the PV industry. This is the reason why Hevel has decided to start a project on modernizing and transforming its micromorph module production line, which includes a large number of PECVD systems (KAI-MT PECVD reactors from TEL Solar), into a new SHJ line. The successful conversion of Hevel's production line for the manufacture of SHJ solar cells and modules was completed in April 2017 using an in-house SHJ solar cell technology developed by its R&D Center for Thin Film Technologies (TFTE – an R&D unit of Hevel).

The annual production capacity was increased from an initial 97MWp (for the micromorph line)

to 160MWp during the first phase of the project, with an average SHJ cell efficiency of 21% being demonstrated in mass production. Meyer Burger's SmartWire Cell Technology (SWCT) was chosen for interconnection in SHJ module assembly. During the second phase of the project (June 2017–May 2019), the production capacity of Hevel's production line was increased to 260MWp, with an average cell efficiency of 22.8% obtained in mass production.

Technology development

As can be seen in Fig. 1, SHJ cells have very simple structure and it takes only six process steps to fabricate them. Typically, the SHJ cell is composed of an n-type c-Si wafer coated on both sides with thin intrinsic and doped a-Si:H layers. The ultrathin intrinsic a-Si:H layers, with typical thicknesses of a few nanometres, have a crucial effect on the performance of SHJ cells. The aim of these layers is to suppress surface recombination by chemical passivation of dangling bonds on the c-Si wafer surface with the formation of Si-Si and Si-H bonds, as well as to prevent defect generation by dopant atoms during the deposition of doped layers. The doped layers are fully covered with indium tin oxide (ITO) films, followed by screen-printing of contact metal grids for current collection using a low-temperature conductive (LTC) Ag paste. To enhance the properties of the ITO layers and contact grids, low-temperature annealing is required.

Wafers for SHJ cells

As in the case of all high-performance c-Si solar cells, wafer quality is key to achieving high-efficiency SHJ cells. Although record efficiency values reported in the literature have been obtained using high-purity float zone (FZ) c-Si wafers, the development of the Czochralski process and the continuous improvement of polysilicon quality have allowed the impurity concentrations in CZ wafers to be reduced while keeping production costs reasonable. As a result, the open-circuit voltage (V_{oc}) of SHJ cells has recently reached values as high as 750mV.

Up to now, only monocrystalline CZ wafers have been used for large-scale manufacturing of SHJ solar cells. The electronic properties of monocrystalline silicon wafers for high-efficiency solar cells are determined by impurities and

“The simple structure of SHJ solar cells, in combination with their high efficiency and low-temperature processing, makes them very attractive to the PV industry.”



For Next Generation Solar Technologies Trust the Adhesives Experts

Whether its thinner wafers, heterojunction and tandem cells or high-density modules, **rely on Henkel know-how**. We've been inventing market-leading electrically conductive adhesives (ECAs) for over six decades.

Henkel's custom ECA's for solar deliver:

- **Maximum cell efficiency** – Eliminate thermal damage to the cell
- **Improved CTM losses** – Reduce resistive losses and improve module level efficiency
- **High yield** – Prevent cell warpage, string alignment issues and tight process windows
- **Fundamental reliability** – Eliminate solder cracking and low-temperature solder fatigue
- **Longevity** – Deliver best-in-class power degradation over service lifetimes
- **Reduced costs** – Compatible with busbarless cells, < 40% silver reduction
- **Scalability** – Engineering services ensure designs are fit-for use at scale
- **Fast time-to-market** – Equipment Sets co-designed with LOCTITE®, ensuring productivity targets met
- **Partnership trust** – Leader in ECA technology at the GW scale. Zero field failures to date.



For more information, call 1-888-943-6535, scan the QR code or visit us online at henkel-adhesives.com/electronics

All marks used are trademarks and/or registered trademarks of Henkel and its affiliates in the U.S., Germany and elsewhere.
© 2019 Henkel Corporation. All rights reserved. (08/19)



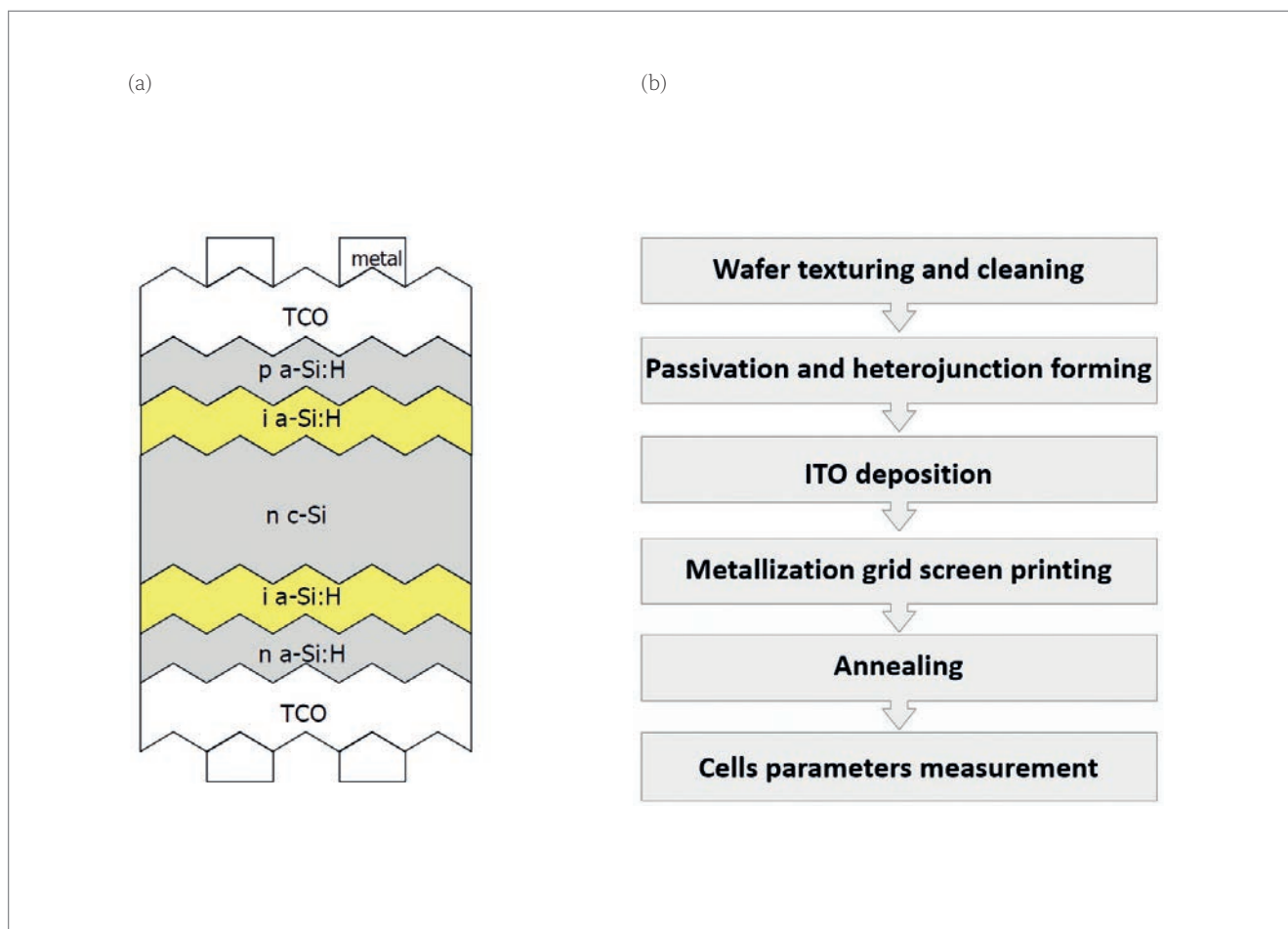


Figure 1. (a) Schematic cross-sectional view of a conventional SHJ solar cell. (b) The main steps of the SHJ cell fabrication process sequence.

dopant concentrations. Since the measurement of these parameters require special techniques that can hardly be used in the mass production process, the minority-carrier lifetime and wafer resistance are usually measured in practice and constitute the main parameters for determining the quality of wafers or ingots. These parameters usually vary along and across ingots, and their profiles depend on the details of the ingot growth process and post treatment. Consequently, it has been proposed to use the measured lifetime/resistance ratio as a cumulative measure of wafer and heterojunction qualities. Recent studies have also shown that for SHJ cells with $V_{oc} > 750\text{mV}$, passivated wafers with a lifetime-to-resistivity ratio above $4\text{ms}/\Omega\text{cm}$ must be used.

The most significant advantage of SHJ technology in terms of cost reduction is that all process steps are performed at low temperatures ($< 250^\circ\text{C}$), favouring the use of thin wafers for SHJ solar cell production. Recent progress in wafer slicing technology as a result of the implementation of diamond wire technology has resulted in the mass production of low-cost wafers with thicknesses less than $160\mu\text{m}$. Wafers with an as-cut thickness of $150\mu\text{m}$ have recently been successfully implemented in the SHJ production process without module power losses, as illustrated in Fig. 2. Although

further reductions in SHJ cell thickness are also possible without significant losses in efficiency, the implementation of thinner wafers in mass production is currently limited by handling issues, resulting in excessive wafer breakage rates.

A slight decrease in I_{sc} here is partially compensated by the V_{oc} gain, leading to a very small ($< 0.1\%$) efficiency loss when switching to $150\mu\text{m}$ as-cut wafer thickness in the cell production. At the module level, the cell efficiency loss is fully compensated by a 10% decrease in cell-to-module (CTM) ratio. The overall benefit of switching to $150\mu\text{m}$ wafers is on average around 1–1.5W per module.

The latest update to wafers was carried out in May 2019. The existing SHJ production line is able to adapt wafers of size $157.35\text{mm} \times 157.35\text{mm}$ (M2+ wafer type). The use of such wafers with an optimized contact grid design leads to a power increase per cell of 0.15W (Fig. 3). Hevel's R&D Center is also currently working on further developments using M4 and M6 wafers as well as full square wafers and wafers with lower oxygen concentration.

“An enhanced cleaning procedure is necessary for the production of high-efficiency SHJ cells.”

Wafer texturing and cleaning

As with other c-Si PV technologies, wet chemical treatment is the first step in the SHJ cell production sequence. The following steps are usually included:

- Etching of the highly defective surface part of the wafer (surface damage etch – SDE).
- Forming of the special surface morphology (texture) which reduces light reflection from the wafer surface (TEX).
- Cleaning of the wafer surface to remove organic and metal impurities.

While the first two steps based on isotropic (SDE) and anisotropic (TEX) alkali etching are similar to those used in other silicon PV technologies, the last step is significantly different. To obtain high-quality surface passivation, the wafer surface should be extra clean. An enhanced cleaning procedure is therefore necessary for the production of high-efficiency SHJ cells; this includes the removal of

residual organic, ionic and metallic contamination (originating from the wet etching/texturing solutions) from c-Si wafer surface. In addition, heavy deionized (DI) water rinse steps are used between each chemical treatment. The wet chemical treatment ends with a short HF dip, which removes native oxide and passivates the c-Si surface with hydrogen atoms prior to the a-Si:H PECVD processes.

Much effort has been devoted at Hevel to stabilizing and optimizing the wafer texturing and cleaning processes. One of the steps of the optimization was a change to a single-component texturing additive; such an optimization enabled an increase in batch lifetime and a reduction in the consumption of chemical reagents.

Surface passivation and junction formation

High-quality surface passivation is key to achieving high values of V_{oc} in high-efficiency silicon-based solar cells. An insertion of thin (< 10nm) hydrogenated amorphous silicon (a-Si:H) layers between the c-Si wafer and the doped a-Si:H layers leads to higher V_{oc} values in comparison to those registered in the case when intrinsic

VON ARDENNE 

www.vonardenne.biz

GWATT
IGA ATT

XEA|nova® L
up to 10 000 wafers/h

XENIA
width: up to 3 m

FUTURE-PROOF COATING EQUIPMENT
MAXIMUM PERFORMANCE FOR MINIMUM CAPEX PER GIGAWATT

Are you looking for coating equipment with a low cost of ownership for crystalline or thin-film photovoltaics and for technologies such as HJT, IBC, CIGS or passivated contacts? We can provide you with future-proof technology and system solutions for all scales of production.

Visit our booth at the EU PVSEC 2019 (booth E5) for more information.

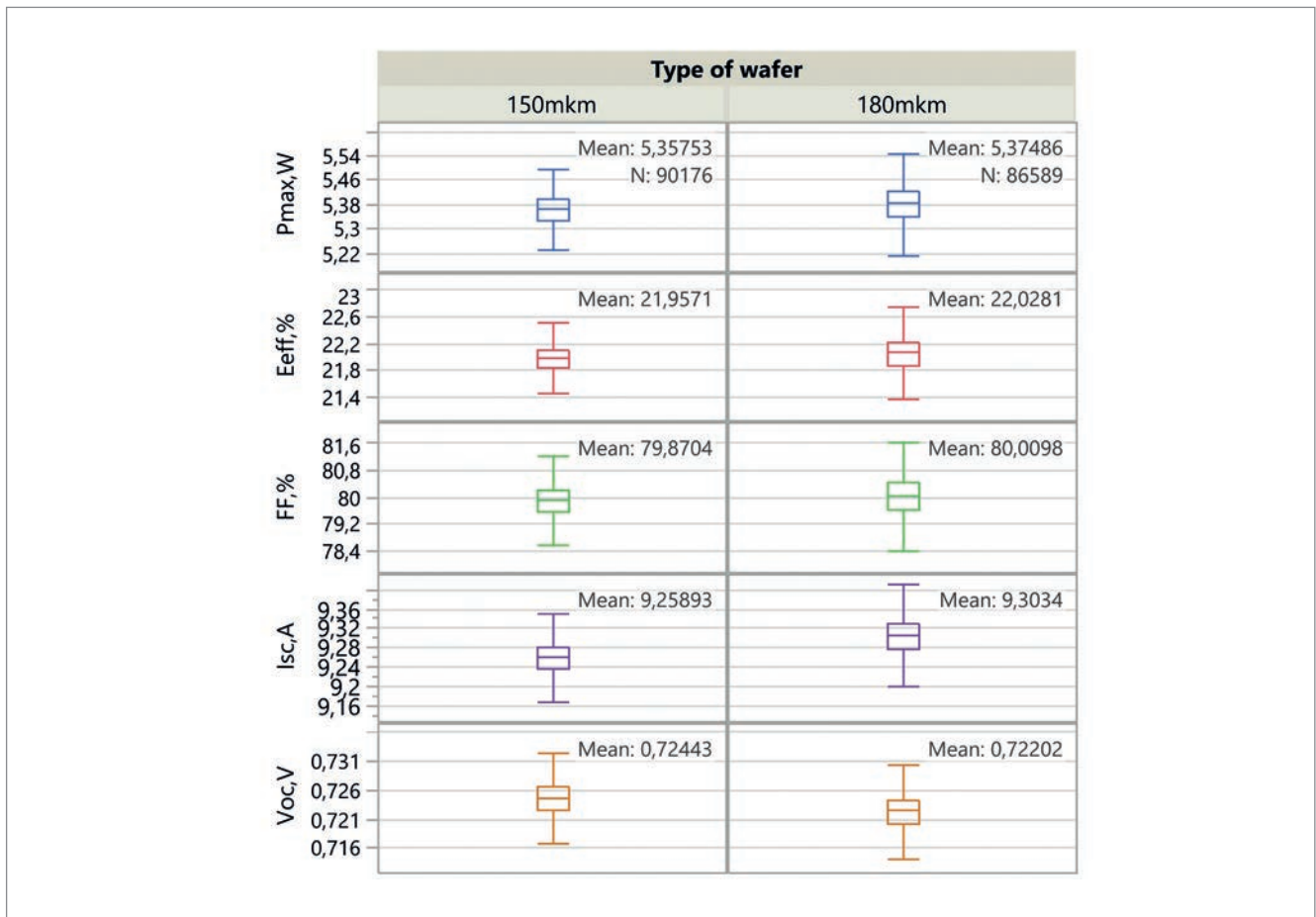


Figure 2. Results of 150µm-thick wafer implementation.

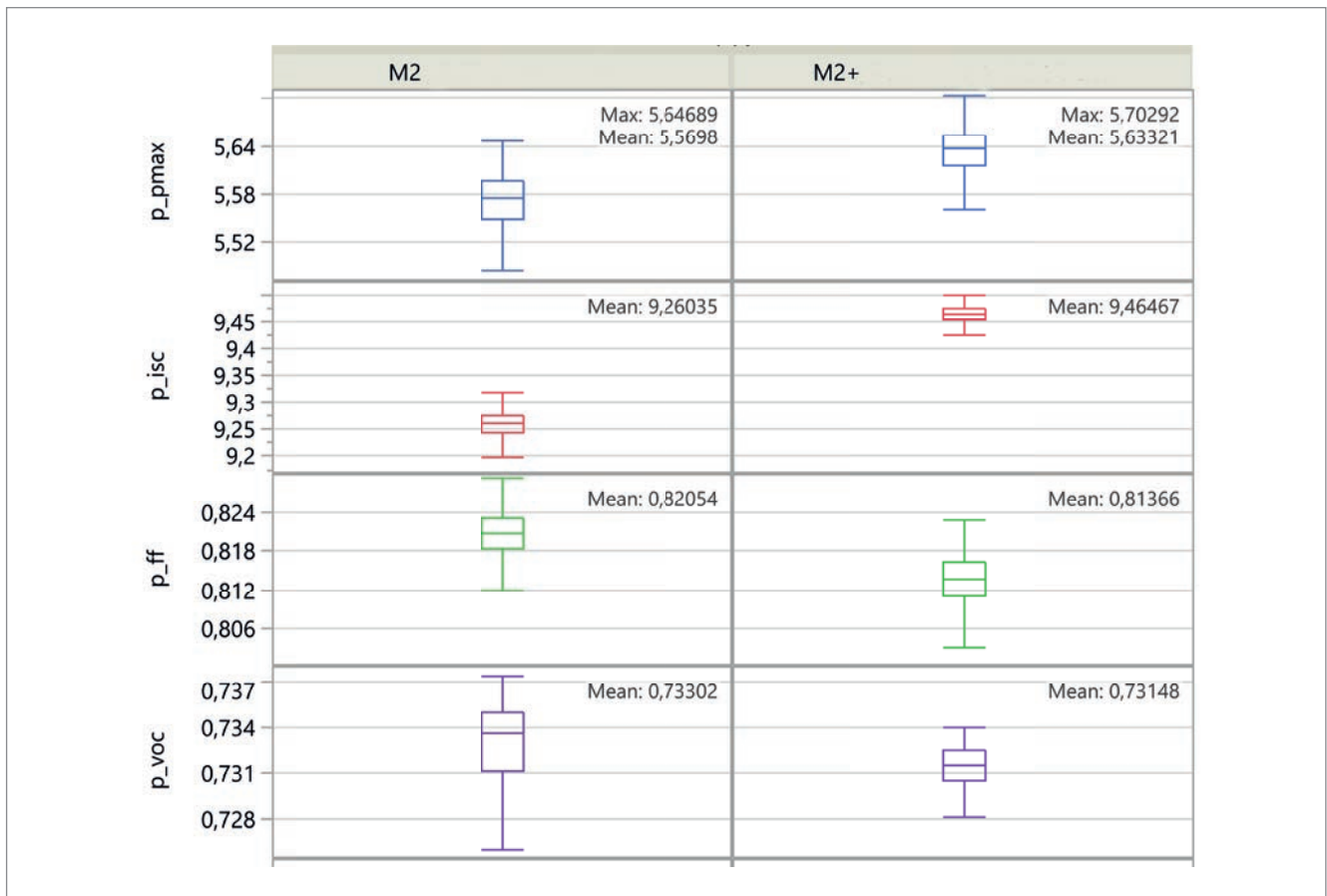


Figure 3. Results of larger-area wafer (M2+) implementation.

“Thinner rear ITO layers with higher transparency could increase the cell efficiency as a result of the better utilization of light in the IR part of the spectrum.”

a-Si:H layers are absent. In the last two decades, the surface passivation of SHJ cells has been essentially improved by many research groups, resulting in V_{oc} values close to 750mV; this is approaching the theoretical limit (760mV) and underlines the particular appeal of this technology.

As a rule, a necessary condition for good surface passivation is that the a-Si:H/c-Si interface should be atomically sharp, meaning that silicon epitaxial growth is avoided, i.e. no crystalline material is deposited. This can be achieved by a proper tuning of the a-Si:H film properties during the deposition process. In practice, a-Si:H layers are commonly grown by the PECVD method using parallel-plate capacitively coupled plasma discharge in pure silane or in silane-hydrogen mixtures at temperatures close to 200°C. It appears that the most critical process parameters for surface passivation are the hydrogen-to-silane gas flow

ratio and the RF power density, whereas the gas pressure may affect the film thickness uniformity.

The properties of doped layers can also have a big impact on cell performance: for example, an appropriate tuning of the thickness and doping profile of the n layer resulted in a 0.5% gain in cell efficiency, whereas in the case of the p layer the gain was about 0.1%.

Transparent conductive oxides

ITO layers are commonly used in SHJ cells as transparent conductive oxide layers, and it is very important to optimize their properties, in particular for the production of bifacial HJT solar cells. An investigation of the various stoichiometric contents of ITO sputter magnetron targets has been carried out at Hevel's R&D Center. It was found that thinner rear ITO layers with higher transparency could increase the cell efficiency as a result of the better utilization of light in the IR part of the spectrum. Such an improvement resulted in a module power increase of 3.7W because of the lower CTM loss, as well enabling a reduction in the cost of cell production, since 90:10 ITO targets are about 6% cheaper than standard 97:3 ITO targets. The optimized

THE WET PROCESSING COMPANY

R | E | N | A |

RENA BatchTex SHJ

Proven wet chemical texturization & cleaning for mass production of silicon heterojunction solar cells

Visit us!
EU PVSEC
RE India Expo
www.rena.com

recipes for ITO layers were implemented at Hevel's production line in Q1 2018.

Another approach taken for ITO layer optimization was the addition of an Ar/H₂ mixture during magnetron sputtering (Fig. 4); this method resulted in a power increase of 20mW per cell. In addition, many experiments are still ongoing with other special magnetron targets having higher Hall mobility. Some of these targets have already been tested at Hevel's R&D Center and showed promising results which justify further testing at the production facility.

To minimize the cost of cell production, the use of so-called *dogbone* targets is now under consideration. Targets of this type could bring about a lower target utilization rate, further decreasing cell production costs. Additional optimizations have been performed whereby the physical vapour deposition (PVD) tray has been changed and contact grid designs have been modified in order to minimize the inactive area losses. The modules assembled with such cells demonstrated an average increase in power of 1.8W.

Metallization

The process requirements for manufacturing SHJ solar cells have several advantages compared with those for conventional homojunction c-Si solar cells. The first advantage is the low thermal budget during the heterojunction formation; the deposition temperature of a-Si:H and ITO layers is usually less than 250°C. Second, the time required to form the a-Si:H/c-Si junctions and contact layers is also shorter for SHJ cells than for conventional c-Si solar cells based on

	Standard BOM	Optimized BOM and cell
P_{max} [W]	304	328
V_{pmax} [V]	34.72	36.66
I_{pmax} [A]	8.76	8.94
I_{sc} [A]	9.4	9.42
V_{oc} [V]	43.34	43.94
FF [%]	74.6	79.3

Table 1. Mean production values for the module I–V characteristics with standard and optimized BOM, including cell power optimization.

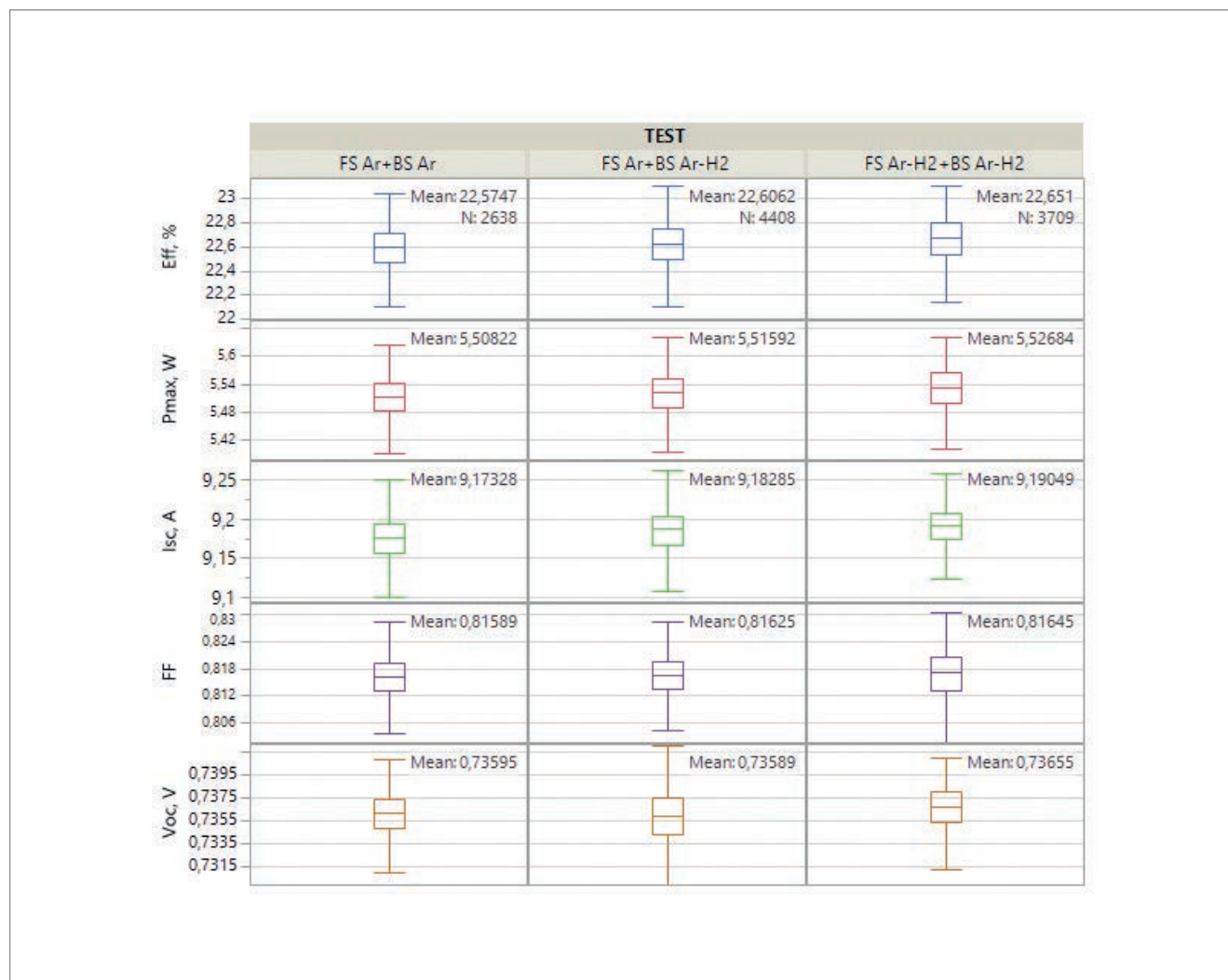


Figure 4. Results of ITO layer optimization by adding an Ar/H₂ mixture during magnetron sputtering.

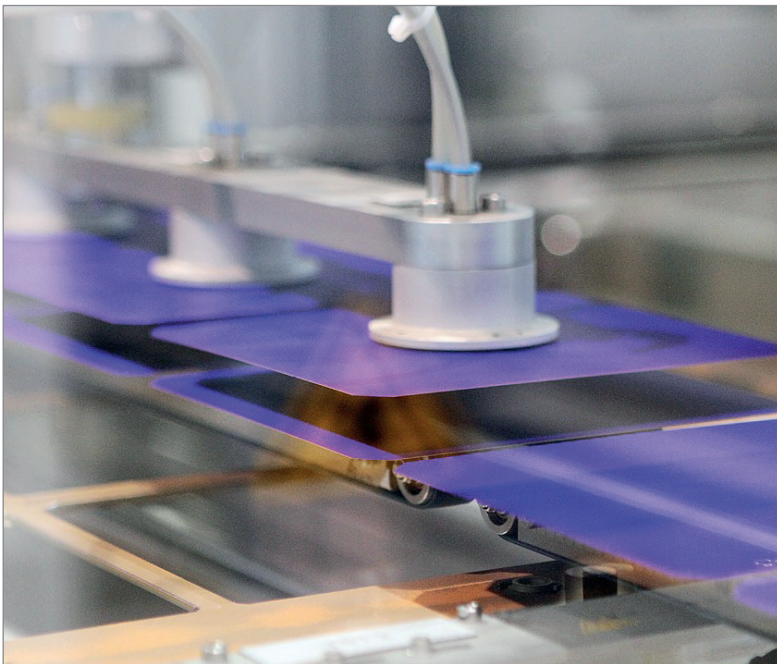


Figure 5. Hevel's production line.

thermal diffusion processes. Third, wafer bowing is suppressed because of the low process temperature and symmetric structure of SHJ solar cells.

There are disadvantages, however, to using low-temperature processes, the main one being that standard fire-through metallization techniques (with firing temperatures in the range 800–900°C) cannot be employed for SHJ cells. This

is because the a-Si/c-Si heterojunction cannot withstand process temperatures above 200–250°C, at which point the hydrogen effusion from the internal surfaces of the heterojunction leads to a detrimental effect on cell performance. For this reason, the so-called *low curing temperature (LCT) silver paste* is commonly used for the metallization of SHJ cells via screen-printing, which is currently the state-of-the-art technology for the metal grid deposition.

Cell interconnection and module assembly

The interconnection of SHJ cells is a stumbling block for the whole process chain: soldering, which is used for the interconnection of conventional c-Si cells, is not compatible with LTC Ag paste, which has to be applied instead of the standard fire-through silver paste because of temperature restrictions for the a-Si/c-Si heterojunction. The low-temperature type of paste has higher bulk resistivity (two to three times that of high-temperature pastes) and low adhesion after soldering. Commonly, Ag busbars easily peel off the ITO surface with forces well below 1N/mm.

To overcome this limitation, new cell interconnection technologies have been proposed, such as gluing the ribbons using electrically conductive adhesive (ECA), or multiwire interconnection using the low-temperature attachment of a foil with embedded InSn-coated wires (Meyer Burger's SmartWire Connection

Technology – SWCT). InSn alloy with a low melting point of around 120°C has good adhesion to both the Ag paste and the ITO layer itself; hence a metallurgic contact between the wire and the cell surface is established after temperature treatment. SWCT technology does not require very precise positioning of the ribbons relative to the metallization grid, which is one of the major challenges for multiwire technology. The initial attachment of the cells to the wires in SWCT does not require precise soldering of the wires to the solder pads and is commonly done by an adhesive-layer-containing foil, which allows the use of a large number (up to 24) of relatively thin wires of diameter 200–250µm.

With an optimization of the SWCT module assembly bill of materials (BOM) – by tuning the optical properties of the lamination foils and the electrical properties of the wires – a gain of 9W for a 60-cell module has been achieved at Hevel compared with the standard BOM, with no increase in material costs (see Table 1).

Overall improvements in cell production (higher FF, leading to lower CTM) and in module assembly on Hevel’s production line have enabled an average increase in power from 300W to 318W during the period Q4 2017 to Q2 2019.

In June 2019 Hevel started the ramp-up of a new assembly line for glass–glass modules using glued five-busbar cells; a full ramp-up is scheduled for July 2019. New bifacial modules will bring an extra gain in production capacity, as they can deliver up to 30% additional module output in power plants.

Another advantage of Hevel’s new assembly line is the implementation of special light-capturing ribbon (LCR); its ability to diffuse reflected light can yield a module efficiency increase of up to 4% (according to producer data). The next generation of Hevel’s modules will therefore have higher efficiency along with higher durability and stability as a result of a glass–glass configuration that enables lower module degradation.

Conclusions

In a record-breaking project schedule, Hevel has converted its low-capacity (97MWp) micromorph module production line into a moderate-capacity line (260MWp) for the manufacture of high-efficiency SHJ cells/modules by implementing an in-house cell production process developed by its daughter company R&D Center TFTE (Figs. 5 and 6). In less than two years after shutting down the thin-film line, an average cell efficiency of 22.8% has been achieved (with maximum efficiencies above 23.5%), resulting in a 60-cell module power of on average 318W (with a maximum module power of 328W) in mass production.

Acknowledgements

The authors wish to thank their equipment suppliers for their support in the equipment

implementation in Hevel’s production line, as well as Skolkovo Foundation for granting access to their laboratory equipment

About the Authors



Igor Shakhray has been the CEO of Hevel Group since 2015. He studied economics at Irkutsk State Economic Academy and received an MBA in asset management from RANEPA. Under his leadership,

commercial operation of Hevel’s solar module production line was set in motion and steered to full capacity in 2015, and the thin-film fab line was converted to heterojunction technology in 2017.

Dr. Alexey Abramov has been the head of the solar energy department at Hevel’s R&D Center TFTE since 2010. He received his M.S. in quantum electronics from St. Petersburg State Polytechnical University, Russia, in 1993 and his Ph.D. in semiconductor physics from A.F. Ioffe Physical Technical Institute RAS, St. Petersburg, in 2001. From 2004 to 2010 he worked at CNRS and the École Polytechnique, Paris, as a researcher in the field of amorphous and nanocrystalline thin-film semiconductors and their applications in PV and large-area electronics.

“Overall improvements in cell production and in module assembly on Hevel’s production line have enabled an average increase in power from 300W to 318W during the period Q4 2017 to Q2 2019.”



Figure 6. Visual control station on Hevel’s production line.

Dr. Sergey Abolmasov has been a senior process engineer at Hevel's R&D Center TFTE since 2013, where he focuses on the development of thin-film silicon and silicon heterojunction solar cells. He received his D.Sc. in plasma physics from Kyushu University, Fukuoka, Japan, in 2003. From 2003 to 2010 he worked in the plasma technology sector as a researcher at Kyoto and Tohoku Universities, Japan, and at Samsung SDI Co. Ltd., Korea. From 2010 to 2013 he was with CNRS, École Polytechnique, France, working on amorphous/microcrystalline silicon solar cells.

Dr. Ekaterina Terukova has worked for Hevel's R&D Center TFTE since 2011 and is currently a team leader in the solar energy department. She studied materials science at St. Petersburg Polytechnical University, Russia. Her research interests include materials for solar cell fabrication and also solar module assembly. Her main activity is implementation of new materials and processes for Hevel's production line.

Dr. Dmitriy Andronikov is the chief process engineer at Hevel's R&D Center TFTE. He received his Ph.D. in condensed matter physics from St. Petersburg

State University, Russia, in 2013. From 2008 to 2011 he was a research fellow at Ioffe Physical Technical Institute, St. Petersburg, Russia, where he worked on amorphous silicon deposition. Since 2011 has been working at Hevel R&D, initially as a senior process engineer and subsequently as the chief process engineer, with a main focus on PECVD processes for silicon heterojunction solar cells and PV module assembly techniques.

Enquiries

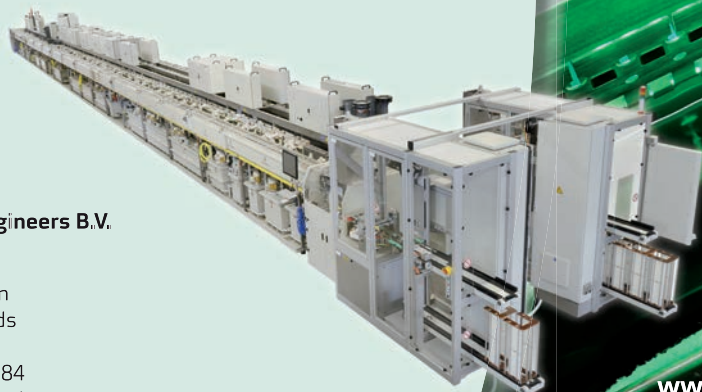
Hevel Group
 Profsoyuznaya Str., 65 bld.1
 117342, Moscow, Russia

Tel: +7 (495) 933 06 03
 Email: a.berdnikova@hevelsolar.com
 overseas@hevelsolar.com
 Website: www.hevelsolar.com/en

Meco Plating Equipment

Copper metalization for high efficiency solar cells

- HJT, IBC, bifacial, PERC, TOPCon
- HJT plating: > 24.0%
- > 65% reduction of metalization costs
- Inline process up to 30 - 100 MW tool capacity
- IEC61215 certified
- Eco-friendly processes with maximum material recycling
- 40 years of plating experience
- More than 800 plating tools installed
- Installed base at leading PV manufacturers



Besi

Meco Equipment Engineers B.V.

Marconilaan 2
 5151 DR Drunen
 The Netherlands

T: +31 416 384 384
 meco.sales@besi.com

www.besi.com

Heraeus Photovoltaics- Leading the Future of PV



- ☀ High quality metallization products
- ☀ One-stop total solution of PV value chain
- ☀ Efficiency gains 0.2% every year
- ☀ Sophisticated customer modification solution
- ☀ Fast responding technical services



PERC-based shingled solar cells and modules at Fraunhofer ISE

Puzant Baliozian, Nils Klasen, Nico Wöhrle, Christoph Kutter, Hannah Stolzenburg, Anna Münzer, Pierre Saint-Cast, Max Mittag, Elmar Lohmüller, Tobias Fellmeth, Mohammad Al-Akash, Achim Kraft, Martin Heinrich, Armin Richter, Andreas Fell, Alma Spribille, Holger Neuhaus & Ralf Preu, Fraunhofer Institute for Solar Energy Systems ISE, Freiburg, Germany

Abstract

Achieving high output power densities p_{out} of silicon-based PV modules requires an increase of cell efficiency as well as a reduction of cell-to-module (CTM) losses. Solar cell shingling, an approach first introduced in the 1950s, targets the reduction of CTM losses mainly by: 1) eliminating the cell spacing through the overlapping of neighbouring cells; 2) decreasing the shading losses by covering the busbar with a neighbouring cell's active area; and 3) reducing the series resistance losses at the interconnection level. This paper reports on the latest advances in passivated emitter and rear cell (PERC)-based shingled solar cell activities at Fraunhofer ISE. The approach taken is to fabricate 6" host wafers from Czochralski-grown silicon and separate them after metallization and contact firing into bifacial p-type shingled passivated edge, emitter and rear (pSPEER) solar cells. The separation is performed by laser-assisted processes: 1) laser scribing and mechanical cleaving, or 2) thermal laser separation. Since the separation process leaves the edges without the intended passivation, high edge recombination rates are expected. For that reason, a photoluminescence-based method to characterize edge recombination has been developed and verified by Quokka3 simulations. In order to further increase the pSPEER output power density p_{out} for a cell without the intended edge passivation, a post-metallization/separation edge passivation method, i.e. Passivated Edge Technology (PET), has been developed. The implementation of PET in pSPEER^{PET} solar cells leads to an enhanced designated area $p_{\text{out}} = 23.5\text{mW/cm}^2$ (considering an additional rear-side irradiance $G_r = 100\text{W/m}^2$). In the transition to shingled-module assembly, the study follows up with the cure kinetics of electrically conductive adhesives (ECAs) and mechanical-model-based methods to gain a better understanding of the joint between pSPEER cells within strings. A CTM analysis using the SmartCalc.CTM software shows a comparison of a parallel-stringing topology with a matrix topology of the cell interconnection. The reduced form factor of shingled solar cells makes them very appealing and effective for use in integrated module products, which is demonstrated by a successful automotive application, additionally profiting from the high p_{out} attained. Drawing from the authors' expertise in customized module and surface design, a vehicle-integrated PV solution with a highly aesthetic appearance is presented.

Introduction

Just two years after the first fabricated silicon-based solar cell [1], the shingled interconnection of solar cells was introduced in a 1956-filed patent (see Fig. 1(a)) [2]. Subsequently, numerous patents were filed for various applications, such as satellite solar cell arrays [3], different interconnection patterns/

geometries, and thermally stable shingle arrays [4]. Early publications, including results for shingled solar cells, target 1) low-illumination applications in electronic devices [5]; and 2) prototype vehicles with limited power-generation areas [6].

Commercial modules with shingled solar cells are currently available on the market [7,8], with a projection trend indicating an increasing market share in the upcoming years [9]. The recent patents (see the example in Fig. 1(b) [10,11], as well as reports in the literature [12–15]) highlight the increase in research activities relating to the shingling concept. Shingling is a process whereby neighbouring cells are mechanically and electrically interconnected by overlapping the rear-side busbar of one cell with the following neighbouring cell's front-side busbar, thus creating a visually busbarless string of shingled cells and, in turn, shingled modules.

Shingling leads to an increase in module output power density p_{out} because of the increase in active cell area and the low electrical resistance in the interconnection. The appealing homogeneous appearance raises interest in their use in vehicle-integrated PV (VIPV) and building-integrated PV (BIPV) applications. Even further increases in p_{out} can be achieved by using bifacial solar cells, which make use of the albedo light impinging from the rear side [16,17]. See Fraunhofer ISE's previous *Photovoltaics International* paper [24] for a discussion of shingling bifacial solar cells, such as bifacial passivated emitter and rear cells (PERC, biPERC) [18,19], passivated emitter, rear locally diffused (PERL) cells [20], passivated emitter and rear totally diffused (PERT) cells [21], heterojunction (HJT) cells [22], or TOPCon [23] cells.

The market shift towards PERC solar cells in the upcoming years [9] implies a shrinkage of the market share of aluminium back-surface field (Al-BSF) solar cells. The main shift in the market towards PERC solar cells is due to the clear advantages of the concept in terms of efficiency potential by having dielectrically passivated rear sides in comparison to the Al-BSF. PERC solar cells feature local contacts created by local contact openings (LCO) and subsequent metallization steps, which allows the PERC cell architecture to be designed for bifacial light collecting. This biPERC is obtained by replacing the full-area metallization on the rear side by a grid metallization that allows the harvesting of light from the rear side as well. Adapting the rear-side

“Shingling leads to an increase in module output power density because of the increase in active cell area and the low electrical resistance in the interconnection.”

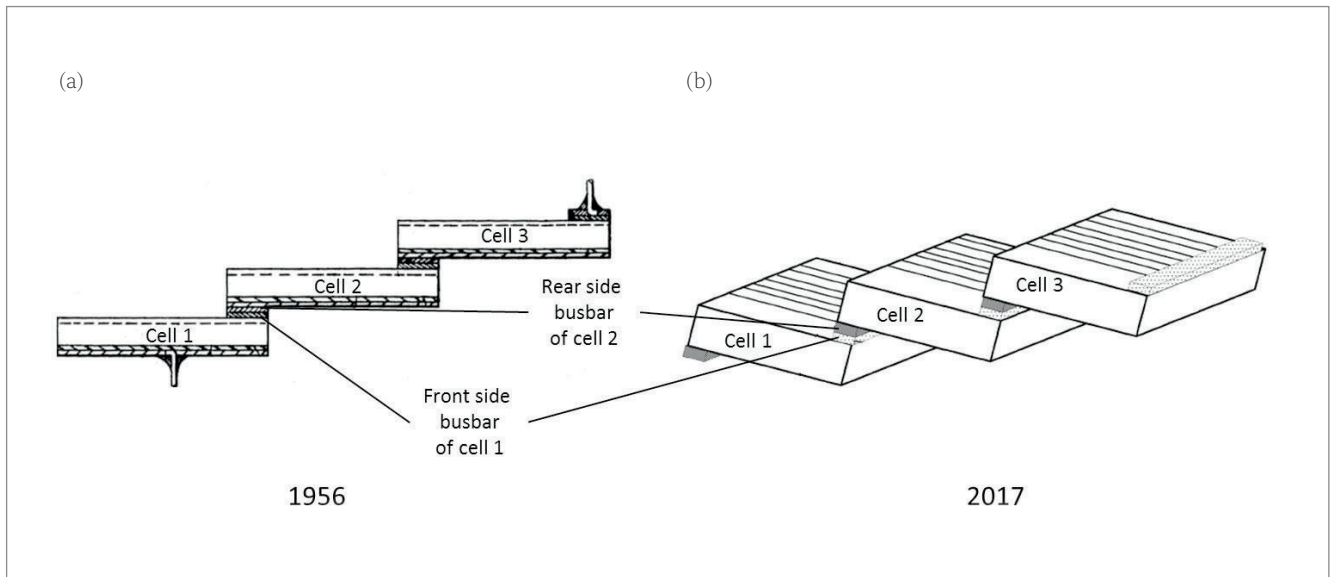


Figure 1. (a) Schematic showing a string of three shingled cells, adapted and labelled from an earlier 1956 patent [2]. (b) Schematic showing a string of three shingled cells in a recent 2017 patent (adapted and labelled) [11]. The similarities in (a) and (b) show the clear revival of the concept of shingling presented in both patent sketches. In cell shingling, the front and rear busbars of two neighbouring cells form the electrical and mechanical interconnection of two neighbouring cells.

passivation layers boosts the light coupling from the rear side. Although the concept of shingling can be applied to different cell architectures such as PERC, HJT, TOPCon and others (as explained in Wöhrle et al. [24]), the main focus in this paper is PERC-based shingle cells fabricated from 6" Czochralski-grown (Cz-Si) wafers, which are then integrated in the shingled module.

In the first part of this paper, Fraunhofer ISE's current fabrication process is presented, along with the characterization results for bifacial p-type shingled passivated edge, emitter and rear (pSPEER) solar cells [25] ready for shingled-module integration. The laser-assisted separation processes used for the fabrication of shingle cells are also described. Further investigation of the separated edge quality by modelling, simulations and photoluminescence (PL) measurements of the edge is discussed. In addition, Fraunhofer ISE's Passivated Edge Technology (PET), a post-metallization/separation edge passivation concept, is introduced. In the second part, as an essential step towards cell interconnection, available testing methods, along with the crucial properties of electrically conductive adhesives (ECAs), are presented. The paper also compares possible shingling design topologies and suggests numerous applications shown in demonstrated products, such as a PV-integrated car roof.

pSPEER solar cell concept and process

To obtain a bifacial shingle pSPEER cell, only one additional process step is needed compared with a large-area cell: the laser-assisted separation process. This separation process is preferably done after the back-end processes of the 6" host wafer have been completed (typically after firing). As reported in Baliozian et al. [25], pSPEER solar cells can be fabricated by just modifying the back-end processes.

Other than the additional separation process step, the fabrication also requires the adjustment of the metallization layouts in order to obtain several shingle cells from each host wafer. In other words, PERC precursors (with deposited passivation layers) from an industrial production line can be used, and shingle cells of desired sizes can be manufactured. A specific fabrication batch of pSPEER cells using precursors is discussed later.

Current–voltage measurement of pSPEER cells

Rapid and precise current–voltage (I – V) measurements are a prerequisite for the characterization of shingle solar cells. The grid geometry, especially the adversely placed rear-side grid and the small cell size, poses new challenges for the I – V measurement set-up. Conventional measurement units with contacting pins are feasible for R&D purposes.

One option for measuring the cells is the use of inlays in the shape of conventional wafers, as shown in Fig. 2(a). The pSPEER cells are placed in the inlays and then electrically contacted by two I – V pin array strips on each of the front- and rear-side busbars, as shown in Fig. 2(b). Two additional arrays (one on each side) are used for mechanical stability purposes and therefore not electrically connected. To ensure the validity of the measurements, the I – V tester is calibrated with pSPEER cells measured at Fraunhofer ISE CaLab PV Cells. As a result of the measurement, a total area measurement (including the busbars) is obtained. Since the busbars are intended to be covered after interconnection, the efficiency of the area excluding the busbar area, or *designated area*, is of interest. Such designated area results can be obtained by subtracting the busbar area from the total cell area to determine the designated area short-circuit

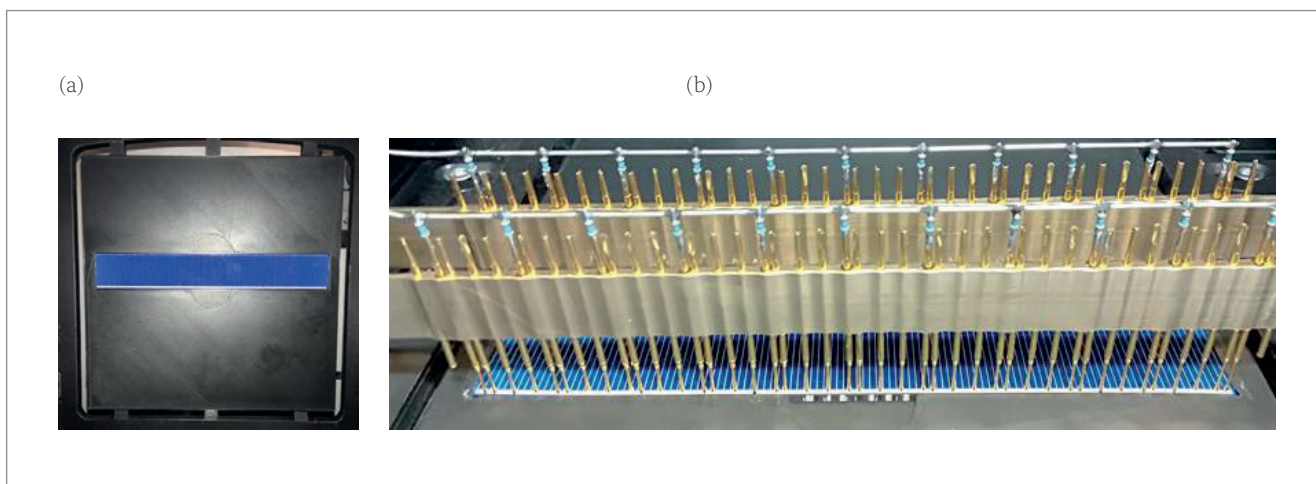


Figure 2. (a) Photograph of an inlay for pSPEER cells, which allows the use of a conventional $I-V$ measurement unit. In this set-up, the pSPEER cell can be measured by two contacting $I-V$ pin arrays that electrically contact the front and rear busbars. (b) Photograph of a front-side busbar contacted by the $I-V$ pin array.

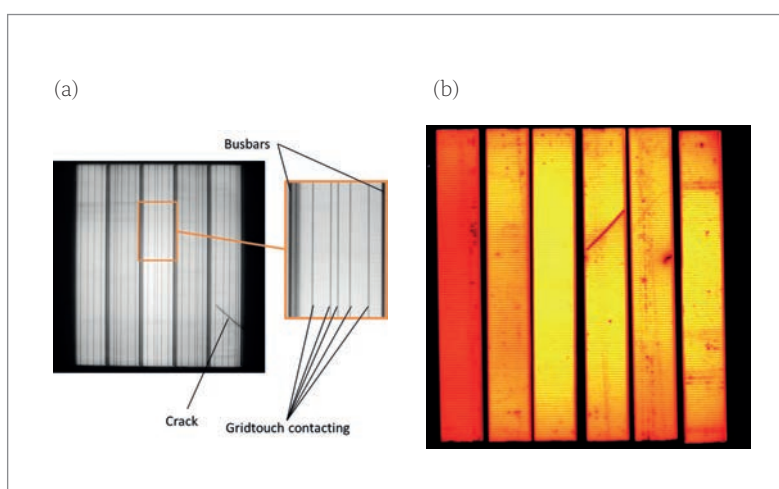


Figure 3. (a) Inline EL image of a finished host wafer before separation, contacted by a GridTOUCH unit. A microcrack can be identified in the lower right part of the cell, which would lead to a rejection of this pSPEER cell strip after separation. (b) PL image of separated pSPEER cells (not the same cell as in (a)). The PL image can uncover additional damage induced by the laser-assisted separation step; this covers edge-related flaws as well as new cracks or the like due to the additional handling. With a feasible automation system, multiple pSPEER cells could be measured simultaneously, making the procedure fast enough for inline characterization.

current density $j_{sc,des}$

For a production line this set-up is suboptimal, as the throughput in terms of equivalent measured cell power scales down with the shingle size. Consequently, alternative approaches for measuring the efficiency of shingled cells are being investigated. The goal is to measure the cells on the host wafer with the conventional technique before the laser separation of the cell strips. Since the front and rear busbars are placed in an alternating pattern, the host wafers cannot simply be contacted with pin arrays like a conventional cell with busbars. GridTOUCH technology, with an orientation parallel to the busbars, is therefore preferred (see Fig. 3(a)). With this method, the efficiency information about the bundle

of six yet to be separated shingles can be determined. Local information can be obtained by forward dark electroluminescence (EL), a common capability of today's $I-V$ testers.

Laser separation, however, might introduce edge cracks, or even shunts, which also need to be inspected. One available option is to make use of inline contactless PL technology immediately after separation in order to detect flawed cells. Because of the wide field of view of the PL camera and the short measurement intervals of contactless measurements, several shingle cells can be measured simultaneously (assuming suitable automated handling of shingle cells), thus avoiding the previously mentioned throughput bottleneck. Fig. 3(b) shows a sample PL image of the measurement of six separated pSPEER cells.

pSPEER solar cell batch

The latest results for pSPEER cells are published in Baliozian et al. [26]. For this specific batch, industrial pre-processed precursors that feature a phosphorus-doped emitter passivated by a silicon nitride (SiN_x) layer were used (see Fig. 4(a)). The rear side is coated by a typical aluminium oxide (AlO_x) and SiN_x stack. The base resistivity of samples from a comparable batch is measured to be in the range $0.3\Omega\text{cm} \leq \rho_B \leq 0.9\Omega\text{cm}$.

The processing begins with laser LCO, carried out at Fraunhofer ISE by means of an infrared laser process. The external rear-side contacts, silver in this case, also known as the rear-side busbars, are first screen printed (the external silver contacts are analogous to the printed rear-side pads of 6" PERC cells). The rear-side aluminium grid is then applied, covering the LCO; this results in a silver busbar which is confined between aluminium grid contacts (see Fig. 4(b)). Next, the front-side silver contact grid is printed, and contact firing is performed in an industrial fast-firing oven. Six pSPEER cells of dimensions $22\text{mm} \times 148\text{mm}$ are obtained after the laser scribing and mechanical cleaving separation

“Laser separation might introduce edge cracks, or even shunts, which also need to be inspected.”

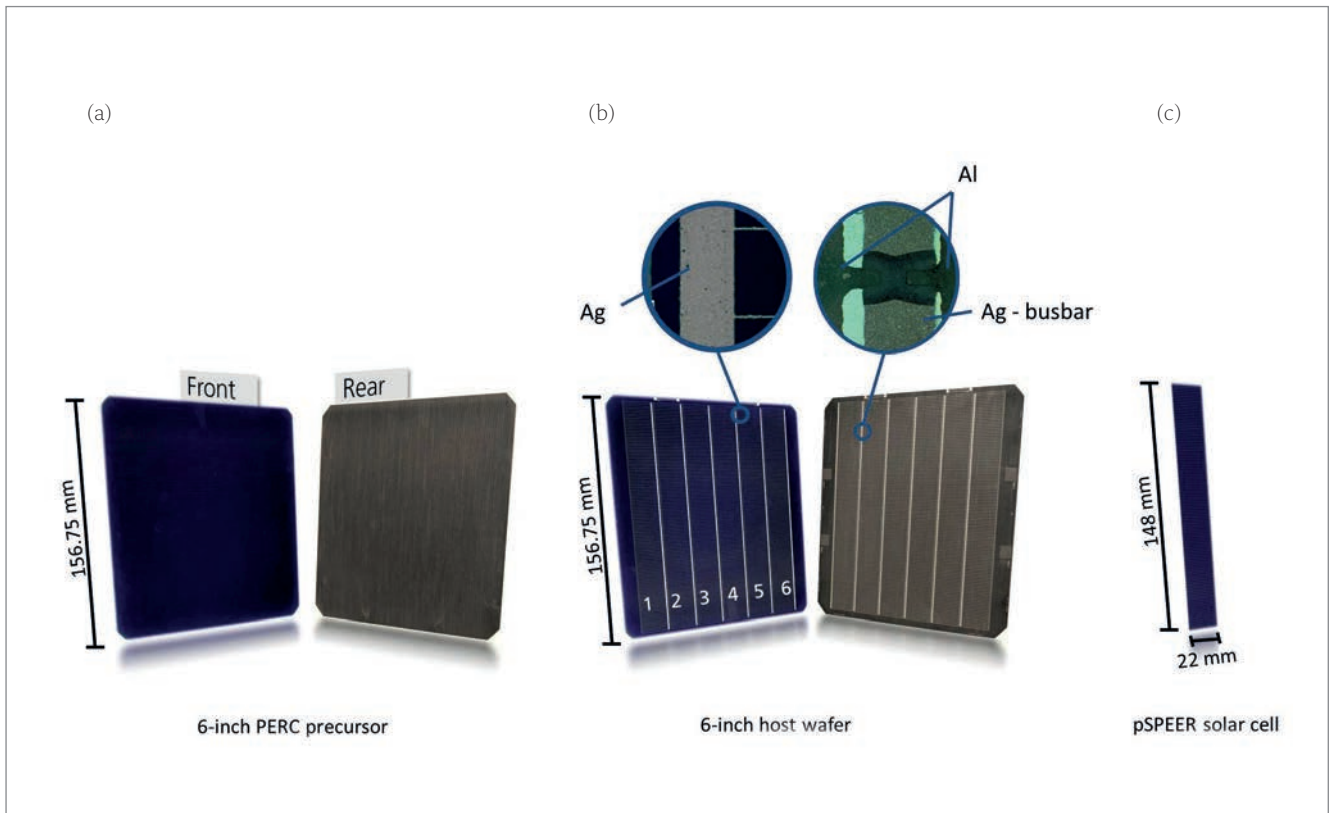


Figure 4. Scanned images of the front and rear sides of: (a) 6" industrial PERC precursor; (b) host wafer with front- and rear-metallization layouts (the microscope images show the metal contacts); (c) pSPEER solar cell of dimensions 22mm × 148mm. The precursors are not optimized for bifacial use, which explains the yellowish colour of the rear side.

process (see Fig. 4(c)). Such pSPEER cell dimensions are chosen to be utilized for research purposes because of the flexibility they offer when different industrial wafer formats are used.

For the characterization of the fabricated pSPEER cell, the measurements are taken at standard testing conditions (STC; $G_t = 1,000\text{W/m}^2$). As reported in Baliozian et al. [26], for the specific pSPEER cell with a nominal size $22\text{mm} \times 148\text{mm}$, I - V measurements show a peak designated area front-side efficiency of $\eta_f = 21.4\%$, as shown in Table 1. The pSPEER cell yields an open-circuit voltage

$V_{oc} = 666\text{mV}$, a fill factor $FF = 79.8\%$, a pseudo-fill factor $pFF = 82.3\%$, and a short-circuit current density $j_{sc,des} = 40.2\text{mA/cm}^2$. The measurement of the same cell's rear side, also at STC, results in a designated-area rear-side efficiency $\eta_r = 13.7\%$, featuring $V_{oc} = 654\text{mV}$, $FF = 79.7\%$ and $j_{sc,des} = 26.2\text{mA/cm}^2$. Consequently, a bifaciality factor $\beta = \eta_r/\eta_f = 0.64$ is determined. The pSPEER cell achieves a designated total output power density $p_{out} = 22.8\text{mW/cm}^2$ (calculated by considering an additional rear-side illumination with an irradiance $G_t = 100\text{W/m}^2$).

In the case of this particular cell, the rear-side $j_{sc,des}$ is $\Delta j_{sc,des} = 14\text{mA/cm}^2$ lower than that of the front side; this difference is due to the high metallization fraction of the rear side compared with that of the front. Additionally, the optical properties of the rear side of the specific precursors utilized are not optimal, as they have not been adjusted for bifacial use. The difference in V_{oc} between the rear- and front-side measurements, or ΔV_{oc} , is $\sim 12\text{mV}$; this difference is due to the lower rear-side $j_{sc,des}$ and, to a lesser extent, to edge recombination, verified using the one-diode model equation.

On the other hand, the difference in pFF between a 6" bifacial PERC cell fabricated in a parallel batch and the separated pSPEER cell, or ΔpFF , is $\sim 1.2\%_{abs}$; this shows the effect of edge recombination as a result of the separation process. As a by-product of the separation process, the edges are sparingly passivated with a thin native silicon oxide layer with no planned additional edge passivation process. To enhance the performance of the separated cell, an additional edge passivation process is therefore needed. The approach taken to decrease edge recombination by the selected

	η [%]	V_{oc} [mV]	$j_{sc,des}$ [mA/cm ²]	FF [%]	pFF [%]	β [1]
Front side	21.4	666	40.2	79.8	82.3	0.64
Rear side	13.7	654	26.2	79.7	81.6	

Table 1. I - V data for the pSPEER solar cell with the highest output power density p_{out} [26]. The designated area short-circuit current density values are obtained by subtracting the busbar area from the total measured cell area $A_{tot} = 3,263\text{mm}^2$.

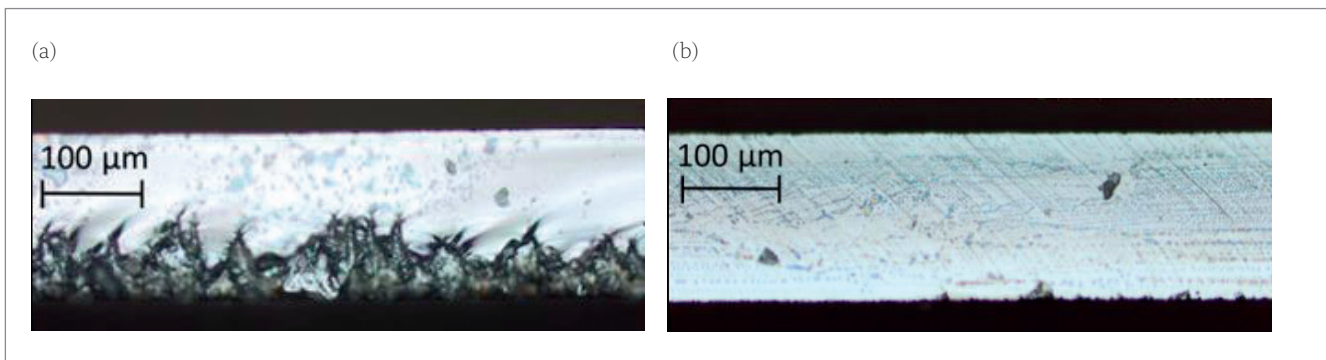


Figure 5. Microscopy images of pSPEER cell edges obtained by laser-assisted separation processes: (a) LSMC and (b) TLS [32].

laser-assisted separation process, as well as an additional edge passivation process, is discussed in upcoming sections.

Laser-assisted separation techniques and characterization

The most common way of separating shingle cells is to do a laser scribe followed by a mechanical cleave (LSMC). The laser scribe makes use of a pulsed laser to ablate the silicon along the entire separation path; the resulting laser perforation then enables an effortless separation by mechanical cleaving. The laser ablation, however, leads to melting and restructuring of the silicon in the cut region, resulting in an optically visible rough surface, as seen in Fig 5(a). The destruction of the crystalline structure leads to a high number of defects at the edge. Since the shingle cells obtained have a high perimeter-to-area ratio, the damaged edges lead to significant losses.

Thermal laser separation (TLS) [27,28] is a gentle, kerfless alternative to LSMC separation. A short scribe beginning at the wafer edge is conducted by an infrared laser to initiate a crack. Subsequently, a continuous wave infrared laser (TLS cleave laser),

followed by a water- and air-cooling jet, is guided over the wafer surface. The heating followed by cooling leads to thermal stress in the material, resulting in a crack propagation from the initial crack along the guided path. The process results in a smooth shingle cell edge surface, as shown in Fig 5(b).

The TLS process, shown schematically in Fig. 6(a), is highly dependent on a variety of process parameters, including the cleave laser power, the feed rate, and the distance between the laser spot and the cooling spot on the sample [29]. The cleave process can be monitored by infrared imaging, whereby an elliptical shape of the laser spot on the sample (see Fig. 6(b)) is displayed. Depending on the cleave parameters, the heat distribution on the sample, as well as the total dissipated heat, can be optimized in order to achieve smooth separation edges and a straight separation path.

Since the TLS process does not lead to melting of the silicon but rather to cracking, this method is expected to cause fewer crystal defects and hence lower electrical losses. Almost no ablation takes place during TLS (only in the short initial scribe), which makes it an almost dust-free process. This is particularly attractive for high-throughput industrial applications [29,30]. Additionally, TLS-separated cells are mechanically more stable than LSMC-separated cells [31].

Model updates in the simulation tool Quokka3

The silicon solar cell modelling tool Quokka3 [33] has a dedicated extension for dealing with shingled cell technology, in order to improve the speed of modelling strip cells. It uses the recently integrated 'multidomain modelling', which can combine two or more simulation domains for modelling large-area devices while maintaining a small calculation mesh [34]. Solar cells with edge effects, half cells and shingled solar cell designs can be modelled using this approach.

A pSPEER cell is simulated with a core domain and one edge domain, as depicted in Fig. 7. The effective symmetry elements have the size of just the finger pitch multiplied by the finger length (approximately 1.3mm × 25mm) instead of half

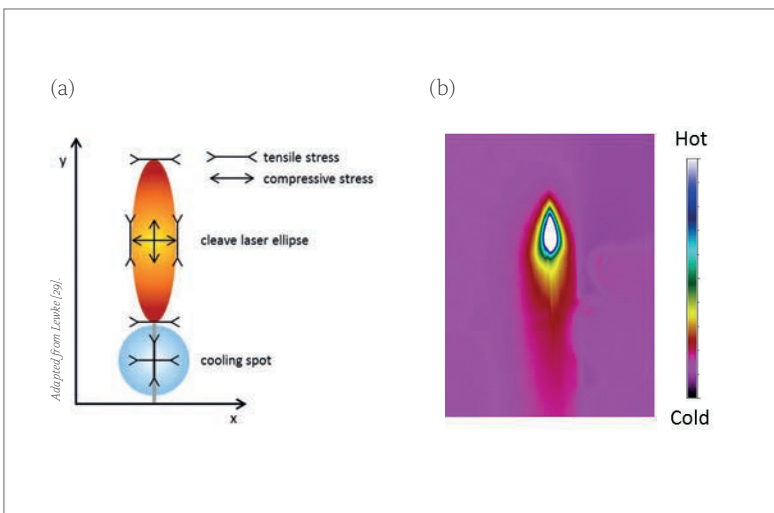


Figure 6. (a) Schematic of the TLS process. After a short laser scribe on the edge of the wafer to initiate a crack, a continuous-wave infrared laser is used to induce heat, directly followed by a water- and air-cooling jet; this leads to thermal stress and cracking of the substrate. (b) Infrared image displaying the heat profile on the substrate resulting from the laser followed by the cooling spot. The shape and size of the elliptical laser spot influence the TLS cut quality.

the strip cell (approximately 25mm × 150mm) as performed in previous publications [35]. This reduces the simulation time from several hours to just a few minutes for each $I-V$ curve. The edge domain features surface recombination models for the space charge and the bulk region, which can be addressed with the recombination parameters $j_{01,edge}$ or $S_{eff,edge}$ and $j_{02,edge}$. The integration of emitter windows along the edge with adjustable sheet resistances and surface recombination is also enabled.

Analytical model for edge recombination

In addition to having an excellent numerical modelling option for shingle cells, a simplified analytical model is useful for calculating the recombination at the edge of the solar cell; for details see Saint-Cast et al. [36]. The edges can be distinguished as linear recombination centres either close to or at the p-n junction; this is in contrast to local recombination on the rear surface (e.g. rear-contact recombination), where the recombination is mainly limited by the diffusion of minority carriers through the wafer from the front to the rear.

If it is assumed that translation along the axis of the defect in the system does not vary, it is possible to reduce the number of dimensions of the system to two. Another assumption is that the linear defect is the only source of inhomogeneity in this system. The high recombination rate at the edge (compared with the rest of the cell) induces a lower p-n junction potential difference (or a lower excess carrier density) in its proximity. The gradient of this potential leads to a flow of electrons and holes towards the defect – we are dealing with a carrier transport problem. In this model it is assumed (hypothesis 1) that over small distances (>1mm) relative to the size of the device (>1cm), the flow of the lateral carriers will be limited by resistive losses. In order to simplify this problem even further, it is assumed (hypothesis 2) that the vertical transport in the emitter and the bulk is small compared with the lateral transport, and can be modelled by simple sheet resistances (ρ_e for the emitter and ρ_b for the bulk).

Fig. 8 shows a schematic of the problem in three dimensions and a comparison with the developed model; the 3D problem is reduced to a single dimension as a result of the above-mentioned assumptions. The origin of the x axis is defined to be the location of the linear defect (edge). The local potential difference $V(x)$ at the p-n junction is calculated analytically.

Under open-circuit conditions, the p-n junction voltage decreases towards the edge because of the recombination at the edge. In Fig. 9, the p-n junction voltage is plotted as a function of position for six different illumination intensities. The 1 sun illumination intensity is defined for the sun spectrum AM1.5G at a power density of 1,000W/m². In this case an equivalent generation is achieved by monochromatic illumination at 808nm with a photon flux density $j_\gamma = 2.5 \times 10^{17} \text{cm}^{-2} \text{s}^{-1}$ by illuminating

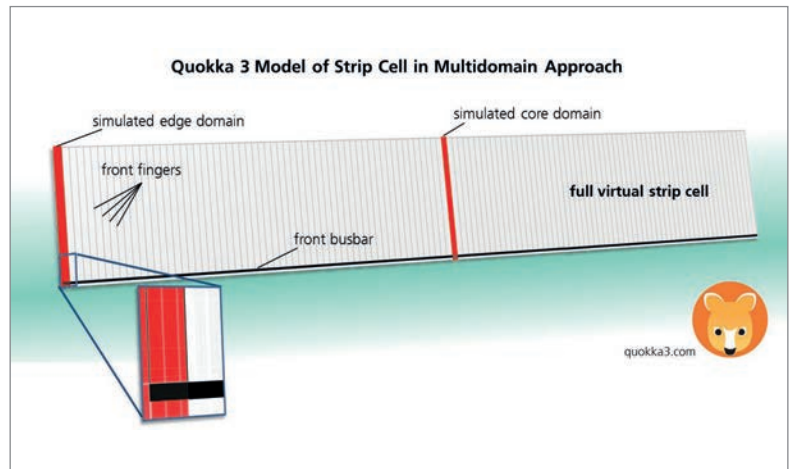


Figure 7. Schematic of the implementation of Quokka3’s multidomain approach for a strip cell. The red front and core parts symbolize the two domains that are actually simulated. The greyed areas result from the cell’s symmetry and do not need to be simulated in addition. This way, the duration of the simulation is greatly reduced.

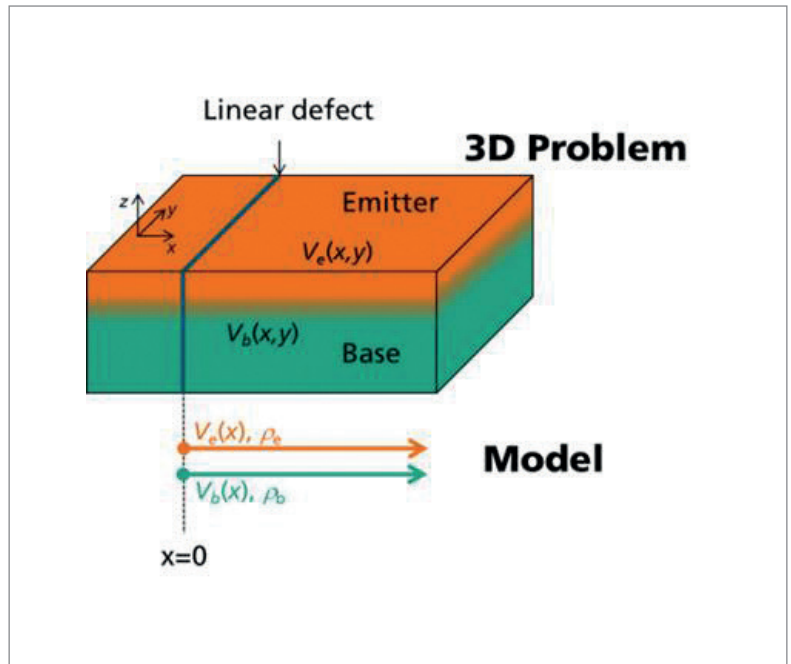


Figure 8. Schematic of the problem in three dimensions, and a comparison with a simplified interpretation of a linear defect in a solar cell.

a reference solar cell of thickness $W \approx 160\mu\text{m}$ at a temperature $T = 300\text{K}$. For low illumination, the p-n junction voltage is affected by the edge over a much greater distance than for high illumination. The results of the models were compared with 2D drift-diffusion simulations using Quokka3, and found to be in good agreement, within a deviation of $\pm 3\text{mV}$. For this example, the recombination parameter at the edge is $j_{02,edge} = 19\text{nA/cm}$, which corresponds to a ‘worst-case’ value as identified by Fell et al. [37].

The benefit of such a model is the simplification of the analysis of measured cell parameters,

“A simplified analytical model is useful for calculating the recombination at the edge of the solar cell.”

Adapted from Saint-Cast et al. [36].

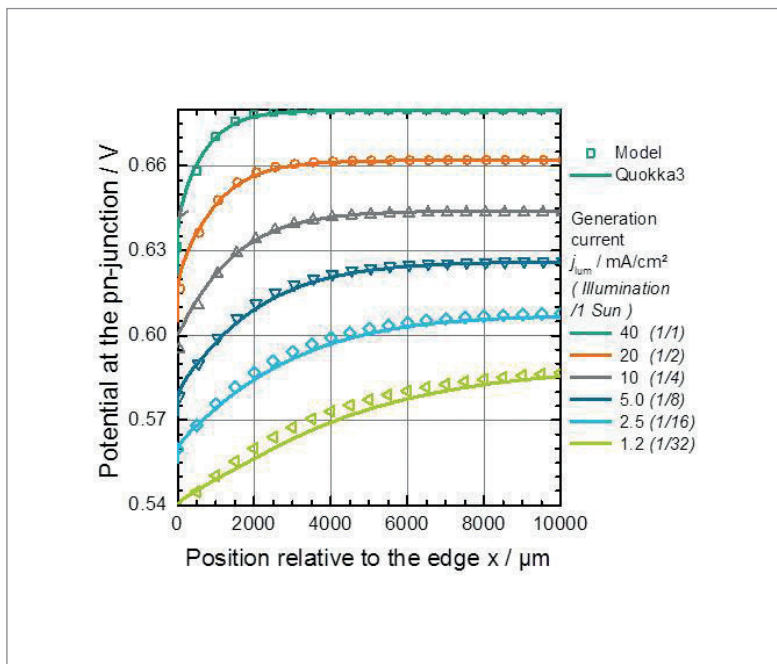


Figure 9. Potential difference at the p-n junction as a function of distance from the edge for different illumination intensities, with $iV_{oc} = 680\text{mV}$, $\rho_e + \rho_b = 180\Omega/\text{sq}$ and $j_{0\text{edge}} = 19\text{nA/cm}$.

which allows one to determine the recombination parameters at the edge (see next section); it also helps in understanding the physical principles behind edge recombination. This assumed model, verified by numerical simulation, shows that the transport mechanism of the carrier which recombines at the edge is mainly resistive.

Edge recombination analysis using PL measurements

Because the impact of edge recombination has been seen in the I - V parameters of the finished cells and in the modelling, there is clearly a demand for

suitable in-depth characterization of this type of recombination. With reference to the investigation in Stolzenburg et al. [38], a new approach is presented to quantify edge recombination by using PL measurements combined with Quokka3 device and luminescence modelling. The main focus is to determine and separate the contribution of the two relevant edge recombination losses, as also proposed in Wöhrlé et al. [35]: 1) recombination at the bulk edge, described by an effective surface recombination velocity $S_{\text{eff,edge}}$; and 2) recombination at the p-n junction edge, described by an edge-length-specific non-ideal recombination parameter $j_{0\text{edge}}$.

Boron-diffused and $\text{Al}_2\text{O}_3/\text{SiN}_x$ surface passivated n-type float-zone silicon wafers ($\rho_B = 1\Omega\text{cm}$) with three differently processed wafer edges are investigated. The wafer is separated by: 1) TLS through the emitter layer from the front side; 2) TLS with a distance d_{EW} of $300\mu\text{m}$ between the emitter and the edge (emitter window); and 3) diamond cutter scribing and subsequent manual mechanical cleaving through the emitter layer.

The PL image of the three different edge types is depicted in Fig. 10(a) at an illumination intensity of 0.02 suns. The corresponding PL profiles in Fig. 10(b) clearly show a decrease towards the edges and a distinction between the differently processed edges. As a result, the TLS-cleaved edge through the emitter is not as affected by edge recombination as the mechanically cleaved edge. Further, the expected positive influence of an emitter window [35,39] due to the missing conductivity of minority carriers through the emitter to the edge is also observed.

For the quantification of the edge recombination, data from 2D PL simulations using Quokka3 are fitted to the experimental PL data. For this, a lifetime calibration is performed [40] and subsequently a fit by varying the two free parameters $S_{\text{eff,edge}}$ and

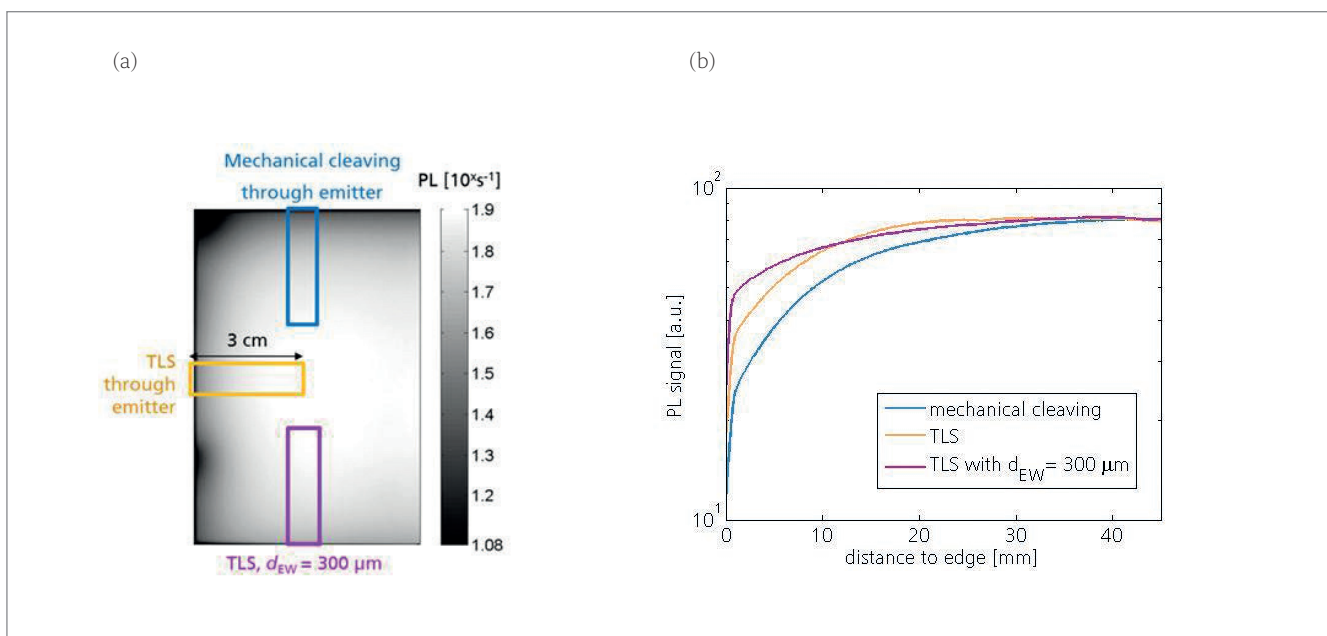


Figure 10. (a) Logarithmically scaled PL image at 0.02 suns, showing the three differently affected edges; (b) corresponding PL profiles averaged over the corresponding areas indicated by the coloured rectangles.

$j_{oz,edge}$. A combined fit to six different illumination intensities (0.02 to 1 suns) allows the $S_{eff,edge}$ and $j_{oz,edge}$ values to be distinguished. The best agreement between simulation and experiment for the TLS edge separated through the emitter is visible in Fig. 11, while the best-fit parameters for the investigated edges are listed in Table 2.

A comparison of these results with the worst-case assumption for an unpassivated edge proposed by Dicker [41] and Fell et al. [37] ($S_{eff,edge} \geq 10^6$ cm/s and $j_{oz,edge} = 13$ or 19 nA/cm, respectively) indicates that the values obtained in the present study are smaller, suggesting that some kind of native passivation is present on the edges. In particular, $j_{oz,edge}$ is similar to the values given in the study by Rühle et al. [39], who also reported 5 nA/cm for a mechanically cleaved unpassivated edge.

The method presented here can be used for extracting detailed information about the edge recombination. Since the overall goal is to optimize silicon solar cell performance, the comparison of mechanical cleaving and TLS leads to the conclusion that the TLS process causes lower edge losses and is therefore a promising separation method for shingle cells. Furthermore, the method is not constrained by specific sample parameters and can be employed for different high-efficiency silicon solar cells as well as for edge-passivated wafers in order to obtain detailed information about the edge recombination.

Post-metallization Passivated Edge Technology (PET)

Reports of some edge passivation approaches for reducing recombination at the edges can be found in previous studies. In one approach, for example, the formation of an emitter window by keeping the p-n junction a few hundred micrometres away from the separation edge reduces dangling bond recombination at the exposed space charge region [5,42]. Another approach is heavy doping of the entire separation path, creating an ‘edge surface field’, which induces the repulsion of carriers and reduces recombination at those intended regions [43]. Furthermore, a method proposing the generation of isolation trenches in the emitter also aims to reduce the flow of carriers towards the edges. An isolation trench can be realized by a laser ablation process, an additional wet-chemical etching and subsequent passivation of the trenches by, for example, thermally grown silicon oxide or polysilicon [44]. Although all these approaches lead to a reduction in edge recombination, the industrial feasibility is limited by the fact that the processes involved have to be performed at the front end, prior to metallization, and these processes can be numerous and perhaps costly.

It has also been reported that native silicon dioxide grown on chemically treated edges reduces perimeter recombination detected mainly in low-illumination conditions [45,46]. Moreover, the passivation of the p-n junction and/or the base directly at the edge by means of dielectric layers with high charge

“The TLS process causes lower edge losses and is therefore a promising separation method for shingle cells.”

density has also been studied as a possible method for edge passivation [47]. However, the removal of damaged silicon induced by the separation process is seen to be necessary in order for a high-quality oxide passivation to form on the edge, as reported in Altermatt et al. [48].

On the other hand, a post-metallization/separation edge passivation method seems to be challenging: for this, an industrially feasible, or potentially feasible, edge passivation process is essential. A technical challenge is the stability of the metal contacts, which can degrade in post-firing thermal processes, as shown in Kontermann [49] and Chan et al. [50].

PET, developed at Fraunhofer ISE, aims to combine TLS separation, resulting in edges with less damage, with a high-quality edge passivation, without harming the solar cell contacts. The pSPEER cell that has undergone PET processing (pSPEER^{PET}) demonstrates an improved front-side designated area efficiency $\eta_f = 22.1\%$ and a total output power density $p_{out} = 23.5$ mW/cm² (considering a rear-side irradiance $G_r = 100$ W/m²). Further details of these pSPEER^{PET} solar cells and the PET process can be found in Baliozian et al. [51].

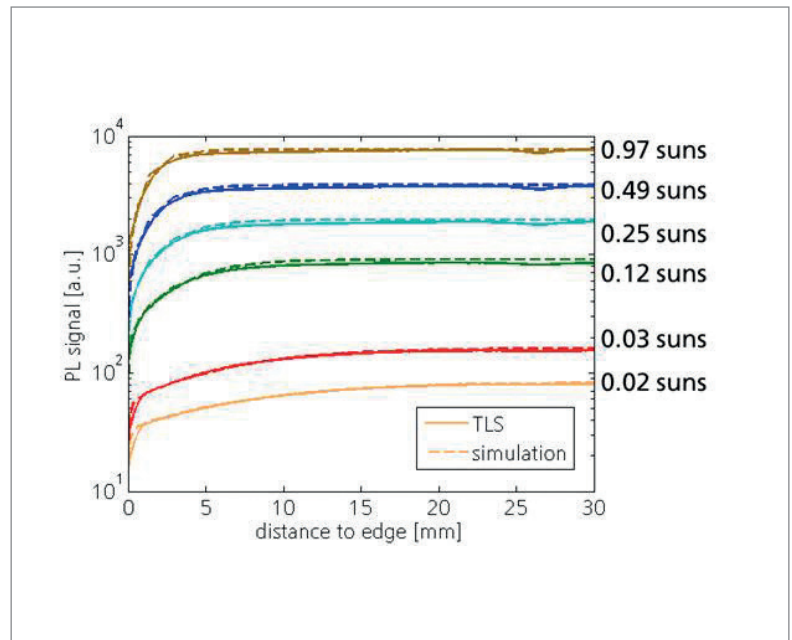


Figure 11. Comparison of the experimental and simulated data of the TLS edge using the best fit, which is shown for all six illumination intensities for the TLS edge with $j_{oz,edge} = 3$ nA/cm and $S_{eff,edge} = 10^5$ cm/s.

Edges	$j_{oz,edge}$ [nA/cm]	$S_{eff,edge}$ [cm/s]
TLS through emitter	3	10^5
TLS ($d_{EW} = 300\mu\text{m}$)	–	10^5
Mechanical cleaving through emitter	5	$\geq 10^6$

Table 2. Best-fit parameters for the three different unpassivated edge types.



Figure 12. A string of shingled solar cells produced by the TT1800 stringer, ready for module integration.

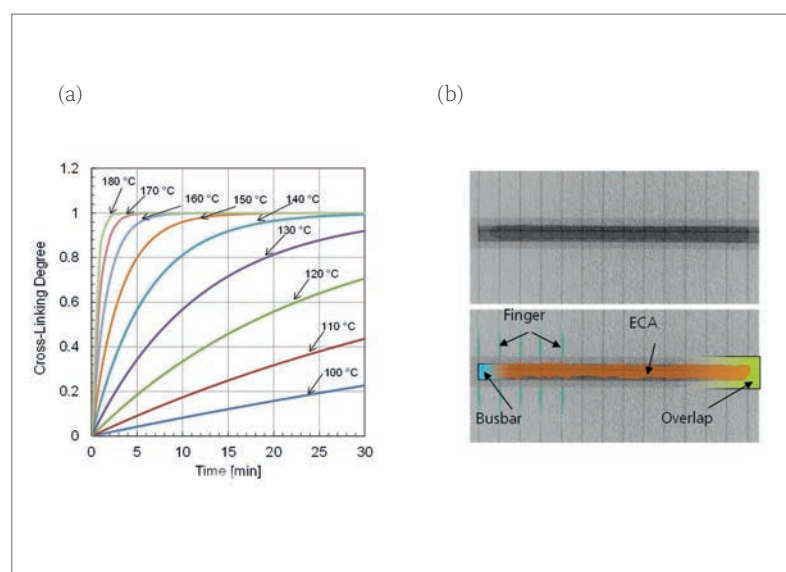


Figure 13. (a) Cure kinetics calculation derived from DSC measurements for an ECA, showing the cross-linking degree as a function of curing time and temperature. (b) X-ray transmission analysis of a shingle joint between neighbouring pSPEER cells (top image shows raw data; bottom image is shaded and labelled for better visibility).

Interconnection

In contrast to conventional solar modules, shingled-cell interconnection requires no ribbon or wire. Solar cells are interconnected directly within a small overlapping area, in a similar way to that of roof tiles. Such interconnection is realized in four steps:

1. Application of the ECA
2. Placement of the cells by a pick and place process
3. Curing (optional)
4. Lamination (with integrated curing)

The technologies for ECA application available at Fraunhofer ISE are dispensing, stencil printing and screen printing. On a lab scale, ECAs are either

manually dispensed or applied using semiautomatic stencil and screen-printing processes. Additionally, a fully automated industrial-scale stringer (TT1800, developed in a joint cooperation with the stringer manufacturer teamtechnik) [52] is accessible for producing shingle strings of various lengths from cells of different sizes and geometries (see Fig. 12). Stencil and screen printing allow an arbitrary layout of the ECA in the joint and the optimization of ECA consumption. Furthermore, a robot-based pick and place process [53] allows the manufacturing of matrix shingle interconnection (discussed in more detail in the next section).

In contrast to soldering, ECAs interconnect the solar cells not by melting and solidifying but by a chemical cross-linking reaction, which is thermally activated; the reaction rate depends on temperature and typically starts at temperatures above 100°C. Curing durations can range from a few seconds to several minutes at temperatures of 150°C. This enables a combined lamination and curing process [54] as an alternative to an extra curing step before lay-up.

Since the key element in shingling is the joint between the solar cells, the module performance is highly dependent on the applied ECA; a thorough suitability assessment of ECAs is therefore crucial in order to ensure a reliable interconnection. A cure kinetics model based on differential scanning calorimetry (DSC) measurements has been developed [55] for specific optimizations of the temperature time profile in the stringing or lamination process to ensure a fully cured joint (see Fig. 13(a)).

Non-destructive X-ray transmission imaging yields information about the geometry and homogeneity of the manufactured joint with respect to cavities, even through the glass in the final laminate (see Fig. 13(b)). Destructive imaging methods include the fabrication of module cross sections after accelerated ageing tests in accordance with IEC 61215 [56], while optical methods, such as light microscopy and scanning electron microscopy (SEM), can be used to identify failure mechanisms inside the joint.

To support these experimental findings, structural-mechanical finite-element simulations allow a deeper understanding to be gained of the underlying effects in the joint when subjected to, for example, cycling temperatures or mechanical loads. Here, the characterization of the ECA bulk material with respect to its mechanical behaviour is an important input for the simulations.

Dynamic mechanical analysis (DMA) is performed to measure and model the viscoelastic properties of ECAs [57]. Fig. 14(a) shows typical DMA data of one material system used at Fraunhofer ISE to interconnect shingle solar cells. This specific material shows distinctive viscoelasticity between 40 and 120°C for frequencies ranging from 0.5 to 50Hz. Even though ECAs contain a high proportion of metal fillers to ensure electrical conductivity, the remaining organic binder matrix causes a viscoelastic behaviour.

“The key element in shingling is the joint between the solar cells.”

By shifting these discrete sets of data via the use of the principle of time–temperature superposition, a master curve can be constructed (see Fig. 14(b)); this curve describes the relaxation spectrum of the material at a reference temperature, usually chosen to be the glass transition temperature T_g . Several rheological models exist that approximate such mechanical properties with spring-damper systems. A Comsol Multiphysics software implementation to carry out finite-element method (FEM) studies is performed by a fit of the data with the Generalized Maxwell Model [58]; a smooth representation of the data is achieved with $i = 20$ Maxwell arms. On the basis of this material modelling, FEM studies of the strings of shingled solar cells subjected to (thermo)mechanical loads have been carried out and published in Klasen et al. [57].

Module technology and application areas

The integration of solar cells into PV modules changes their output power because of optical and electrical effects. Absorption in module layers, reflection at optical interfaces, or resistive losses in solar cell interconnection are typical loss channels within a PV module.

In addition, when inactive module areas (e.g. cell spacing) are added, the geometrical reference area is increased. As a result, not only the output power of a cell but also the efficiency of the device is altered [59,60]. The cell-to-module (CTM) analysis, a methodology introduced by Haedrich et al. in 2014 [61], provides a versatile tool to assess these effects in module integration. Gains and losses are assigned to important module components (e.g. junction boxes, ribbons) and are shown as physical mechanisms, allowing the evaluation of module design and materials and the comparison of different module technologies.

The methodology provides a simple key figure to describe the success of module integration in terms of power or efficiency. The CTM ratio is the module power or efficiency divided by the initial cell power or efficiency; a ratio less than one represents a loss resulting from the integration of solar cells into the module, whereas a ratio greater than one indicates a gain.

Mittag et al. [62] have extended the CTM methodology to deal with shingled modules. All models are integrated into Fraunhofer ISE's SmartCalc.CTM software – a flexible, precise and user-friendly calculation tool for analysing CTM ratios for different module technologies (<https://www.cell-to-module.com>). Case studies performed with SmartCalc.CTM show that shingling technology significantly increases $CTM_{efficiency}$ ratios compared with conventional modules because of the elimination of cell spacing and interconnector shading.

In 2018 Fraunhofer ISE reintroduced the 'matrix shingle' topology, patented by Schmidt and Rasch

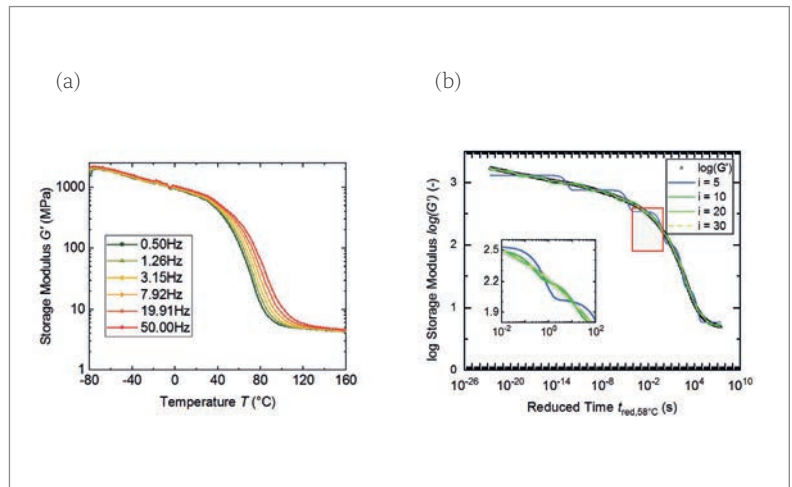


Figure 14. (a) Temperature-dependent stiffness of an ECA, measured at different excitation frequencies. (b) Corresponding master curve at T_g derived from a shift of the data in the time domain and the use of the Generalized Maxwell Model to fit the data, with different numbers of Maxwell elements to achieve a smooth representation.

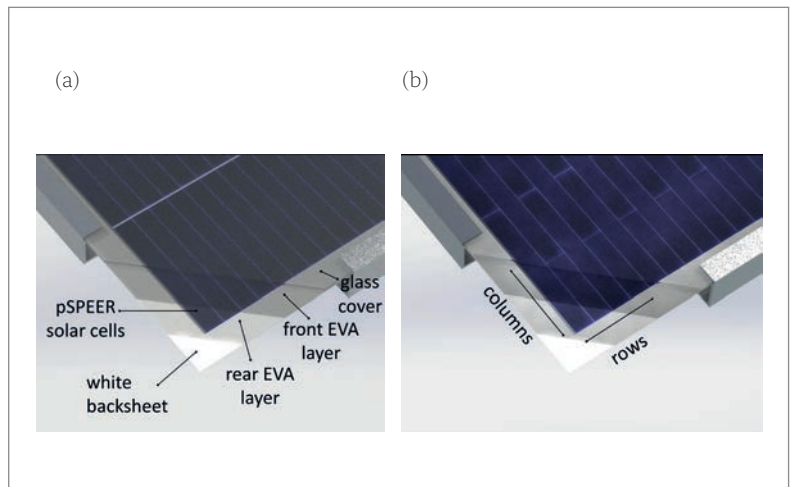


Figure 15. (a) Parallel string-based shingling topology, with string spacing. (b) Matrix-shingling topology, without inactive areas.



Figure 16. Top view of a bifacial matrix-shingled module (60-cell equivalent, rear side).

“The results of the CTM analysis show that matrix shingling is an effective approach for further increasing the module efficiency and power density of shingled modules.”

in the early 90s [63]. Matrix shingling is a further improvement to string-based shingling and features increased cell packing and power density. As in string-based shingling (see Fig. 15(a)), matrix shingling entails the interconnection of cell rows in series by overlapping the solar cells vertically. Additionally, the cell strips of the subsequent cell row are shifted horizontally, resulting in a topology similar to that of a brick wall (see Fig. 15(b)). This means that within a single row the solar cells are connected in parallel via the overlapping front and rear busbars of horizontally adjacent cells. Because of the resulting series-parallel connection scheme, an improved module performance under partial shading conditions is achieved [15]. At the Intersolar Europe exhibition in 2018, Fraunhofer ISE demonstrated for the first time (to the authors' knowledge) a bifacial, matrix-shingled module in a 60-cell equivalent format (see Fig. 16).

To illustrate the potential of the matrix-shingling approach, a comparative CTM analysis was performed for a conventional string-shingled module and a matrix-shingled module. The matrix topology

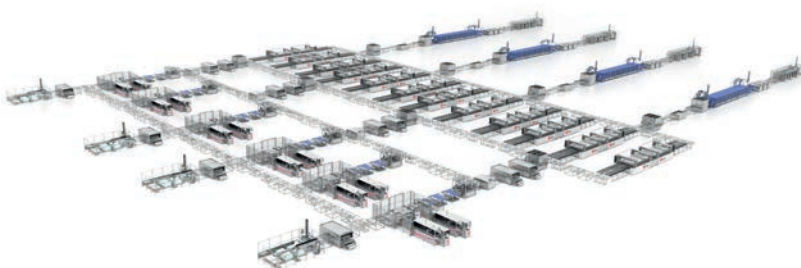
consists of 78 rows with six pSPEER solar cells in each row, while the string topology features six strings with 78 cells in each string. The cell power and the cell overlap are held constant for both topologies. The string design features a 2mm gap between neighbouring strings, whereas the matrix topology has no spacing. The module margins are kept the same; as a result, the matrix module can use a 1cm-smaller glass. Both modules incorporate a 3.2mm-thick glass with an anti-reflection coating, a 0.45mm-thick EVA encapsulant with a low UV cut-off, and a white TPT backsheets. The characteristics of the cells used are listed in Table 3, while the module topologies are summarized in Table 4.

The module power of the matrix-shingled module is found to be slightly less than that of the string-shingled design ($-2W_p$) because the gains from backsheets reflection in the string spacing areas are absent (compare k_{11} in Figs. 17 and 18). Since the matrix module is smaller and its cell packing is denser, the efficiency of the matrix topology is slightly increased in that design, with a power density improvement of $0.71W/m^2$ (+0.36%), as seen in Table 5.

The results of the CTM analysis show that matrix shingling is an effective approach for further increasing the module efficiency and power density of shingled modules. The benefit of the matrix approach becomes more relevant for bifacial modules with transparent back covers, when the reflection



SOLAR PV MODULES MANUFACTURING LINES



Turnkey solutions from 80MW to 1GW

Solutions and services throughout the entire value chain:

- Tabber & Stringer
- Interconnection
- Laminator
- PV Module Testing
- General automation
- Customized solutions
- Full service package
- Training and know-how transfer

Suitable for different technologies:

- Glass-glass and Bifacial modules
- Half cell modules
- Multiwire technology
- High production capacity

gains from inactive spacing areas are not applicable.

The limited space availability on cars, planes or other vehicles require new approaches for module design. Matrix shingling is particularly interesting in the case of VIPV, where a high power density and enhanced performance under partial shading conditions is essential. In addition, a pleasing optical appearance with invisible solar cells is desirable in VIPV. Matrix shingling delivers a very uniform optical appearance by virtue of the absence of cell interconnector ribbons and cell or string spacing.

Unfortunately, solar cells usually have a dark appearance and lack the special look that some products require in terms of bright and brilliant colours. Fraunhofer ISE's bionic Morpho-Color® (a spectrally-selective photonic structure which replicates the same physical effect the morpho butterfly uses to achieve the brilliant optical appearance) fulfils that requirement and allows the customized design of PV modules with a wide choice of colours, but with a power loss of only $-7\%_{rel}$ [64]. The combination of matrix shingling and Morpho-Color enables virtually invisible PV integration. To demonstrate the potential of this approach, a 2D curved matrix-shingled module with Morpho-Color coating was manufactured, demonstrating new possibilities for VIPV (see Fig. 19).

The high power density, the improved shading tolerance and the excellent aesthetics make matrix shingling highly suitable for integrated PV applications, such as BIPV or VIPV, as illustrated in Fig. 20. In an environment where high efficiencies, an attractive optical appearance and an excellent shading tolerance are essential, matrix shingling offers a very attractive solution.

Summary

The revival of the shingling concept for solar cells comes with a clear advantage potential in terms of an increase in the output power density p_{out} of modules. To achieve this goal, a number of challenges have to be tackled within the entire PV chain, from cell processing to module processing.

With an adaptation of the metallization layout and an advanced laser-assisted separation process, pSPEER solar cells can be fabricated in readiness for shingled-module integration. The laser-scribed and mechanically cleaved pSPEER solar cell yields a designated area front-side efficiency $\eta_f = 21.4\%$, measured at STC. A total designated area output power density $p_{out} = 22.8\text{mW/cm}^2$ is achieved, when considering an additional rear-side irradiance $G_r = 100\text{W/m}^2$.

The recombination in the edge region is better understood by means of an analytical model, verified by numerical Quokka3 simulations. In addition, a PL-based method offers further insight into edge recombination. The method shows that the thermal laser separation process (through the emitter) leads to enhanced results in comparison to the diamond-

cutter-scribed and mechanically cleaved edge separated through the emitter, quantified by the parameter $j_{02,edge} = 3\text{nA/cm}$.

At Fraunhofer ISE, a post-metallization/separation Passivated Edge Technology (PET) is under development, allowing higher cell efficiencies without compromising the stability of the metal contacts. A pSPEER cell processed with PET (pSPEER^{PET} solar cell) has achieved a designated $\eta_f = 22.1\%$ and $p_{out} = 23.5\text{mW/cm}^2$ (considering an additional $G_r = 100\text{W/m}^2$). The use of appropriate ECAs for the shingling interconnection, as well as a curing process, is necessary. The behaviour of the ECA material is seen to be viscoelastic.

The matrix-shingling topology demonstrates advantages with regard to superior aesthetics, thus making the approach attractive for integrated PV. A good example of the use of a matrix-shingled module is a vehicle-integrated roof module; the PV module is barely discernible, since the Morpho-Color glass surface integrates seamlessly into the car's structural form.

Acknowledgements

The work reported here was conducted within the framework of the PV-BAT 400 project (Contract No. 0324145), funded by the German Federal Ministry of Economics and Energy (BMWi). The authors would like to thank all their colleagues in the Fraunhofer ISE photovoltaic divisions for their contributions to advanced PV R&D.

References

- [1] Chapin, D.M., Fuller, C.S. & Pearson, G.L. 1954, "A new silicon p-n junction photocell for converting solar radiation into electrical power", *J. Appl. Phys.*, Vol. 25, No. 5, p. 676.
- [2] Dickson, J.D.C. 1960, "Photo-voltaic semiconductor

	pSPEER technology
Cell dimensions [mm ²]	156.75 × 22.00
Cell total area efficiency [%]	20.04
Cell power (STC) [W _p]	0.703
Ribbons	n/a

Table 3. Characteristics of the simulated cells used for both shingled-module concepts.

	String shingled	Matrix shingled
Number of cells		468
Overlap [mm]		1.55
String spacing [mm]	2	–
Top/bottom margins [mm]		36.7
Side margins [mm]		18
Glass format [mm]	3.2 × 1,667 × 987	3.2 × 1,667 × 977

Table 4. Topology characteristics for each shingled-module concept.

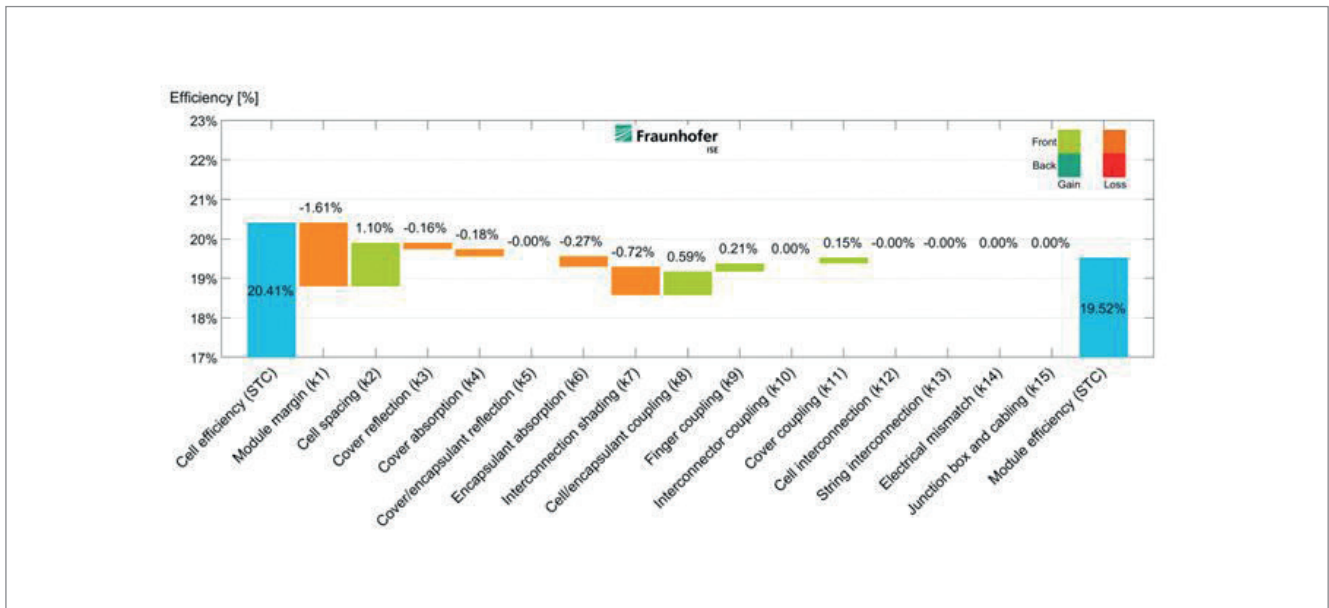


Figure 17. CTM_{efficiency} diagram for the string-shingled module at STC.

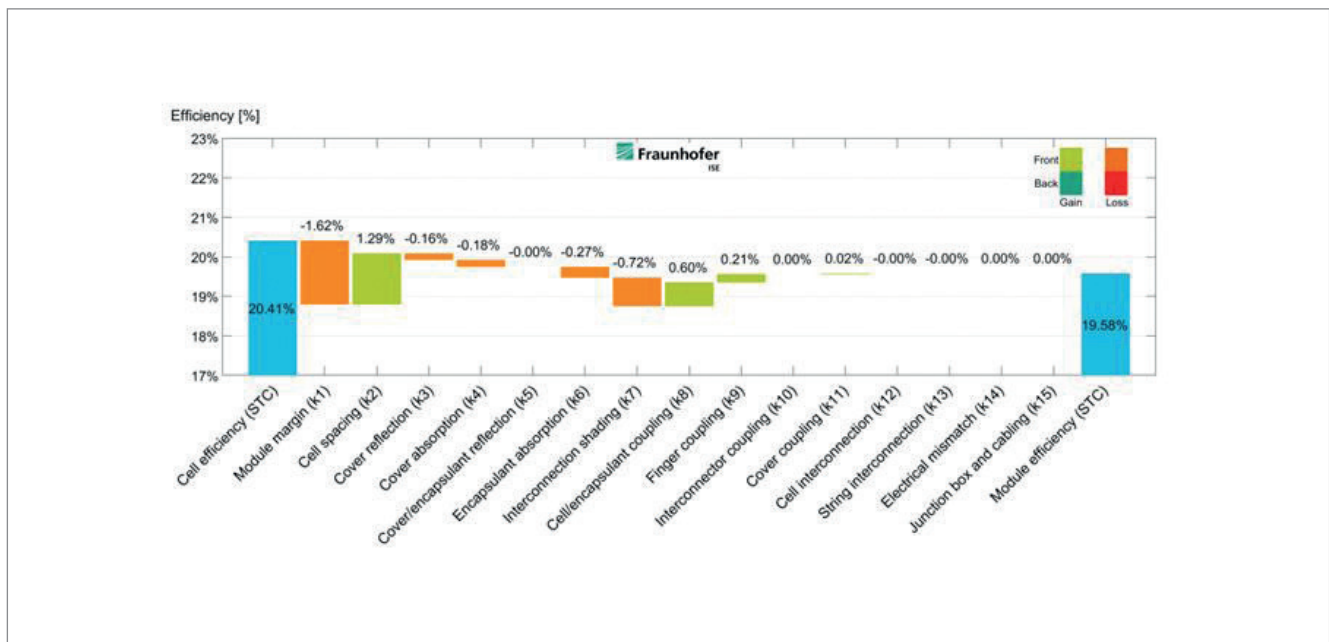


Figure 18. CTM_{efficiency} diagram for the matrix-shingled module at STC.

	String shingled 1,667 × 987mm ²	Matrix shingled 1,667 × 977mm ²	$\Delta_{\text{abs.}}$
Cell input power [W _p]	329.49	329.49	0
Module power [W _p]	323.27	321.15	-2.12
Power density [W/m ²]	196.48	197.19	+0.71
Module efficiency [%]	19.52	19.58	+0.06
CTM _{power} ratio [%]	98.11	97.47	-0.64
CTM _{efficiency} ratio [%]	95.69	95.98	+0.29

Table 5. CTM analysis results for both shingled-module concepts.

apparatus or the like”, US Patent 2,938,938.

[3] Nielsen, R.J. & Rongved, L. 1963, “Satellite solar cell assembly”, US Patent 3,116,171.

[4] Leinkram, C.Z. & Oaks, W.D. 1973, “Shingled array of solar cells”, US Patent 3,769,091.

[5] Glunz, S.W. et al. 2002, “High-efficiency silicon solar cells for low-illumination applications”, *Proc. 29th IEEE PVSC*, New Orleans, Louisiana, USA, pp. 450–453.

[6] Zhao, J. et al. 1997, “20000 PERL silicon cells for the ‘1996 World Solar Challenge’ solar car race”, *Prog. Photovolt: Res. Appl.*, Vol. 5, No. 4, pp. 269–276.

[7] SunPower, “SunPower P-Series Solar Panel” [https://www.sunpower.de/sunpower-p-series-solar-panel].

[8] Canadian Solar Inc., “High density shingle modules” [https://www.canadiansolar.com/solar-panels/hidm.html].

[9] ITRPV 2019, “International technology roadmap

“The high power density, the improved shading tolerance and the excellent aesthetics make matrix shingling highly suitable for integrated PV applications.”

for photovoltaic (ITRPV): 2018 results”, 10th edn (Mar.) [https://itrpvdma.org/en/].

[10] Morad, R. et al. 2015, “Shingled solar cell module”, US Patent 2015/0349167 A1.

[11] Heng, J. et al. 2018, “Module fabrication of solar cells with low resistivity”, Tesla Motors Patent 10,115,839.

[12] Tonini, D. et al. 2017, “Shingling technology for cell interconnection: Technological aspects and process integration”, *Proc. 33rd EU PVSEC*, Amsterdam, The Netherlands.

[13] Rudolph, D. et al. 2017, “Cell design optimization for shingled modules”, *Proc. 33rd EU PVSEC*, Amsterdam, The Netherlands.

[14] Schulte-Huxel, H. et al. 2019, “Interconnect-shingling: Maximizing the active module area with conventional module processes”, *Proc. 9th SiliconPV*, Leuven, Belgium.

[15] Mondon, A. et al. 2018, “Comparison of layouts for shingled bifacial PV-modules in terms of power output, cell to module factor and bifaciality”, *Proc. 35th EU PVSEC*, Brussels, Belgium.

[16] Luque, A. et al. 1984, “Diffusing reflectors for bifacial photovoltaic panels”, *Solar Cells*, pp. 277–292.

[17] Kopecek, R. et al. 2015, “Bifaciality: One small step for technology, one giant leap for kWh cost reduction”, *Photovoltaics International*, 26th edn.

[18] Blakers, A.W. et al. 1989, “22.8% efficient silicon solar cell”, *Appl. Phys. Lett.*, Vol. 55, No. 13, pp. 1363–1365.

[19] Dullweber, T. et al. 2016, “PERC+: industrial PERC solar cells with rear Al grid enabling bifaciality and reduced Al paste consumption”, *Prog. Photovolt: Res. Appl.*, No. 12, pp. 1487–1498.

[20] Lohmüller, E. et al. 2017, “Bifacial p-type silicon PERL solar cells with screen-printed pure silver metallization and 89% bifaciality”, *Proc. 33rd EU PVSEC*, Amsterdam, The Netherlands.

[21] Meier, S. et al. 2017, “Fast co-diffusion process for bifacial n-type solar cells”, *Solar RRL*, Vol. 1, No. 1.

[22] de Wolf, S. et al. 2012, “High-efficiency silicon heterojunction solar cells: A review”, *Green*, Vol. 2, No. 1.

[23] Feldmann, F. et al. 2017, “Evaluation of TOPCon technology on large area solar cells”, *Proc. 33rd EU PVSEC*, Amsterdam, The Netherlands.

[24] Wöhrle, N. et al. 2017, “Solar cell demand for bifacial and singulated-cell module architectures”, *Photovoltaics International*, 36th edn, pp. 48–62.

[25] Baliozian, P. et al. 2018, “Bifacial p-type silicon shingle solar cells – the ‘pSPEER’ concept”, *Solar RRL*.

[26] Baliozian, P. et al. 2018, “Bifacial pSPEER solar cells for shingle modules”, *Proc. 35th EU PVSEC*, Brussels, Belgium, pp. 410–413.

[27] Lewke, D. et al. 2015, “Thermal laser separation –



Figure 19. Curved matrix-shingled car roof module presented at Intersolar 2019.



Figure 20. Illustration of an integrated PV-active car roof.

A novel dicing technology fulfilling the demands of volume manufacturing of 4H-SiC devices”, *MSF*, Vol. 821–823, pp. 528–532.

[28] Röth, J. et al. 2015, “Thermal laser separation (TLS) dicing process study – A new technology for cutting silicon solar cells for high-efficiency half-cell modules”, *Proc. 31st EU PVSEC*, Hamburg, Germany, pp. 716–718.

[29] Lewke, D. 2018, *Untersuchung und Minimierung lateraler Rissabweichungen beim Thermischen Laserstrahlreparieren*. Aachen: Shaker Verlag.

[30] Koitzsch, M. et al. 2013, “Improving electric behavior and simplifying production of Si-based diodes by using thermal laser separation”, *Proc. 24th SEMI ASMC*, pp. 400–403.

[31] Eiternick, S. et al. 2014, “Loss analysis for laser

- separated solar cells”, *Energy Procedia*, Vol. 55, pp. 326–330.
- [32] Baliozian, P. et al. 2018, “Bifacial shingle solar cells on p-type Cz-Si (pSPEER)”, *Proc. 8th SiliconPV*, Lausanne, Switzerland.
- [33] Fell, A. et al. 2017, “The concept of skins for silicon solar cell modeling”, *Sol. Energy Mater. Sol. Cells*, Vol. 173, pp. 128–133.
- [34] Fell, A. & Altermatt, P.P. 2019, “Detailed 3D full-cell modeling in Quokka3: Quantifying edge and solder-pad losses in an industrial PERC cell”, *AIP Conf. Proc.*, Vol. 1999, No. 020007, pp. 1–5.
- [35] Wöhrle, N. et al. 2017, “The SPEER solar cell Simulation study of shingled bifacial PERC technology based stripe cells.”, *Proc. 33rd EU PVSEC*, Amsterdam, The Netherlands, pp. 844–848.
- [36] Saint-Cast, P. et al. 2019, “Extracting metal and edge recombination parameters which are compatible with multi-dimensional cell simulations”, *Proc. 36th EU PVSEC*, Marseille, France.
- [37] Fell, A. et al. 2018, “Modeling edge recombination in silicon solar cells”, *IEEE J. Photovolt.*, Vol. 8, No. 2, pp. 428–434.
- [38] Stolzenburg, H. et al. 2019, “Edge recombination analysis of silicon solar cells using photoluminescence measurements”, *Proc. 9th SiliconPV*, Leuven, Belgium.
- [39] Ruhle, K. et al. 2015, “Impact of edge recombination in small-area solar cells with emitter windows”, *IEEE J. Photovolt.*, Vol. 5, No. 4, pp. 1067–1073.
- [40] Giesecke, J.A. et al. 2011, “Minority carrier lifetime imaging of silicon wafers calibrated by quasi-steady-state photoluminescence”, *Sol. Energy Mater. Sol. Cells*, Vol. 95, No. 3, pp. 1011–1018.
- [41] Dicker, J. 2003, “Analyse und Simulation von hocheffizienten Silizium-Solarzellenstrukturen für industrielle Fertigungstechniken”, Dissertation, Faculty of Physics, University of Konstanz.
- [42] Fellmeth, T. 2014, “Silicon solar cells for the application in low concentrator systems – Development and characterization”, Dissertation, Faculty of Science, University of Tübingen.
- [43] Mulligan, W.P. et al. 2000, “Development of chip-size silicon solar cells”, *Proc. 28th IEEE PVSC*, Anchorage, Alaska, USA, pp. 158–163.
- [44] Zhao, J. et al. 2000, “Peripheral loss reduction of high efficiency silicon solar cells by MOS gate passivation, by poly-Si filled grooves and by cell pattern design”, *Prog. Photovolt: Res. Appl.*, pp. 201–210.
- [45] Hermle, M. et al. 2003, “Analysis of edge recombination for high-efficiency solar cells at low illumination densities”, *Proc. 3rd WCPEC*, Osaka, Japan, pp. 1009–1012.
- [46] Dicker, J. 2003, “Analyse und Simulation von hocheffizienten Silizium-Solarzellenstrukturen für industrielle Fertigungstechniken”, Dissertation, Faculty of Physics, University of Konstanz.
- [47] Kuhn, R., Fath, P. & Bucher, E. 2000, “Effects of pn-junctions bordering on surfaces investigated by means of 2D-modeling”, *Proc. 28th IEEE PVSC*, Anchorage, Alaska, USA, pp. 116–119.
- [48] Altermatt, P.P., Heiser, G. & Green, M.A. 1996, “Numerical quantification and minimization of perimeter losses in high-efficiency silicon solar cells”, *Prog. Photovolt: Res. Appl.*, Vol. 4, No. 5, pp. 355–367.
- [49] Kontermann, S. 2009, “Characterization and modeling of contacting crystalline silicon solar cells”, Dissertation, University of Konstanz.
- [50] Chan, C. et al. 2017, “Instability of increased contact resistance in silicon solar cells following post-firing thermal processes”, *Solar RRL*, Vol. 1, No. 11, 1700129 (1–5).
- [51] Baliozian, P. et al. 2019, “Post-metallization ‘Passivated Edge Technology’ of separated bifacial shingle pSPEER solar cells”, *IEEE J. Photovolt.* [submitted for publication].
- [52] Fraunhofer ISE 2019, “Adhesive process developed for shingle cell technology”, Press Release [<https://www.ise.fraunhofer.de/de/presse-und-medien/presseinformationen/2019/klebeverfahren-fuerschindeltechnologie-entwickelt.html>].
- [53] Klasen, N. et al. 2017, “Shingled cell interconnection: A new generation of bifacial PV-modules”, *Proc. 7th Worksh. Metalliz. Interconn. Cryst. Sil. Sol. Cells*, Konstanz, Germany.
- [54] Wirth, H. 2018, “Encapsulation form for a shingled photovoltaic module”, WO 2018/087008 A1.
- [55] Geipel, T. & Eitner, U. 2013, “Cure kinetics of electrically conductive adhesive”, *Energy Procedia*, Vol. 38, pp. 340–347.
- [56] IEC 61215-1-1, 2016, “Terrestrial photovoltaic (PV) modules – Design qualification and type approval – Part 1-1: Special requirements for testing of crystalline silicon photovoltaic (PV) modules.
- [57] Klasen, N. et al. 2019, “FEM simulation of deformations in strings of shingled solar cells subjected to mechanical reliability testing”, *Proc. 8th Worksh. Metalliz. Interconn. Cryst. Sil. Sol. Cells*, Konstanz, Germany.
- [58] Ward, I.M. & Sweeney, J. 2013, *Mechanical Properties of Solid Polymers*. Chichester, UK: Wiley.
- [59] Hädrich, I. 2014, “Unified methodology for determining CTM ratios: Systematic prediction of module power”, *Proc. 4th SiliconPV*, ‘s-Hertogenbosch, The Netherlands.
- [60] Pfreundt, A. et al. 2018, “Rapid calculation of the backsheets coupling gain using ray groups”, *Proc. 35th EU PVSEC*, Brussels, Belgium.
- [61] Hädrich, I. et al. 2014, “Unified methodology for determining CTM ratios: Systematic prediction of module power”, *Sol. Energy Mater. Sol. Cells*, Vol. 131, pp. 14–23.
- [62] Mittag, M. et al. 2017, “Cell-to-module (CTM) analysis for photovoltaic modules with shingled solar cells”, *Proc. 44th IEEE PVSC*, Washington DC, USA.
- [63] Schmidt, W. & Rasch, K.-D. 1990, “New interconnection technology for enhanced module efficiency”, *IEEE Trans. Electron Dev.*, Vol. 37, No. 2, pp. 355–357.
- [64] Bläsi, B. et al. 2017, “Morpho butterfly inspired coloured BIPV modules”, *Proc. 33rd EU PVSEC*, Amsterdam, The Netherlands, pp. 2630–2634.

About the Authors



Puzant Baliozian received a B.Sc. in physics from the American University of Beirut in 2014, and an M.Sc. in renewable energy engineering and management from the University of Freiburg in 2016 for his thesis work

completed at Fraunhofer IPM in the field of magnetocaloric energy conversion. He is currently a Ph.D. candidate at Fraunhofer ISE, and his main area of research is the development of p-type SPEER solar cells by focusing on the laser-assisted separation and edge passivation processes.



Nils Klasen studied chemical and process engineering at Karlsruhe Institute of Technology (KIT). He completed his master's thesis on large-area processing of perovskite solar cells at the Light Technology

Institute (LTI) in 2015. In 2017 he began his Ph.D. studies within the module technology group of Fraunhofer ISE, and is focusing on the reliability of shingled cell interconnections.



Nico Wöhrle studied physics at the University of Freiburg, Germany, and received his diploma degree in 2012 for his work at Fraunhofer ISE on optical simulation of silicon solar cells. With a fellowship from the German Federal

Environmental Foundation (DBU), he received his Ph.D. from the University of Freiburg in 2016 for his work on simulation of PERC solar cells. He is currently a researcher at Fraunhofer ISE, where he focuses on simulation and inline characterization of solar cells as well as on the conceptual development of p-type PERC solar cells.



Christoph Kutter obtained his B.Sc. in environmental engineering from the Hamburg University of Applied Sciences in 2015, for which he investigated the correlation between the LCOE of PV power plants and

module design. In 2018 he received his M.Sc. in renewable energy engineering and management from the University of Freiburg for his thesis on the topic of CTM analysis of decorated integrated PV modules. As a scientist at Fraunhofer ISE, his current research focus is the development of module technology for integrated PV applications (BIPV, VIPV).



Hannah Stolzenburg studied physics at the University of Göttingen. She received her M.Sc. in 2018 with a focus on material and solid-state physics while spending one semester studying physics at the University of Ghent. For

her master's thesis she investigated the interface between p-type silicon and aluminium oxide using

deep-level transient spectroscopy. She is currently a Ph.D. student at Fraunhofer ISE, carrying out research on characterization and quantification of edge losses in silicon solar cells.



Anna Münzer received her B.Sc. in physics with a focus on semiconductor physics in 2015, after which she studied renewable energy engineering and management at the University of Freiburg. In 2018 she

started working as an engineer at Fraunhofer ISE, where she is currently working on TLS process development in the research of shingled solar cells.



Pierre Saint-Cast received his M.Sc. and an engineering degree from the Polytechnic Institute of Grenoble in 2007. In 2012 he received his Ph.D. from the University of Konstanz, Germany. Since 2008 he has been

with Fraunhofer ISE, where his research interests include the development of passivation layers for solar cell applications, especially PECVD of Al₂O₃ layers, and the analytical modelling of electrical transport in Si solar cells devices. He is currently the project manager and product manager for PERC solar cells at Fraunhofer ISE.



Max Mittag studied industrial engineering and management at the Freiberg University of Mining and Technology. In 2010 he completed his diploma thesis at Fraunhofer ISE and joined the PV module

technology department. He is the head of the module efficiency team, and his current work includes CTM efficiency analysis, techno-economical assessments, and the development of new PV module concepts.



Elmar Lohmüller studied physics at the University of Tübingen, and at Nelson Mandela Metropolitan University, Port Elizabeth, South Africa. He received his diploma degree in 2010 for his work at

Fraunhofer ISE on the development of p-type MWT-PERC solar cells, and then his Ph.D. from the University of Freiburg in 2015 for his work on the development of n-type MWT solar cells. He is currently a researcher at Fraunhofer ISE and focuses on the development of p-type PERC solar cells.



Tobias Fellmeth studied physics at the University of Konstanz, and received his diploma degree in 2009 for his work at Fraunhofer ISE on the development and characterization of MWT concentrator solar cells. He

subsequently received his Ph.D. from the University of Tübingen in 2014 for his work on silicon-based, low-concentrator solar cells. Currently a scientist and project manager at Fraunhofer ISE, he focuses on the development of bifacial PERC and TOPCon solar cells.



Mohammad Al-Akash was awarded his B.Sc. in energy engineering by the German Jordanian University. In 2019 he received his M.Sc. in renewable energy engineering and management from the University of

Freiburg. His master's thesis focused on the evaluation of different post-metallization edge passivation methods of p-type SPEER solar cells.



Achim Kraft studied electrical engineering at the University of Applied Science in Hanover, and renewable energies at the University of Applied Science in Berlin. He obtained his master's in renewable

energies before joining Fraunhofer ISE as a Ph.D. student in 2012. He received his Ph.D. in the field of plated copper front-side metallizations for silicon solar cells from the Albert Ludwig University of Freiburg, Germany, in 2015. Since then his research has focused on solar cell interconnection technologies and processes at Fraunhofer ISE, where he is head of the interconnection technologies team in the module research group.



Martin Heinrich completed his Ph.D. at the National University of Singapore in 2015, where he worked for two years at SERIS, and then for two years at Fraunhofer ISE. As a group leader at University of

Freiburg, he focused on solar cell engineering and was the coordinator of the Solar Energy Engineering online study programme. In 2017 he joined the module technology department at Fraunhofer ISE and is the coordinator of the PV for Mobility programme.



Armin Richter received his Ph.D. in physics from the University of Konstanz, Germany, in 2014 for his work on n-type silicon solar cells with front-side boron-doped emitters and an in-depth

characterization of aluminium-oxide-based silicon surface passivation. His current research interests include atomic layer deposition of functional thin films (e.g. passivation layers, electron/hole transport layers, TCOs) and in-depth characterization of dielectric surface passivation layers, as well as the development of high-efficiency silicon solar cells along the whole process chain and 3D device simulations.



Andreas Fell carried out his Ph.D. thesis work at Fraunhofer ISE, Germany, on the topic of modelling and simulation of laser processes for silicon solar cells. From 2011 to 2015 he was a research fellow at the Australian

National University, where he developed laser processes and device simulation capabilities for silicon solar cells. In 2016 and 2017 he held a Marie-Curie fellowship position at Fraunhofer ISE, dedicated to developing the Quokka3 solar cell simulator and advancing solar cell modelling, which continues to be his research focus.



Alma Spribille, studied energy and environmental management at the European University of Flensburg, Germany. She completed work for her diploma thesis as an industrial engineer at Fraunhofer ISE, concerning

MWT solar cells, in 2010, after which she joined the MWT Solar Cells & Printing Technology group. Since December 2017 she has been head of the Process Integration – Structuring and Metallization team.



Holger Neuhaus holds a Ph.D. from the University of New South Wales. He was a development engineer at Pacific Solar Pty Ltd, and then worked for more than 15 years at SolarWorld AG, where he was initially responsible for

quality assurance and technology in cell production, and later headed the global R&D activities along the entire value chain. In 2018 he joined Fraunhofer ISE and is in charge of module technology.



Ralf Preu studied physics at the universities of Freiburg and Toronto, and economics at the University of Hagen, Germany. After being awarded a Ph.D. degree in electrical engineering, he joined Fraunhofer ISE

in 1993 and has worked in different fields in PV, including system monitoring, silicon solar cell and module technology, characterization and simulation. He is the director of the PV Production Technology division at Fraunhofer ISE, where his main focus is R&D of advanced silicon solar cell technology and its transfer to industrial production. He also teaches photovoltaics at the University of Freiburg.

Enquiries

Puzant Baliozian
Fraunhofer Institute for Solar Energy Systems ISE
Heidenhofstraße 2
79110 Freiburg, Germany

Tel: +49 (0)761 4588 5383

Email: puzant.baliozian@ise.fraunhofer.de

R&D spending analysis of 21 key PV manufacturers in 2018

Mark Osborne, Senior News Editor, *Photovoltaics International*

Abstract

Photovoltaics International's annual analysis of PV manufacturers, research and development (R&D) spending in 2018 includes 21 companies that were public listed on various stock exchanges around the world. R&D spending data was taken from audited annual financial reports and converted to US dollars at the time of the reports being published. The analysis in this 2018 report is intended to provide a good representation of global R&D spending trends in the PV wafer, cell and module segments of the upstream solar market.

Company updates

Since the adoption of new selection criteria for PV manufacturers to be included in the 2017 report, several companies have merged (Neo Solar Power (NSP), Gintech and Solartech) to form a new Taiwan-based company, United Renewable Energy (URE). These three companies have therefore been deleted from the 2018 report and replaced with the new URE name.

Included in the analysis for many years has been 'Solar Module Super League' (SMSL) member Hanwha Q CELLS, which delisted from NASDAQ in October 2018, negating the need to file a 2018 annual report. The renamed Q CELLS is therefore not included in the 2018 report.

“For the second year in a row, spending exceeded the US\$1bn level.”

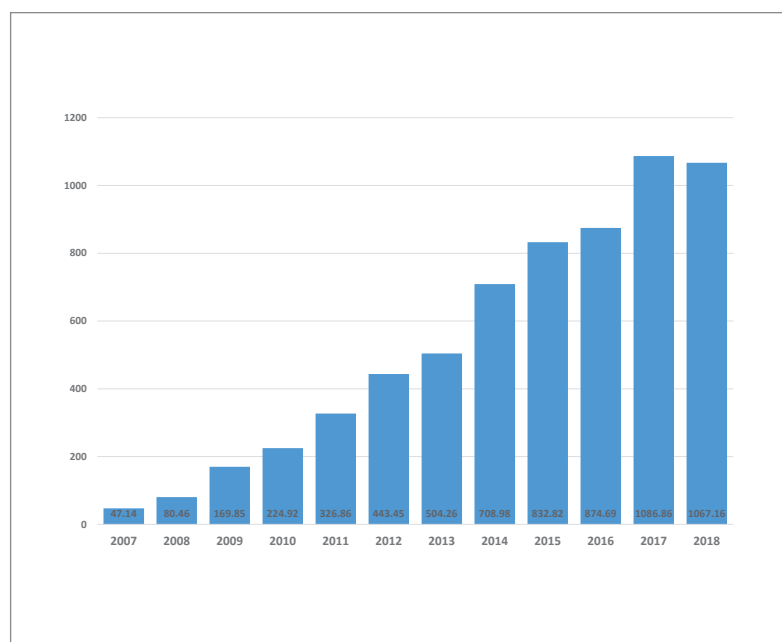


Figure 1. Total annual cumulative R&D expenditure (US\$m) of 21 PV manufacturers 2007–2018.

In an effort to maintain a good representation of global R&D spending trends, several companies (Tianjin Zhonghuan Semiconductor (TZS), Zhongli Talesun, Solargiga and Comtec) have been included for the first time in the 2018 analysis. Historical R&D spending figures for the new additions have also been included in the 2018 report.

The PV industry remains highly dynamic, however, and before this report was published, China-based PV manufacturer Hareon Solar became technically bankrupt, had ceased all manufacturing and was subsequently delisted from the Shanghai Stock Exchange (SSE) in July 2019. Luckily, the company had published its 2018 annual report before the delisting and is included in this R&D report. However, because of the delisting, Hareon Solar is not expected to be covered in the 2019 report. In August 2019 another company, Hanergy Thin Film, delisted from the Hong Kong Stock Exchange, indicating it would not be publishing further audited annual reports, and consequently is also not expected to be covered in the 2019 report.

More positive developments involve the expected re-inclusion of two SMSL members, Trina Solar and JA Solar, in the 2019 report, because of preparations, which are at various stages, to relist on Chinese stock exchanges. Also planning a public listing is China-based major merchant solar cell producer, Aiko Solar. These are therefore expected to have meaningful positive benefits in the coverage of global R&D spending trends in 2019.

R&D spending trends in 2018

The cumulative annual R&D spending of 21 key PV manufacturers reached a total of US\$1,067.16m (US\$1.06bn) in 2018. For the second year in a row, spending exceeded the US\$1bn level, although it is down slightly from the US\$1,086.86m (US\$1.08bn) cumulative annual R&D spending of the 20 key PV manufacturers in 2017 (Fig. 1).

It is interesting to note that R&D spending doubled over the five-year period from 2013 (US\$504m) to 2017 (US\$1.08bn). Almost all the 20 PV manufacturers in the analysis were public in 2013, and all of them by 2014.

Spending pattern divergence

A continued trend since 2014, however, has been the growing number of companies that lowered

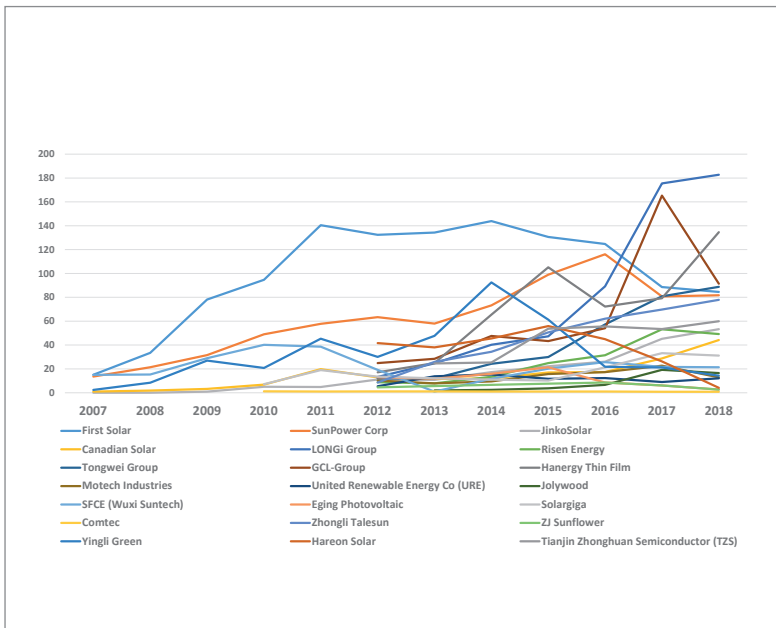


Figure 2. Total annual cumulative R&D expenditure (US\$m) of 21 PV manufacturers 2007–2018.

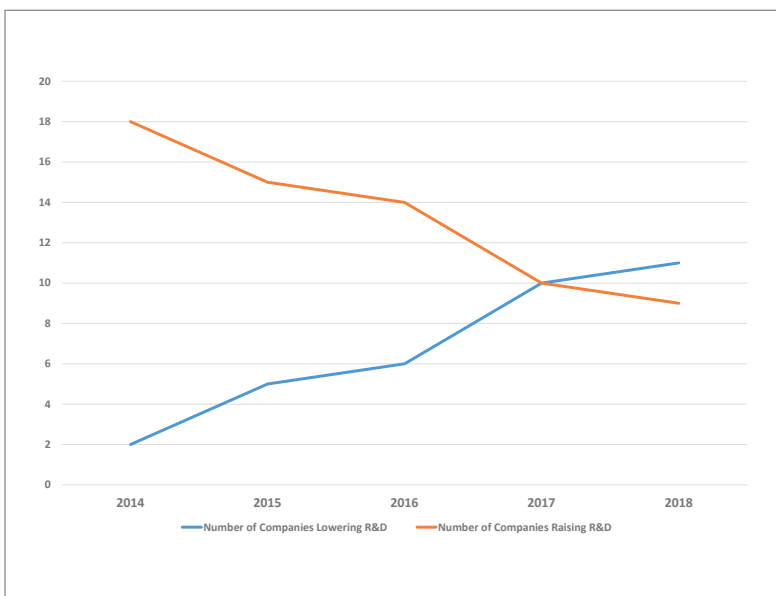


Figure 3. Trends of the number of companies spending less or more on R&D 2014–2018.

R&D spending, compared with those increasing spending on a year-on-year basis (Fig. 2).

As the chart in Fig. 3 highlights, only two companies lowered R&D spending in 2014, while the crossover point was reached in 2017, when 10 companies reduced spending, compared with the previous year. This trend continued in 2018, when for the first time the number of companies lowering spending (11) exceeded the number (9) increasing R&D spending.

Since 2015 there have also been two companies (First Solar and Yingli Green) that have reduced

spending for four consecutive years. In the 2018 analysis, two companies (Eging PV and Hareon Solar) have been lowering spending for three consecutive years, while two companies (ZJ Sunflower and Wuxi Suntech) have been lowering spending for two consecutive years.

As noted in the 2017 report, the spending pattern divergence has been due primarily to the financial condition of some of the companies, such as Yingli Green, Hareon Solar, SunPower and others, in the past. However, the growing number of companies reducing spending in 2018 is also a result of the weaker downstream PV market in China, after the Chinese government announced the ‘531 New Deal’, which put a halt to utility-scale and DG markets, as installations were viewed to have far exceeded plans and the market was subsequently overheating.

As stated in the previous year’s report, First Solar’s sequential decline in spending is more to do with its production shift to the large-area Series 6 modules and the construction of three new manufacturing plants than any financial issues, as the company remains technically sold out for several years to come.

It is also interesting to note from the trends in Fig. 2 that, since 2012, only two companies (LONGi Group and Zhongli Talesun) have consistently increase R&D spending, year on year.

Other companies that increased spending in 2018 include JinkoSolar, Canadian Solar, SunPower, Tongwei, Hanergy Thin Film, URE, TZS and Comtec (Fig. 4).

R&D spending rankings

Following on from topping the spending rankings in 2017, LONGi Group maintains its position at the top for 2018. The company increased R&D expenditure from US\$175.5m in 2017 to US\$182.7m in 2018, marking the seventh consecutive year of increased spending (Fig. 5). Hanergy Thin Film was the second biggest spender on R&D in 2018, reporting expenditure of US\$134.6m, up from US\$79.2m in the previous year, when it was ranked fifth. Both LONGi Group and Hanergy Thin Film were the only companies to surpass US\$100m in R&D spending in 2018.

Despite a significant reduction in year-on-year spending, GCL Group is ranked third with spending of US\$91.4m, down from US\$165.2m in 2017, when ranked second only to LONGi Group.

Moving up the rankings is Tongwei Group, reporting R&D expenditure of US\$88.8m in 2018, compared with US\$53.4m in the previous year. The company is therefore ranked fourth in 2018, up from seventh in 2017.

Dropping down one position in the rankings are First Solar and SunPower with spending of US\$84.5m and US\$81.7m respectively in 2018. First solar is ranked fifth-highest R&D spender in 2018 and SunPower sixth highest.

Zhongli Talesun, which has been included in the

“Following on from topping the spending rankings in 2017, LONGi Group maintains its position at the top for 2018.”

report for the first time, had R&D expenditure of US\$77.9m in 2018, up from US\$69.8m in the previous year. The company would have been ranked sixth in 2017, but actually falls one position to seventh in 2018.

Tianjin Zhonghuan Semiconductor (TZS) is another new entrant to the report. The company had R&D expenditure of US\$59.9m in 2018, up from US\$53.5m in the previous year. As a result, it is ranked eighth, down one position if it had been represented in the 2017 report.

Leading SMSL member, JinkoSolar, increased R&D spending to US\$53.3m in 2018, up from US\$45.2m in 2017. Although this was record spending for the company, its ninth-ranked position means it has dropped from its eighth-place ranking in 2017.

Risen Energy lowered R&D spending in 2018 to US\$49.2m, compared with US\$56.4m in the previous year. As a result, the company falls from being ranked sixth in 2017 to tenth in 2018.

Second-ranked SMSL member, Canadian Solar, has significantly increased R&D expenditure year on year. In 2018, spending topped US\$44.2m, up from US\$28.7m in 2017 – a 53% increase. Despite the marked increase, Canadian Solar’s ranking drops from ninth in 2017 to eleventh in 2018.

New to the rankings in 2018 is Solargiga, reporting R&D expenditure of US\$31.2m, down slightly from US\$33.2m in 2017. The company is ranked twelfth in 2018 and would have been ranked above Canadian Solar in 2017, had the company been included in the previous report.

Ranked thirteenth is Wuxi Suntech. R&D expenditure in 2018 was US\$21.4m, almost identical but slightly down from US\$21.75m in 2017. However, because of the previously highlighted changes to some of the companies excluded and included in the 2018 analysis, Wuxi Suntech actually ranks one position higher at thirteenth.

Jolywood experienced a similar situation to Wuxi Suntech, jumping several positions to rank fourteenth in 2018, compared with its ranking of seventeenth in 2017, despite decreasing R&D spending from US\$19.2m in 2017 to US\$16.5m in 2018.

Although Yingli Green again lowered R&D spending in 2018, its ranking position remains unchanged at fifteen. Yingli Green’s spending in 2018 was US\$14.3m, down from US\$21.2m in 2017.

Taiwan-based Motech significantly cut R&D spending in 2018, impacting its ranking position. The company had spending of US\$12.9m in 2018, down around 48% from US\$22.7m in 2017. As a result, it drops from being ranked thirteenth in 2017 to sixteenth in 2018. However, despite the deep cuts in R&D, Motech is ahead of its nearest country rival, URE.

Before Gintech, Solartech and NSP combined under NSP, while changing the name to URE in 2018, their total R&D spending as separate businesses was US\$14.89m in 2017. Under the URE name in 2018, the R&D spending declined to

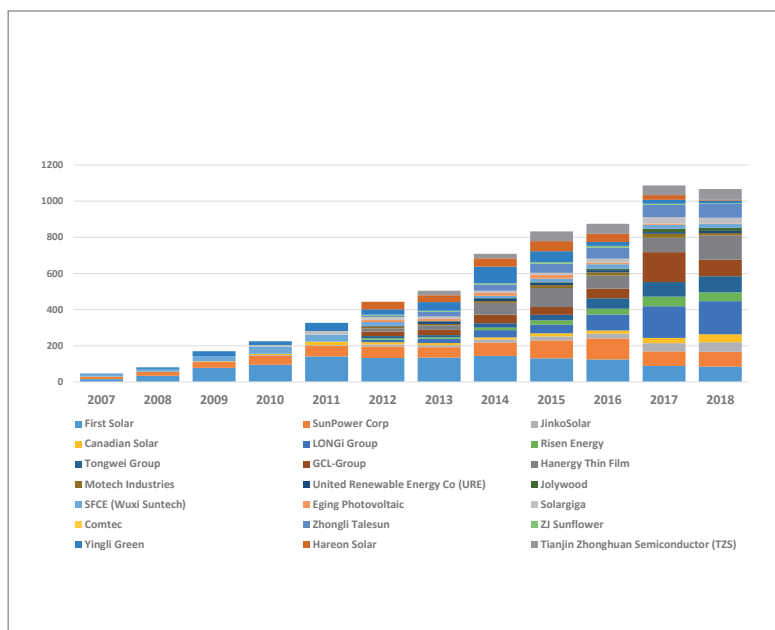


Figure 4. Annual R&D expenditure (US\$m) of 21 PV manufacturers (public listed) 2007–2018.

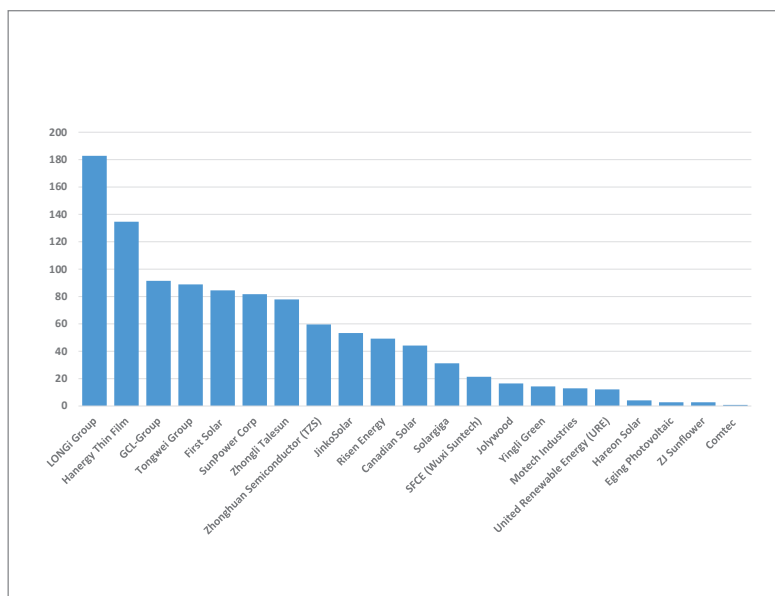


Figure 5. Annual R&D expenditure (US\$m) of 21 PV manufacturers ranked (public listed) in 2018.

US\$12.1m. However, with Gintech and Solartech rolled into NSP, the R&D spending of NSP in 2017 was US\$9m, indicating that R&D spending as the renamed URE actually increased. Despite the merger, URE is ranked seventeenth in the 2018 rankings, only one position above where NSP stood in the 2017 rankings.

The collapse of Hareon Solar means the company falls from being ranked tenth in 2017 to eighteenth in 2018. R&D spending was only US\$4.1m, down from US\$26.2m in 2017. The company will not be ranked next year.

Eging Photovoltaic reported R&D expenditure of US\$2.7m in 2018, down from US\$6.1m in 2017, ranking the company in nineteenth position, one down from the previous year.

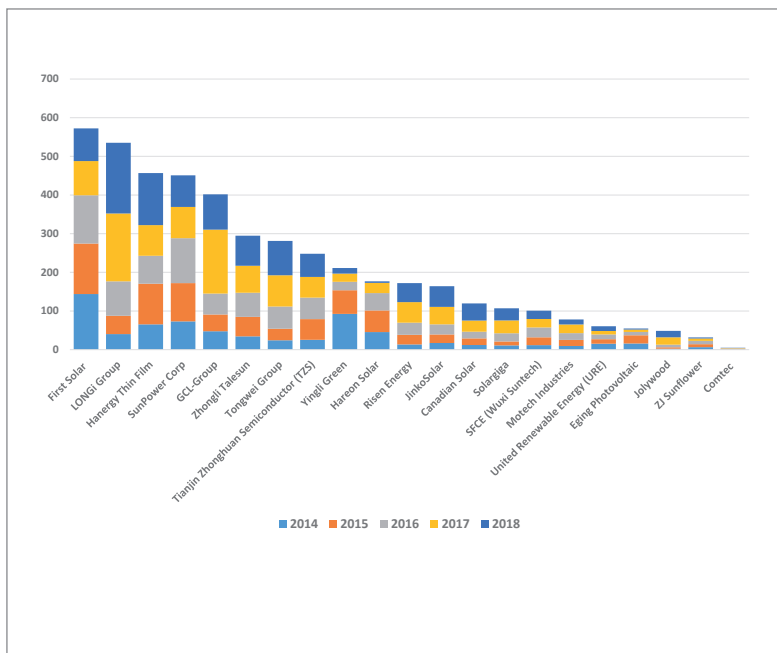


Figure 6. R&D expenditure (US\$m) of 21 PV manufacturers ranked (public listed) 2014–2018.

In twentieth position is new entrant ZJ Sunflower, which had R&D expenditure of US\$2.7m in 2018, down markedly from US\$6.7m in 2017, and the lowest level since 2012.

New entrant Comtec had R&D expenditure of US\$0.86m in 2018, up slightly from US\$0.85m in 2017. The company sits at the bottom of the rankings in twenty-first position for 2018.

Five-year ranking trends

With continued volatility in the PV industry, which R&D spending is not immune to, a look at cumulative company annual expenditures over a period covering the last five years may provide insight into other trends related to R&D expenditure. The chart in Fig. 6 covers the last five years of annual R&D spending of the 21 key PV manufacturers addressed in this report.

There is clearly a group of five companies (First Solar, LONGi Group, Hanergy Thin Film, SunPower and GCL Group) that have become separated from the pack by a minimum of over US\$100m in cumulative R&D spending over the last five years. Despite First Solar and SunPower dropping in the annual rankings, the changes over a five-year period are less pronounced for First Solar, which remains the cumulative R&D spending leader.

These five companies have been in the high US\$500m to the low US\$400m spending range over the last five years. However, SunPower's

“Five years of R&D spending have mainly highlighted the chasm between the lead and second-placed groups, a gap that increasingly looks to be insurmountable.”

position dropped two places in the 2018 rankings, and has also been overtaken by LONGi Group and Hanergy Thin Film in the five-year period. Moreover, GCL Group was closing in fast on SunPower until a significant reduction in R&D spending took place in 2018. LONGi Group and Hanergy Thin Film have been two of the three fastest-growing companies in terms of R&D spending, notably in the last three years, as shown in the chart.

The chart in Fig. 6 also highlights that three companies (Zhongli Talesun, TZS and Tongwei Group) have formed a second strong group with accelerated R&D spending in the last four of the past five years. Zhongli Talesun, TZS and Tongwei Group have R&D spending that ranges between the very high US\$200m level and the mid US\$250m level.

Below TZS, things also look interesting, as the low levels of spending by Yingli Green in the last three years highlight its declining position in the rankings, while Hareon Solar collapsed. This means that the accelerated R&D spending by Risen Energy, JinkoSolar and Canadian Solar in the last two years shows their ability to move ahead of Yingli Green very soon. However, it can also be seen that they remain a significant distance behind the second leading pack of Zhongli Talesun, TZS and Tongwei Group. Despite the potential of Risen Energy, JinkoSolar and Canadian Solar to climb slowly up the ranking, primarily because others are falling by the wayside, there is every chance the gap between them and the second group will widen, locking in the two major SMSL members in the lower middle range. This situation may also be exacerbated by the expected return of two other SMSL members, Trina Solar and JA Solar, to the R&D analysis in 2019.

As for those companies below Canadian Solar, five years of R&D spending have mainly highlighted the chasm between the lead and second-placed groups, a gap that increasingly looks to be insurmountable.

Five years of annual R&D expenditure as a percentage of revenue

Another metric that is being tracked but has not previously been covered in the R&D reports is R&D expenditure as a percentage of revenue. A key reason was the fact that the almost universal ratio of companies' R&D expenditure as a percentage of revenue lies within the 0.8% to 3% range. The exceptions to this have always been First Solar and SunPower, with much higher ratios.

In the first sample chart, shown in Fig. 7, First Solar and SunPower have been included in order to represent the historical high end of R&D expenditure as a percentage of revenue; also included are two major SMSLs (JinkoSolar and Canadian Solar), which have been perennial laggards in total annual R&D spending. A typical

example of a relatively small PV manufacturer has also been included in the form of Eging PV. This selection of companies is a good representation of the historical highs and lows of R&D expenditure as a percentage of revenue.

A key takeaway is that the proprietary technology used by First Solar and Sunpower, compared with the other companies, requires much higher R&D expenditure as a percentage of revenue. However, despite JinkoSolar and Canadian Solar being laggards in total annual R&D expenditure, as well as in expenditure as a percentage of revenue, it has historically had little negative impact on them, as both have become the two largest crystalline PV module manufacturers in the world today.

In the second sample chart, shown in Fig. 8, three major China-based integrated PV manufacturers – LONGi Group, TZS and GCL Group – have been included and are arguably the most closely matched from a business model perspective. The main deviation here is that GCL Group can be deemed the historical major incumbent and has been the largest company in the PV industry by revenue and scale in polysilicon and multicrystalline wafer capacity for many years.

LONGi Group and TZS have become fast-growing companies that have strong R&D spending regimes coupled with strong revenue growth. Indeed, in 2018 both companies’ R&D expenditure as a percentage of revenue declined at almost the same rates, but the reality was that both companies’ total revenue significantly increased, compared with the previous year, while R&D spending increased but clearly at a slower pace than revenue. In contrast, GCL Group reported markedly lower revenue in 2018, compared with the previous year. GCL Group companies have cut R&D spending significantly, year on year, because of financial constraints, causing R&D expenditure as a percentage of revenue to decline.

Therefore, it could be argued that emerging major players that have had high R&D spending in the last five years have gained significant market share against an historical incumbent. GCL, however, has been an investor in TZS as well as SunPower, which muddies the waters for a clear-cut comparison.

Conclusion

Despite continued upheaval in the companies being tracked and those untracked, which will undoubtedly occur in 2019 as well, it remains somewhat remarkable that over US\$1bn was allocated in R&D expenditure in 2018, following a record year and milestone in 2017.

As was the case in 2017, this report highlights that R&D spending trends remained volatile in 2018, still being impacted by some companies

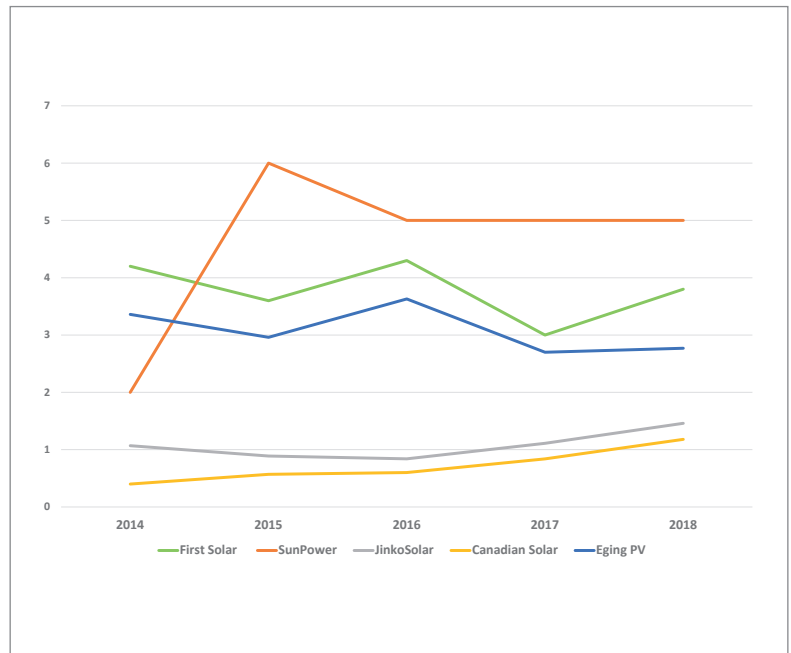


Figure 7. Annual R&D expenditure as a percentage (%) of revenue (sample 1).

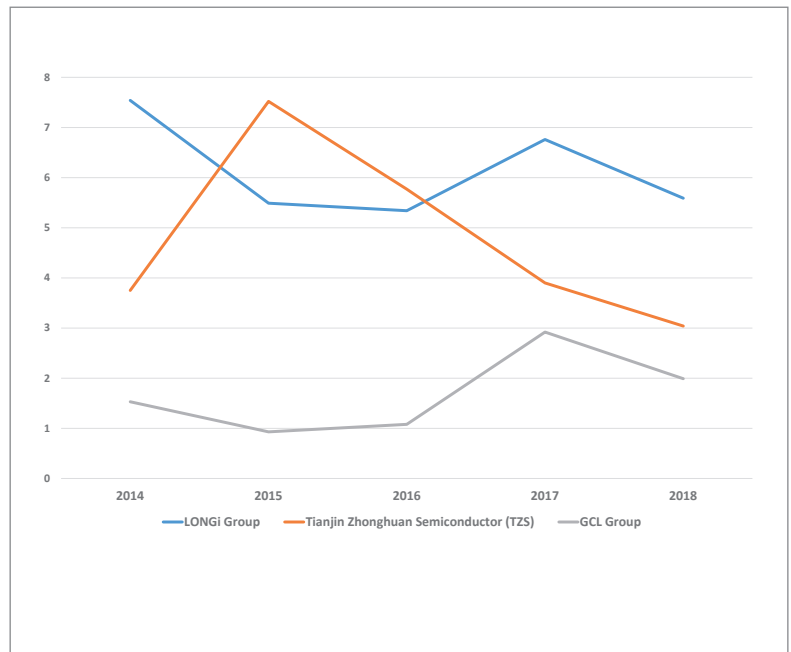


Figure 8. Annual R&D expenditure as a percentage (%) of revenue (sample 2).

driving new technology adoption and market share gains, as well as by other companies being affected by company-specific financial challenges.

This report has also highlighted a clear leadership group of R&D spenders, which could become pivotal to their business strength and the weakening of others.

“R&D spending trends remained volatile in 2018.”

Advertisers and web index

ADVERTISER	WEB ADDRESS	PAGE NO.
Aiko Cells	en.aikosolar.com	Outside Back Cover
Borealis AG	borealisempowersolar.com	7
Ecoprogetti srl	ecoprogetti.com	58
Energy Taiwan	www.energytaiwan.com.tw	33
EU PVSEC 2019	www.photovoltaiic-conference.com/	9
Exateq GmbH	www.exateq.de	37
Heraeus Photovoltaics	www.Heraeus-Photovoltaics.com	62
Henkel AG & Company	henkel-adhesives.co/electronics	53
Innolas Solutions GmbH	www.innolas-solutions.com	11
Intersolar Global	www.intersolar.de	43
Intersolar Mexico 2019	www.intersolar.mx	23
JA Solar	www.jasolar.com	Inside Front Cover
Meco Equipment Engineers B.V	www.besi.com	60
Meyer Berger	www.meyerburger.com	5
Mondragon Assembly	www.mondragon-assembly.com	64
PV CellTech	https://celltech.solarenergyevents.com	29
Photovoltaics International	www.pv-tech.org/photovoltaics-international/overview	29
PV ModuleTech	https://moduletech.solarenergyevents.com	Inside Back Cover
PV-Tech.org	www.pv-tech.org	29
PV-Tech Research	www.pv-tech.org/solar-intelligence/pv-manufacturing-technology-quarterly-report	35
RENA	www.rena.com	56
Sentech Instruments GmbH	www.sentech.com	35
SNEC PV Power Expo 2020	www.snec.org.cn	27
Von Ardenne GmbH	www.vonardenne.biz	54

To advertise within Photovoltaics International, please contact the sales department: Tel +44 (0) 20 7871 0122

THE INDISPENSABLE GUIDE FOR MANUFACTURERS IN SOLAR

NEXT ISSUE:

- Capacity expansion report
- Heterojunction manufacturing
- Tandem perovskites

Photovoltaics International contains the latest cutting edge research and technical papers from the world's leading institutes and manufacturers.

Divided into six sections – Fab & Facilities, Materials, Cell Processing, Thin Film, PV Modules and Market Watch – it is an essential resource for engineers, senior management and investors to understand new processes, technologies and supply chain solutions to drive the industry forward.

An annual subscription to **Photovoltaics International**, which includes four editions, is available at a cost of just \$199 in print and \$159 for digital access.

Make sure you don't miss out on the ultimate source of PV knowledge which will help your business to grow!



SUBSCRIBE TODAY: www.photovoltaiicsinternational.com/subscriptions



The new PV ModuleTech Bankability Ratings list

The new PV ModuleTech Bankability Ratings methodology has recently been outlined clearly across a series of six online PV-Tech articles that explained how PV module suppliers can be graded (from the top AAA-rated to the lowest/highest-risk C-rated). The final ratings system overview can be found on the final of the six articles here, with links to each of the series features highlighted at the bottom of this webpage also.

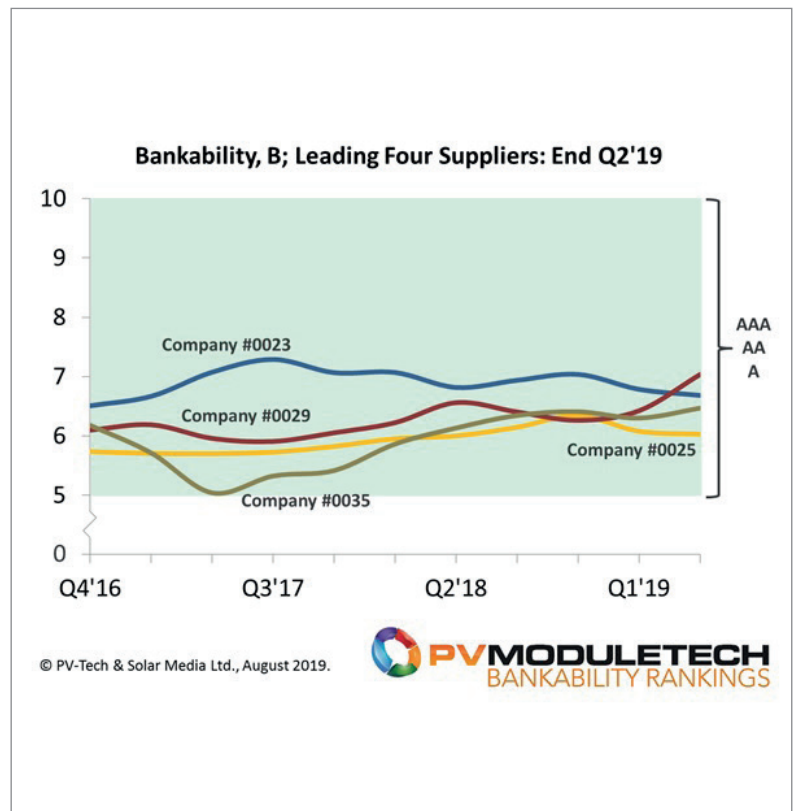
The new PV-Tech Ratings system is the first industry analysis that combines each company's track-record in large-scale global shipments, with its financial health, on a rolling quarterly basis. The analysis uses data collected over 10 years at PV-Tech, across a wealth of manufacturing and financial inputs; these are all covered in the series of six articles on PV-Tech recently.

In contrast to all other tier-based or top/leading-supplier related tables and lists disseminated throughout the industry over the past few decades, the PV ModuleTech Bankability Ratings system uses statistical analysis and modelling, carefully validated against each company's historic and current status within large-scale PV module deployment.

The driver for the new ratings system has been from downstream PV module users and investors who have been constantly confused about which module suppliers were truly bankable, being able to supply volumes with confidence and having a balance-sheet that reduced the risk of imminent bankruptcy or in-house manufacturing re-organization.

This PV ModuleTech Bankability Ratings system finally allows project developers, EPCs, site investors and asset owners to understand the key investment differences across the range of PV module suppliers bidding to supply to commercial, industrial and utility-scale PV solar sites globally. It is ideal for competitive benchmarking, and shows the strengths and weaknesses of each PV module supplier from each of the key manufacturing and financial perspectives. It is perfect for short-listing potential suppliers, prior to factory audits and reliability tests that are essential to meet specific investor requirements.

No module company today meets the top-performer AAA-rated grade, and that this has rarely been obtained by any PV module supplier in the past. This is not too much of a surprise however, as I will explain during the webinars, and



Four PV module suppliers are currently AA-rated, as of the end of Q2'19. The AA-rating grade is the highest any PV module supplier meets today.

is in part arising from a still-fragmented landscape where the market-leaders command typically a 10% market-share of module supply; and where some 200-plus companies fight over business globally. It is also arising from the rather precarious financial health of companies that have been overly-dependent on revenue streams from module sales that have been impacted regularly by ASP declines well above cost-reduction measures implemented internally.

The highest ratings grade achieved by a PV module supplier today is AA-rated, and there are only four companies within this top-performer category only.

The forthcoming PV ModuleTech 2019 conference in Penang, Malaysia on 22-23 October 2019 will see many of the AA-rated and A-rated companies presenting and in attendance. This event will start with a 45-minute talk I will deliver, specific to the PV ModuleTech Bankability Ratings.



PV MODULETECH CONFERENCE

22 - 23 October 2019
Penang, Malaysia

Benchmarking PV module quality, reliability & leading global suppliers

PV Module Tech is a unique event, dedicated to one specific topic. This focus helps in bringing together the right people within the huge PV ecosystem. A must-attend for procurement professionals looking to make smart technology choices.
Ronald Sastrawan, Director of Green Tech Solutions, Munich Re

Great balance of commercial, technical aspects. Good mix of attendees at managerial and senior levels that facilitates productive discussions. Lots of time allocated to networking.
Benjamin Wong, Director of Brand Marketing, LONGi Solar

Very well run and informative event with knowledgeable presenters
Kevin Robinson, Technical Services Manager Middle East and Africa, Jinko Solar

166mm*166mm High Efficiency PERC Cell
Assisting Bifacial Modules with Power Output 450w+

World's First GW-scale Innovation by Aikosolar

Bifacial Cells Metrology and Classification

Provide Highly Reliable Products

